Optimization of computer-assisted intraoperative guidance for complex oncological procedures

by

Mónica García Sevilla

A dissertation submitted in partial fulfillment of the requirements for the degree of Doctor of Philosophy in

Biomedical Science and Technology

Universidad Carlos III de Madrid

Advisor:

Javier Pascau González-Garzón

Tutor:

Javier Pascau González-Garzón

January 2022

A mi familia

"Speaking to you now as one of many patients who has undergone major surgery performed with a machine and who is extremely grateful for the engineers that made that machine and made it safe and effective, I would challenge you: If you are an engineer—or a physicist, computer scientist, or mathematician—do your very best to understand every formula and every algorithm that you encounter that might affect the safety and efficacy of machines in surgery and make it your responsibility to proactively explain these concepts to those who need to understand them.

We're all depending on you."

J. Michael Fitzpatrick

AGRADECIMIENTOS

Estos agradecimientos van dirigidos a todas aquellas personas que han estado conmigo a lo largo de estos cuatro años y que, en mayor o menor medida, han contribuido a que esta etapa haya sido, si no la mejor, una de las mejores de mi vida.

En primer lugar, me siento agradecida por la suerte que he tenido con mi tutor de tesis, **Javi**. Nunca me planteé hacer doctorado, y sé que finalmente me decidí a hacerlo en parte porque sería bajo su supervisión. Javi, trabajar contigo ha sido desde el principio un lujo. No sólo porque siempre has favorecido el buen rollo en el grupo, sino porque eres una persona generosa, razonable, comprensiva y cercana. A tu lado he podido crecer en lo personal y profesionalmente, ganando confianza en mí misma y en mi trabajo, y por eso te estaré siempre agradecida.

Sé que para muchos el doctorado es una etapa difícil porque la hacen en soledad. Por suerte no ha sido mi caso, y he tenido a los mejores compañeros. Con ellos he compartido muchos momentos únicos e inolvidables. Momentos de risas en el despacho, de brainstorming, de tensión en cirugías, de estrés por llegar a un deadline… Los viajes por cursos y congresos (que para mí eran como vacaciones de lo bien que lo pasábamos), las partidas al Mario Kart, los planes de tomar una cerveza, echar un billar o unos dardos después del trabajo, los festivales… Hay tantos momentos y anécdotas que me vienen a la cabeza que podría llenar páginas y páginas.

A **Deivid**, porque sentí una conexión contigo desde el principio y has marcado un antes y un después en mi vida. Todo lo que hemos vivido juntos han sido experiencias increíbles y no puedo esperar a ver qué vendrá después. Te admiro enormemente por tu inteligencia, tu iniciativa y tu valentía. Siempre has estado ahí cuando hacía falta y no te he oído quejarte nunca. Gracias por saber animarme, por el cariño que me das todos los días y por reírte con todas mis tonterías y despistes. Sabes estar en los buenos y malos momentos y por eso y mucho más eres el mejor regalo que me llevo de esta etapa.

A **Rafinha**, mi compi inseparable de experimentos, de brainstorming, de cine, de confidencias, de videojuegos y demás frikadas. Sé que podría tirarme horas hablando contigo de cualquier cosa. Gracias por tus bromas, que me han hecho reír todos los días. Gracias por tu sinceridad. Y gracias por decidirte finalmente a hacer el doctorado, sin ti no habría sido lo mismo. Trabajar a tu lado es genial en todos los sentidos y ojalá podamos volver a hacerlo pronto.

A quien sin duda tengo que agradecer todo lo que he conseguido estos años y haber llegado hasta aquí es a mi queridísima **Ro**. Aunque nuestras andadas empezaron hace más de 10 años en la universidad, mantuvimos la amistad y, gracias a que pensaste en mi cuando buscaban a alguien para entrar a trabajar en el LIM, acabe compartiendo otra etapa más contigo. Y aunque en tu caso decidiste no hacer doctorado y te fuiste a Barcelona, el equipo navegación empezó contigo. Gracias por ser tan buena amiga siempre, dispuesta a escuchar y ayudar. Eres una persona digna de admiración por tu afán de superación, tu positividad, tu iniciativa, tu generosidad, tu alegría, tu espontaneidad, tu sabiduría y tu seriedad cuando hace falta. Gracias por estar ahí después de todos estos años y ojalá podamos compartir más etapas juntas.

A mis padres, **Paloma** y **Fernando**, porque gracias a ellos conozco desde pequeña el mundo de la investigación y la pasión que se puede tener por tu trabajo. Porque me han apoyado siempre con todas las decisiones que he tomado en mi vida y por el cariño y confianza que me dan siempre. Y porque cuando tenía dudas de si hacer o no doctorado porque sentía que no valía, fueron los primeros en convencerme de que sí y me animaron a hacerlo. A mi hermano, **Antonio**, por contagiarme el interés en la tecnología desde pequeñita, por esas horas jugando a la Nintendo y pasándonoslo tan bien. Por su paciencia explicándome programación en primero de carrera, por exigirme y por compartir esa locura y bromas internas con las que solo nosotros nos reímos.

A la gente del LIM, porque hicieron de mi primera experiencia laboral la mejor. A **Eu** por su generosidad y a **Vero** por su paciencia infinita. A **Mariete,** por las risas, los escapes y por ese pedazo Cluedo que montamos juntos. A **Bego,** por su amabilidad, su iniciativa y su apoyo incondicional. A **Alvarito** y **Cristóbal,** por las risas continuas. A **María de la Jara,** por compartir conmigo esa comida en mi primer día. Y a **Clau**, **Inés**, **Alba**, **María**, **Nerea**, **Anita**, **Joaquín**, **Nico**, **Marina** y **Ana** por esas comidas y salidas con la gente del LIM. A la gente de la uni, por ser parte de esa segunda etapa laboral, donde ya empecé el doctorado. A **Estíbaliz**, por su cercanía y amabilidad y por esas charlas y clases que dimos juntas. A **Asier,** por esas clases de alemán que compartimos. A **Blanca**, **Dani, Laura, David**, **Pedro**, **Rigo**, **Patricio** y **Roberto** por formar parte del grupo Juarrates y compartir tantas comidas y reuniones. Y a **Alicia**, **Laura** y **Lucía** por ser tan buenas alumnas y, junto con **Alba**, formar parte de una nueva generación IGT muy prometedora.

A mi querida **Maite**, por acompañarme en esos meses en los que Deivid y Rafa estuvieron fuera. Fuiste como una hermana para mí y el apoyo que necesitaba para preparar esos experimentos y cirugías en tiempo récord. Al final, esos meses fueron clave en mi doctorado y

los resultados que conseguimos han dado lugar a lo que es ahora mi tesis. Fueron meses estresantes, pero a la vez muy divertidos, y eso fue gracias a ti. A **Manu**, porque también compartiste conmigo esos meses y juntos nos reímos un montón y formamos un buen equipo.

A los médicos del Gregorio Marañón con los que hemos colaborado, por su interés en la ciencia y por estar siempre dispuestos a probar cosas nuevas y confiar en nosotros. Al equipo de Cirugía Ortopédica y Traumatología, por ser los primeros en apostar por las nuevas tecnologías y por permitirme hacer investigación en este campo. A **José,** por su paciencia y por estar siempre dispuesto a colaborar. A **Lydia,** por ese experimento con cadáveres y esos papers que compartimos. A **Rubén,** por saber dar la cara ante las cámaras y por sus ideas innovadoras. Al equipo de Cirugía Oral y Maxilofacial, por dejarnos probar tantas cosas nuevas, por ponérnoslo tan fácil y por permitirnos ganar experiencia dentro del quirófano. A **Santiago**, por la pasión que siente por su trabajo, su cercanía y su afán de mejorar, y al resto del equipo por facilitarnos siempre las cosas en el quirófano. También quiero agradecer a **Juan de León** la confianza que puso en mi para trabajar con él desarrollando un sistema de entrenamiento para parto. Aunque finalmente no ha podido entrar en mi tesis, es el proyecto por el que he sentido más pasión y con el cuál he aprendido más y he ganado confianza en mí misma. Gracias por estar siempre dispuesto a colaborar y a explicarme los procedimientos, ha sido un placer trabajar contigo y espero que podamos seguir colaborando en el futuro.

A mis amigos de Baltimore, que hicieron de mi estancia allí una experiencia increíble. A **Sisni,** por acogerme, por contar conmigo para los planes y por hacerme sentir a gusto allí desde el principio. A **Esther**, por su generosidad, su cercanía y por ser tan divertida. A **Andrés** por nuestros planes y por formar parte del team Charles Village People. Al resto del grupo, **Juanan**, **Christy**, **Alex**, **Eliza**, **Martín**, **Ondra**, **Fran**, **Laure**, **Michael**, **Vicente**, **Spencer**, **Felipe** y **Christian** por ser tan majos siempre. Y a mi supervisor de la estancia, **Anand**, por acogerme y permitirme aprender y trabajar en un proyecto suyo con el da Vinci.

A mis amigas de toda la vida, por estar siempre ahí a pesar del tiempo y la distancia, que parece inexistente cada vez que nos volvemos a juntar. A mi consejo de sabias. A **Moni**, por su amistad, su generosidad y su sinceridad. A **Pau**, por su cariño, su fuerza de voluntad y su iniciativa. A **Yui**, por su lealtad y su genialidad, y por acceder a diseñarme la portada de esta tesis. A **Estefi** por las risas y por ser tan divertida siempre. Y a **Carol**, por la amistad, el cariño, por nuestras in-jokes y por las risas y confidencias que compartimos siempre que nos vemos.

A **Javi**, **Natalia**, **Esteban** e **Iván**, mis amigos del máster, por su amistad, su lealtad y cariño, por la etapa que pasamos juntos y por las risas aseguradas cada vez que nos vemos. A los

de la uni, **Alex**, **Álvaro**, **Jorge**, **Lavín**, **Manu**, **Yaiza** y **Pili** por las experiencias que vivimos juntos y porque cuando nos vemos siento que no ha pasado el tiempo. A los Beers Cheers (**Patri**, **Bruno**, **Nuri**, **Calvo**, **Luis**, **Chari** y **Víctor**) por las risas y esas tardes jugando a juegos de mesa. Y a mi **familia canaria**, por incluirnos en seguida en el grupo, por los planes constantes y por hacernos sentir a gusto a David y a mi desde que llegamos a la isla.

Y por último a mi familia por estar siempre ahí. A mi **Jori** por su cariño, por su iniciativa y por esas comilonas y recetas que siempre está dispuesta a compartir. A mis primos **Óscar** y **David** por las risas, y a **Marijose** por esas partidas al "conti" interminables. A mis primas y primo, **los Sevilla**, por tantos años compartidos durante la infancia, adolescencia y juventud. A mis abuelos, **Charo**, **Lola**, **Fernando** y **Antonio**, y a mis tíos, **Toñi**, **José**, **Cuca**, **Marisa**, **Juanjo**, **Isabel** y **Jesús**. Y a mi nueva familia, **Mar**, **Javi** y **Pau**, por vuestro cariño, porque me hacéis sentir como en casa y porque siempre me lo paso genial con vosotros. Gracias a todos, sin vosotros esta experiencia no hubiera sido la misma.

PUBLISHED AND SUBMITTED CONTENT

Journal Articles:

[1] **M. García-Sevilla**, L. Mediavilla-Santos, M. T. Ruiz-Alba, R. Pérez-Mañanes, J. A. Calvo-Haro, J. Pascau. Patient-specific desktop 3D-printed guides for pelvic tumour resection surgery: a precision study on cadavers. *Int J CARS* (2021) https://doi.org/10.1007/s11548-021-02322-3 [Impact factor: 2.924; Q2]

Author contributions: Mónica García Sevilla was responsible for data acquisition, data analysis, and writing the paper. All authors were responsible for conceptualizing the framework, writing, editing, and reviewing the paper.

Contribution completely included in chapter 3. Figures from this paper have been reprinted with permission from the copyright holder, Springer Nature.

[2] **M. García-Sevilla**, L. Mediavilla-Santos, R. Moreta-Martinez, D. García-Mato, R. Pérez-Mañanes, J. A. Calvo-Haro, J. Pascau. Combining Surgical Navigation and 3D Printing for Less Invasive Pelvic Tumor Resections. *IEEE Access* (2021) https://doi.org/10.1109/ACCESS.2021.3115984 [Impact factor: 3.367; Q2]

Author contributions: Mónica García Sevilla was responsible for software development, data acquisition, data analysis, and writing the paper. All authors were responsible for conceptualizing the framework, writing, editing, and reviewing the paper.

Contribution completely included in chapter 4.

[3] **M. García-Sevilla**, R. Moreta-Martinez, D. García-Mato, A. Pose-Diez-de-la-Lastra, R. Pérez-Mañanes, J. A. Calvo-Haro and J. Pascau. Augmented reality as a tool to guide PSI placement in pelvic tumor resections. *Sensors* (2021) https://doi.org/10.3390/s21237824 [Impact factor: 3.576; Q1]

Author contributions: Mónica García Sevilla was responsible for software development, data acquisition, data analysis, and writing the paper. All authors were responsible for conceptualizing the framework, writing, editing, and reviewing the paper.

Contribution completely included in chapter 5.

[4] **M. García-Sevilla**, R. Moreta-Martinez, D. García-Mato, G. Arenas de Frutos, S. Ochandiano, C. Navarro-Cuéllar, G. Sanjuán de Moreta, J. Pascau. Surgical Navigation,

Augmented Reality, and 3D Printing for Hard Palate Adenoid Cystic Carcinoma En-Bloc Resection: Case Report and Literature Review. *Frontiers in Oncology* (2022) https://doi.org/10.3389/fonc.2021.741191 [Impact factor: 6.244; Q2]

Author contributions: Mónica García Sevilla was responsible for software development, data acquisition, data analysis, and writing the paper. All authors were responsible for conceptualizing the framework, writing, editing, and reviewing the paper.

Contribution completely included in chapter 6.

[5] L. Mediavilla-Santos, **M. García-Sevilla**, J. A. Calvo-Haro, M. T. Ruiz-Alba, R. Pérez-Mañanes, J. Pascau, M. Cuervo-Dehesa, F. J. Vaquero Martín. Validación de los modelos de impresión 3D paciente-específicos para cirugía ortopédica oncológica pélvica. *Revista Española de Cirugía Ortopédica y Traumatología* (2021) https://doi.org/10.1016/j.recot.2021.07.001

Author contributions: Mónica García Sevilla was responsible for software development, data acquisition, and data analysis. All authors were responsible for conceptualizing the framework, writing, editing, and reviewing the paper.

Contribution partially included in chapters 3 and 4.

Conference Proceedings:

[1] **M. García-Sevilla**, D. García-Mato, J. Calvo-Haro, R. Pérez-Mañanes, J. Pascau. Optimizing navigation with patient-specific 3D printed guides in pelvic tumor resection surgery. *In: CARS 2019 - Computer Assisted Radiology and Surgery Proceedings of the 33rd International Congress and Exhibition, Rennes, France, June 18–21, 2019. Int J CARS 14, 1–194* (2019) https://doi.org/10.1007/s11548-019-01969-3

Author contributions: Mónica García Sevilla was responsible for software development, data acquisition, data analysis, and writing the paper. All authors were responsible for conceptualizing the framework, writing, editing, and reviewing the paper.

Contribution partially included in chapter 4.

[2] **M. García-Sevilla**, D. García-Mato, R. Moreta-Martinez, S. Ochandiano, M. Tousidonis, C. Navarro-Cuéllar, J. Pascau. Surgical navigation for palate carcinoma resection using a non-invasive 3D-printed reference frame. *In: CARS 2020 - Computer Assisted Radiology and Surgery Proceedings of the 34th International Congress and Exhibition,*

Munich, Germany, June 23–27, 2020. Int J CARS 15, 1–214 (2020) https://doi.org/10.1007/s11548-020-02171-6

Author contributions: Mónica García Sevilla was responsible for software development, data acquisition, data analysis, and writing the paper. All authors were responsible for conceptualizing the framework, writing, editing, and reviewing the paper.

Contribution partially included in chapter 6.

[3] **M. García-Sevilla**, R. Moreta-Martinez, D. García-Mato, A. Pose-Díez-de-la-Lastra, R. Pérez-Mañanes, J. Calvo-Haro, J. Pascau. Augmented reality for improved PSI placement in pelvic tumour resections. *In: CARS 2021: Computer Assisted Radiology and Surgery Proceedings of the 35th International Congress and Exhibition Munich, Germany, June 21-25, 2021. Int J CARS 16, 1-119* (2021) https://doi.org/10.1007/s11548-021-02375-4

Author contributions: Mónica García Sevilla was responsible for software development, data acquisition, data analysis, and writing the paper. All authors were responsible for conceptualizing the framework, writing, editing, and reviewing the paper.

Contribution partially included in chapter 5.

The material from these sources included in this thesis are not singled out with typographic means and references.

TABLE OF CONTENTS

ABSTRACT

The role of technology inside the operating room is constantly increasing, allowing surgical procedures previously considered impossible or too risky due to their complexity or limited access. These reliable tools have improved surgical efficiency and safety. Cancer treatment is one of the surgical specialties that has benefited most from these techniques due to its high incidence and the accuracy required for tumor resections with conservative approaches and clear margins.

However, in many cases, introducing these technologies into surgical scenarios is expensive and entails complex setups that are obtrusive, invasive, and increase the operative time. In this thesis, we proposed convenient, accessible, reliable, and non-invasive solutions for two highly complex regions for tumor resection surgeries: pelvis and head and neck. We explored how the introduction of 3D printing, surgical navigation, and augmented reality in these scenarios provided high intraoperative precision.

First, we presented a less invasive setup for osteotomy guidance in pelvic tumor resections based on small patient-specific instruments (PSIs) fabricated with a desktop 3D printer at a low cost. We evaluated their accuracy in a cadaveric study, following a realistic workflow, and obtained similar results to previous studies with more invasive setups. We also identified the ilium as the region more prone to errors.

Then, we proposed surgical navigation using these small PSIs for image-to-patient registration. Artificial landmarks included in the PSIs substitute the anatomical landmarks and the bone surface commonly used for this step, which require additional bone exposure and is, therefore, more invasive. We also presented an alternative and more convenient installation of the dynamic reference frame used to track the patient movements in surgical navigation. The reference frame is inserted in a socket included in the PSIs and can be attached and detached without losing precision and simplifying the installation. We validated the setup in a cadaveric study, evaluating the accuracy and finding the optimal PSI configuration in the three most common scenarios for pelvic tumor resection. The results demonstrated high accuracy, where the main source of error was again incorrect placements of PSIs in regular and homogeneous regions such as the ilium.

The main limitation of PSIs is the guidance error resulting from incorrect placements. To overcome this issue, we proposed augmented reality as a tool to guide PSI installation in

the patient's bone. We developed an application for smartphones and HoloLens 2 that displays the correct position intraoperatively. We measured the placement errors in a conventional and a realistic phantom, including a silicone layer to simulate tissue. The results demonstrated a significant reduction of errors with augmented reality compared to freehand placement, ensuring an installation of the PSI close to the target area.

Finally, we proposed three setups for surgical navigation in palate tumor resections, using optical trackers and augmented reality. The tracking tools for the patient and surgical instruments were fabricated with low-cost desktop 3D printers and designed to provide less invasive setups compared to previous solutions. All setups presented similar results with high accuracy when tested in a 3D-printed patient-specific phantom. They were then validated in the real surgical case, and one of the solutions was applied for intraoperative guidance. Postoperative results demonstrated high navigation accuracy, obtaining optimal surgical outcomes. The proposed solution enabled a conservative surgical approach with a less invasive navigation setup.

To conclude, in this thesis we have proposed new setups for intraoperative navigation in two complex surgical scenarios for tumor resection. We analyzed their navigation precision, defining the optimal configurations to ensure accuracy. With this, we have demonstrated that computer-assisted surgery techniques can be integrated into the surgical workflow with accessible and non-invasive setups. These results are a step further towards optimizing the procedures and continue improving surgical outcomes in complex surgical scenarios.

LIST OF FIGURES

LIST OF TABLES

LIST OF ABBREVIATIONS AND ACRONYMS

ACC: Adenoid Cystic Carcinoma

AR: Augmented Reality

BSD: Berkley Software Distribution

CAD: Computer-Aided Designs

CAM: Computer-Aided Manufacturing

CAS: Computer-Assisted Surgery

CNC: Computer Numerically Controlled

CT: Computed Tomography

DIC: Digital Image Correlation

FDM: Fused Deposition Modelling

FFF: Fused Filament Fabrication

GPS: Global Positioning System

HDI: Human Development Index

HMD: Head Mounted Display

IGT: Image-Guided Therapy

IQR: Interquartile Range

IR: Infrared

LED: Light-Emitting Diode

MOD: Maximum Osteotomy Deviation

MOL: Mean Osteotomy Length

MRI: Magnetic Resonance Imaging

OTS: Optical Tracking System

PET: Positron Emission Tomography

PLA: Polylactic Acid

PSI: Patient-Specific Instrument

RAS: Right Anterior Superior

RF: Reference Frame

RGB: Red Green Blue

RP: Rapid Prototyping

SD: Standard Deviation

SLA: Stereolithography

SLS: Selective Laser Sintering

VSP: Virtual Surgical Planning

2D: Two-Dimensional

3D: Three-Dimensional

3DP: 3D Printing

1

INTRODUCTION

1.1. Surgical oncology

1.1.1. Cancer

Throughout our lives, our body cells grow, multiply (by division) and die in an orderly and controlled manner. However, sometimes the genes managing cells' function suffer changes modifying how they grow or multiply [1]. These alterations can be caused by external agents such as chemicals (tobacco smoke, arsenic, aflatoxin, etc.), harmful substances (alcohol), infections (human papillomavirus, hepatitis B or C, etc.), ultraviolet and ionizing radiation, or they can be inherited [2]. Unhealthy dietary habits are also one of the main risk factors for developing cancer. Usually, our body detects these damaged cells and eliminates them, but this ability decreases with age [3]. When this occurs, the damaged cells divide uncontrollably, generally forming a mass. This abnormal mass is known as tumor or neoplasm.

Tumors can appear in our body without posing any threat or spreading to create new tumors. When presenting this behavior, they are classified as benign or non-cancerous [4], [5], being usually not problematic. However, they can grow and generate discomfort or become dangerous if they press vital structures such as nerves or blood vessels. On the other hand, if the damaged cells invade the surrounding tissues, drawing nutrients and interfering with body functions, they are considered malignant or cancerous. These cells can spread to other organs traveling through the blood, generating new tumors in other parts of the body. This process is called metastasis and is the leading cause of death from cancer [6], [7].

Cancer can arise from almost any part of our body. The type of cancer is usually classified according to the organ or tissue from where it originated (lung, breast, brain) or by the type of cell that formed it [8]. The main types are carcinoma, melanoma, sarcoma, lymphoma, and leukemia [9]. Carcinomas are the most common, originating in the organs and glands. They are composed of epithelial cells located on the skin or the tissues lining organs (liver or kidneys). There are several subtypes of carcinomas, including adenocarcinomas which occur in the glandular tissues that produce fluids or mucus. Melanomas are also quite common and represent the most dangerous type of skin cancer, formed in the cells giving pigment to the skin. On the other hand, sarcomas are less common. They develop in mesenchymal cells and appear in soft or connective tissues, including muscle, fat, bone, blood vessels, and cartilage. Cancer can also occur without forming a tumor. This is the case of blood cancers such as leukemia. It arises from the bone marrow, generating an excessive production of white blood cells. It is the most common childhood cancer. Lastly, lymphoma is another type of blood cancer affecting the lymphocytes, the cells from the immune system in charge of fighting infections.

1.1.2. Incidence and social impact

In 2020, nearly 20 million people were diagnosed with cancer (**Figure 1.1**), and almost 10 million died from it [10] (**Figure 1.2**). It represents the second leading cause of death in the world. The most common cancers in 2020 were female breast cancer (2.6 million cases), lung cancer (2.21), and prostate cancer (1.41), and those with the highest mortality rates were lung (1.79 million), liver (830000), and stomach (769000).

Cancer could be prevented in 30 to 50% of the cases by avoiding tobacco or alcohol use, having healthy diets, or reducing air pollution. Infections are also one of the main causes of cancer, especially in low- and middle-income countries [11], and only about 5% of cancer cases are caused by inherited genetic mutations [12]. Cancer creates a physical, emotional, and financial impact on individuals and their families and is a significant burden to communities and health care systems [13]. Additionally, limitations in heath access affect cancer diagnosis, treatment, and survival in developing countries [14]. Approximately 70% of deaths caused by cancer occur in these regions due to the high inequalities between countries with a high Human Development Index (HDI) and those with a lower one (**Figure 1.3**). Hence, it is necessary to strengthen health systems by finding cost-effective strategies and sustainable solutions for cancer prevention and treatment.

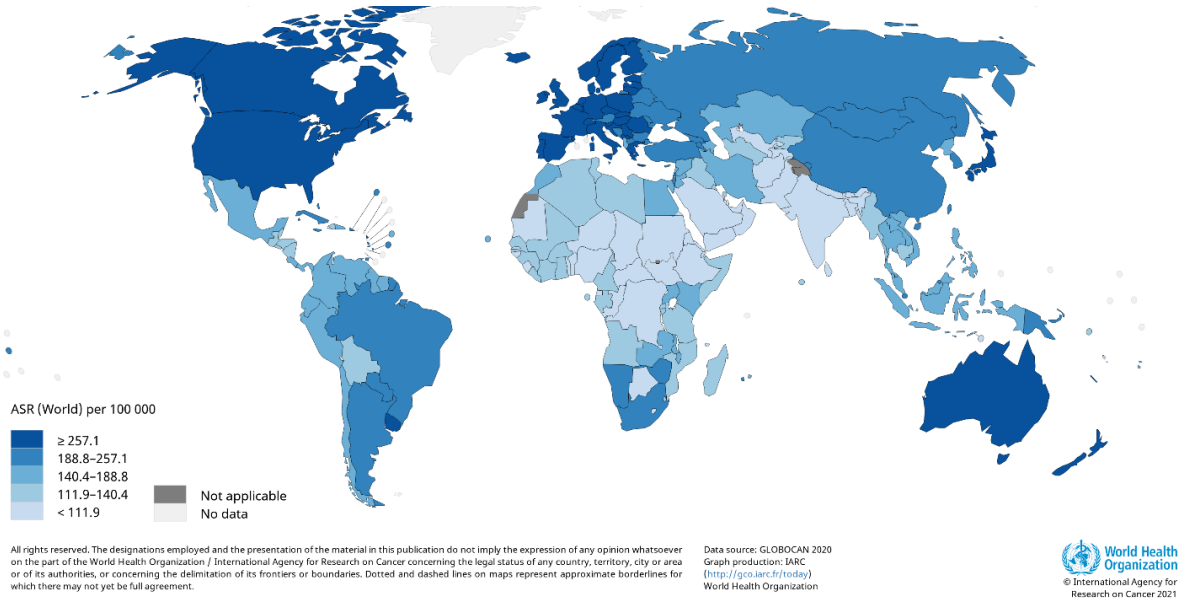

Figure 1.1. World cancer incidence rates. Source: © International Agency for Research on Cancer (IARC) http://gco.iarc.fr/today.

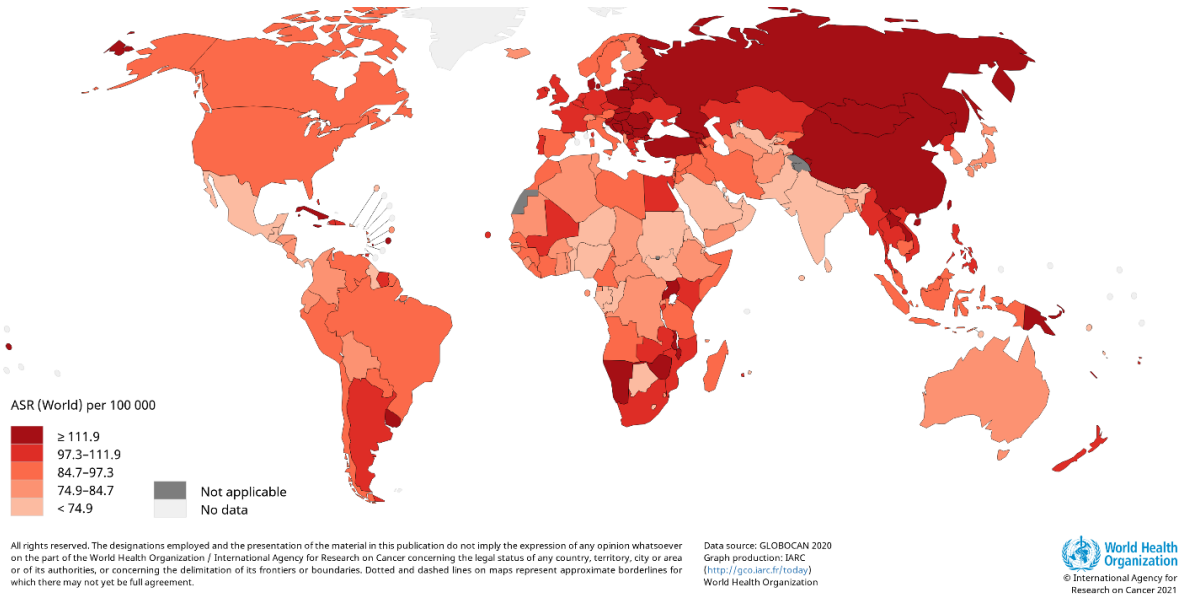

Figure 1.2. World cancer mortality rates. Source: © IARC http://gco.iarc.fr/today.

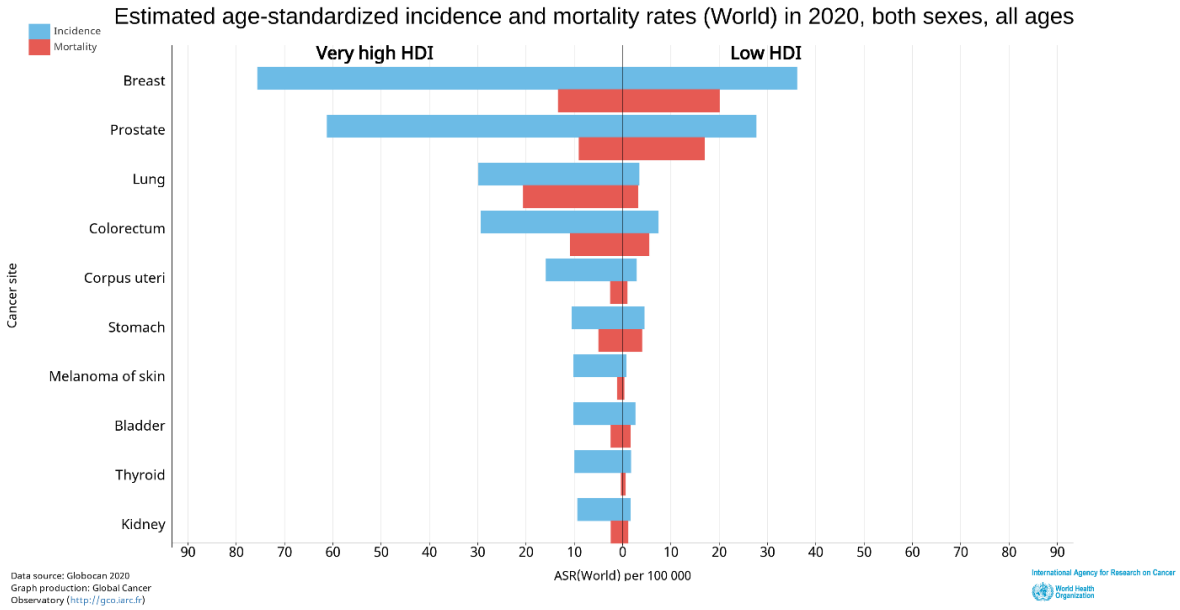

Figure 1.3. World cancer incidence and mortality rates. Comparison between very high Human Development Index (HDI) and low HDI countries. Source: © IARC http://gco.iarc.fr/today.

1.1.3. Screening and diagnosis

Oncology is the branch of medicine that studies cancer and deals with its diagnosis, treatment, and prevention. In the last century, significant advances have been accomplished in this field to gain a deeper understanding of cancer and better diagnose, prevent, and treat it [8]. Until the late 20th century, cancer diagnosis required exploratory surgery to obtain and analyze samples of the affected tissue. However, at the beginning of the 1970s, the advent of new medical imaging techniques such as ultrasounds, computed tomography (CT), magnetic resonance imaging (MRI), and positron emission tomography (PET) enabled diagnosis without surgery [15], [16].

Medical imaging allows clinicians to see the interior of a body through images even before a patient presents symptoms. This process is called screening, and it helps to identify abnormalities that can be indicative of cancer [16]. When this occurs, further tests can then be performed to diagnose and establish adequate treatment if needed. Screening tests can go from imaging procedures to physical exams (e.g., checking for lumps) or laboratory tests (analysis of tissues or blood samples extracted through medical procedures). Cancer risk factors such as age, personal and family history, or bad habits such as smoking are usually considered before and after screening.

Screening has become a routine procedure to prevent more extended diseases such as breast or colon cancer. As cancer presents a better response at initial stages, early detection is a key factor for effective treatment, increasing the probability of survival [14].

1.1.4. Surgical treatment

Once cancer is detected, there are different options for treatment depending on the type, location, and stage. These options include surgery, radiotherapy, chemotherapy, or a combination [8], [14]. The primary purpose of treatment is to cure cancer or prolong a patient's life, but it can also focus on improving the patient's quality of life.

Among the options for cancer treatment, surgery represents the oldest one. It is applied at different cancer stages and for various purposes, including diagnosis, prevention, primary treatment, debulking, reconstruction, or palliative care [17], [18].

When a patient presents symptoms or abnormalities, surgery can be used for diagnosis. Usually, a portion or all the suspicious tissue is removed through surgery for examination under a microscope. This process of obtaining tissue samples is called a biopsy, and it is commonly performed with needles or through small incisions. A pathologist analyzes the extracted tissue to determine whether cancerous cells are present and reports the results to the oncologist who performs the diagnosis. The lymph nodes can also be removed through an intervention to determine the cancer stage and detect if it has spread to other organs or parts of the body. Therefore, it can be used to predict the patient's chance of recovery (prognosis).

Surgery can also be used for prevention. Some non-cancerous lumps, polyps, or abnormal tissues can eventually turn malignant. This scenario is common in colon, breast, and ovarian cancer. Surgeons may recommend in these cases to remove them as a preventive measure. Also, complete removal of the area at risk can be performed in patients with a high predisposition to cancer due to family history.

When a cancerous tumor is confirmed and localized, the most common treatment is tumor removal through surgery. It is also called primary treatment and is the best chance for cure in most cases. In these interventions, surgeons remove the tumor along with nearby tissue that may also be affected. This extra tissue is called surgical or resection margin, and it is examined after surgery to ensure it is clear of cancer cells. It is defined as a negative

margin if no cancer cells are found in the outer edge of the removed tissue. If cancerous cells are found in the outer rim, additional surgery may be necessary.

Sometimes the tumor is located close to delicate structures, and the complete removal may pose a high risk. In these scenarios, debulking is commonly performed, where only a portion of the tumor is removed. These interventions are frequently complemented with other treatments such as chemotherapy or radiotherapy, applied before surgery, intraoperatively, or after surgery to help reduce the tumor size or remove the remaining cancer cells.

After the tumor removal, the patient's appearance or function might be considerably affected, requiring reconstructive surgery during the tumor removal intervention or afterward. In breast cancer, reconstructive surgery can restore the physical shape of the breast. It is also common in maxillofacial surgery, where soft tissue or bone segments from other anatomical regions are used to replace the removed sections that contained or were near the tumor.

When an individual presents an advanced cancer stage where the disease has already spread to other body parts, surgery can also improve the patient's quality of life. A tumor can cause pain to the patient and affect physical function, either because it induces pressure to a nerve or organ or because it blocks the bowel or the intestines. The tumor can therefore be removed through surgery even if it will not cure cancer. An intervention can also stop the bleeding of delicate organs affected by cancer. The most common treatment in these cases involves applying a ligature to the blood vessel or affected structure.

1.2. Computer-assisted surgery (CAS)

Cancer treatment has improved significantly in the last century, reducing incidence and mortality thanks to advances in prevention and treatment. However, for centuries cancer was thought to be incurable. The ancients believed that once it had spread, there was no cure, and surgical treatment would only do more harm [19]. Surgery at that time was very primitive, with a great risk of infection and complications derived from high blood loss.

Surgical procedures did not improve until the late 19th century, driven primarily by the discovery of anesthesia [1]. Surgeons such as Bilroth, Handley and Halsted began to perform surgeries in which they completely removed the tumor as well as lymph nodes near the affected area. Halsted introduced radical mastectomy in breast cancer surgery, where the whole breast, chest muscles, and proximal lymph nodes are removed [20]. He thought that

cancer spread from the tumor to the neighboring structures and that en bloc resections (complete removal) of the tumor and surrounding tissues would eliminate the disease.

Over time it was learned that cancer can spread through the bloodstream, and that surgery often needs to be complemented with systemic treatments before or after the intervention to destroy the spread cells. At the end of the 20th century, chemotherapy and radiotherapy were introduced, contributing to less invasive surgeries by reducing the amount of unaffected tissue removed during surgery [1]. Dr. Bernard Fisher demonstrated that less extensive surgeries supplemented with chemotherapy, radiotherapy, or both are equally or more effective than en bloc resections and reduce morbidity [21]–[24].

The introduction in the 1970s of new medical imaging modalities (CT, MRI, PET or ultrasounds) also significantly impacted the field, allowing the inspection of the disease without the need for exploratory surgery [15]. These techniques could also be exploited for biopsy guidance or to improve radiation therapy by enabling targeted beam energy delivery, sparing the unaffected tissue [1].

In recent years, advances in computing and image processing have allowed the development of new technologies introduced in the surgical workflow to reduce the risks, improve precision and enhance the surgeons' confidence [25], [26]. They can be used preoperatively to plan surgery, during the surgical procedure for guidance and to better identify anatomical structures, or after surgery to assess the intervention [27]. The integration of these technologies in surgical procedures is known as computer-assisted surgery (CAS).

1.2.1. Virtual surgical planning

Surgical planning is the process through which the patient images are visualized prior to surgery to predefine the surgical steps [28]. The different existing imaging modalities, such as CT and MRI, can be used for this purpose. However, CT is preferred due to its volumetric data [29]. Although MRI scans also provide 3D visualization of the anatomical structures, they are known to present volumetric deformations, which can lead to inaccuracies in surgical planning. However, data fusion techniques can combine CT and MRI scans to provide additional information during planning.

Before the introduction of CT images, preoperative images such as X-rays, angiograms, or ultrasounds were recorded and displayed on photographic films to understand the internal patient's anatomy [30]. Nevertheless, these conventional images did not show the

deepness of structures as they reduced 3D objects to a single two-dimensional (2D) view. With the invention of CT in 1971 by Godfrey Hounsfield, the structures inside the body could be captured into images in consecutive slices [31]. The acquired data was intrinsically represented as numbers and converted to images by assigning different gray levels. A decade later, in the 1980s, Vannier et al. [32] performed the first three-dimensional (3D) reconstruction from the CT sectional images.

Nowadays, 3D CT can be acquired faster. From this data, anatomical structures are represented in 2D displays with different shades of gray, allowing a visual interpretation and distinction of hard and soft tissues [33]. This visualization can be improved for each application by modifying image display settings such as window level and width, which is not possible in conventional analog images. Volume rendering displays the image volumes as 3D objects applying opacity and color tables [34]. 3D virtual models of the patient's anatomy can also be generated by image segmentation. This step consists of dividing the image into regions or segments with similar properties such as gray level [35]. These segments can represent anatomical regions such as the skull, mandible, skin, brain, nerves, or other soft- or hard-tissue structures [36].

The generation of these 3D models and their visualization from different angles and depths improves the understanding of the patient's anatomy and facilitates surgical planning [32]. The 3D models can be fragmented to simulate osteotomies (bone cuts) performed during an intervention, repositioned or moved with 6 degrees of freedom, or manipulated in some other way to make treatment decisions [36]. These functionalities translate into a customized treatment adapted to the specific surgical case.

The first software applications for neurosurgery virtual surgical planning (VSP) appeared in the 1990s. These were the StealthStation [37] developed by Medtronic and VectorVision [38] by Brainlab. In the late 1990s, a full computer-based software for planning osteotomies in orthopedic surgery and traumatology was introduced [39]. More recently, some surgical planning systems started to incorporate virtual or augmented reality technology to improve the visualization and facilitate the manipulation of the 3D data. In the 2000s, the surgical planning system VIVIAN (Virtual Intracranial Visualization and Navigation) was developed for neurosurgical interventions for its use in Dextroscope, a virtual reality environment [40]. There are currently many software alternatives available (3DSystems, Invivo5, OsiriX MD, 3D Slicer, Materialise Mimics Care Suite), some specialized in specific

treatments. Companies such as Stryker offer different software applications depending on the surgical procedure, including VSP© Cranial, VSP© Orthognatics, or VSP© Reconstruction. Apart from neurosurgery, VSP is mainly used for oral and maxillofacial surgery, especially for orthognathic and reconstructive surgery, where it becomes a valuable tool to plan the cuts and ensure facial symmetry [36], [41], [42] (**Figure 1.4**). However, more procedures are incorporating these solutions in their surgical workflow, as they have demonstrated several potential benefits, including reducing operative time and gaining control of the final surgical outcome [41] with no associated increase in complications [43], [44].

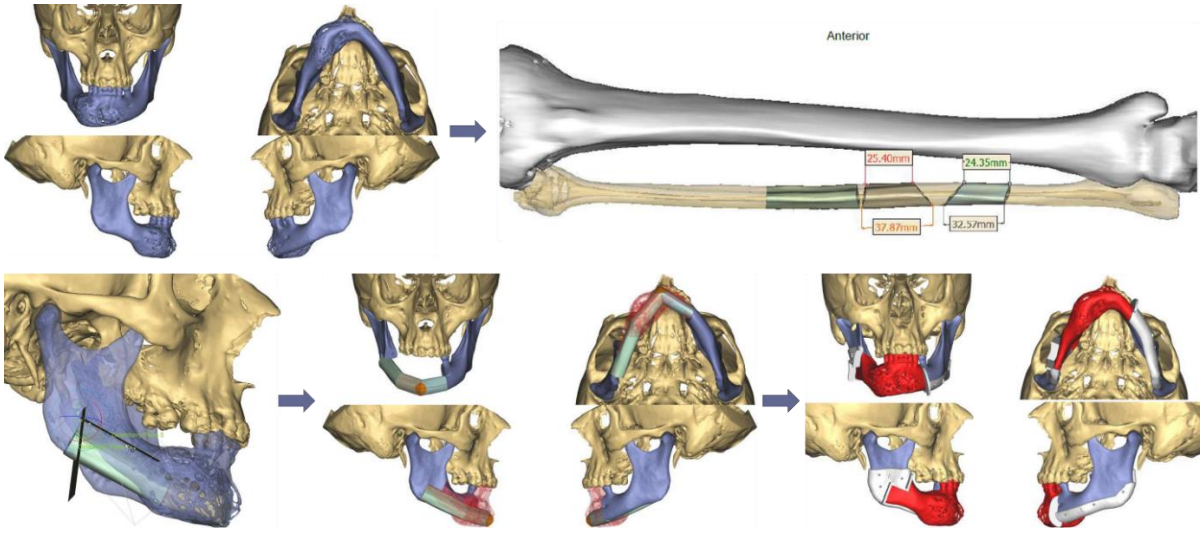

Figure 1.4. Example of virtual surgical planning applied to mandibular reconstruction surgery (figure reprinted with permission of the copyright holder, Springer Nature) [45].

Once preoperative planning has concluded, it can be transferred to the operating room to replicate the simulation precisely. Several tools are available to perform this translation, including 3D-printed guides or implants fabricated through computer-aided design and manufacturing (CAD/CAM), surgical navigation with conventional tracking systems, or navigation based on augmented reality technology.

1.2.2. CAD/CAM

Rapid prototyping (RP) refers to building a model layer by layer starting from the bottom by depositing material in precise shapes [46]. This technique is called additive manufacturing, also known as 3D printing. This method was initially introduced in the industry in the 1980s to rapidly translate the precision of computer-assisted designs (CAD) to final products (CAM) [47]. It was soon adopted by aircraft and automobile industries for fast

production of prototype parts, from where RP gets its name. This technology allows optimizing the design and production of customized models fabricated on demand [48].

Additive manufacturing can be achieved following different processes. The three most extended methods are stereolithography (SLA), selective laser sintering (SLS), and fused deposition modeling (FDM) [49]. SLA works by curing a liquid photopolymer (a photosensitive resin), converting it from liquid to solid layer by layer using a high-powered ultraviolet laser beam. It was invented by the co-founder and chief technology officer of 3D Systems, Charles W Hull, in 1981 [50]. SLS technology uses a laser to sinter powdered material (commonly polyamide or nylon) instead of liquid. This way, the material is bonded together, creating a solid part. This technology was presented in 1986 by Carl Deckard at the University of Texas [51]. FDM, also called fused filament fabrication (FFF), instead of using light to solidify the material, extrudes it through a heated nozzle that melts it. The fed filament pushes the melted material, which is extruded in the build plate and quickly resolidifies. This procedure is the most extended among desktop 3D printers [49].

It was not until 1988 that the first commercial 3D printer (SLA-1) was made available, increasing access to this technology [52]. In the beginning, 3D printers were expensive and difficult to use, requiring much postprocessing of the printed objects. In the 1990s, many companies started exploring this technology [50]. The competition among them propelled innovation, refinement, and a reduction of prices. Open-source initiatives such as the RepRap Project in 2005 gave more access to this technology, while CAD tools also improved and became more available. The expiration of the FDM patent in 2009 became a turning point in the history of 3D printing, making it accessible to the general public [50]. Nowadays, many industries, including healthcare, use 3D printers in their production workflow. Cheaper versions, known as desktop 3D printers due to their reduced size, are available for commercial and consumer applications.

With the widespread of CAD/CAM technology and the availability of 3D medical images from CT and MRI scanners, the healthcare industry soon became interested in translating the anatomical models to 3D-printed objects [36]. Even before the advent of 3D printing, previous solutions such as computer numerically controlled (CNC) milling machines were used to create these replicas from solid blocks of Styrofoam or polyurethane, although the results presented stepped and non-precise surfaces [46]. In 1994, the first biomedical model was manufactured with an SLA 3D printer [53]. Orthopedics and oral and

maxillofacial surgery were the first medical specialties to introduce this technology, probably because only hard parts could be printed at the beginning. Nowadays, almost all surgical specialties use this technology [46].

The most common image modalities used in medical applications to generate 3D models are CT and MRI [46]. However, other alternatives such as Cone Beam CT, PET, and 3D laser or light scanning have also been used [54]–[56]. Data from multiple sources can also be combined to generate the final models [57]. The reconstructed 3D models are exported in a compatible file format (.stl, .obj) [58] and transferred to a printing software such as Cura (Ultimaker B.V., Netherlands) or ideaMaker (Raise3D Inc., Irvine, California, USA). Finally, a printing file (.gcode or .x3g) is sent to the printer with encoded instructions for its fabrication.

The anatomical models can be helpful in preoperative planning, surgical simulation, pre-surgical manipulation of surgical equipment (contouring and modeling), or education [46]. However, the use of 3D printing in medicine is not restricted to the creation of anatomical models (**Figure 1.5 a**). CAD/CAM can also be used to design patient-specific implants, prostheses, splints or external fixators [59]–[62] (**Figure 1.5**). It can also produce customized surgical guides and instruments [63]–[65]. The use of these tools is widely extended in orthopedic surgery for the creation of implants in the pelvis and acetabular cage [66], [67], fixation of tibial fractures [62], [68], and especially for surgical guidance [63], [69]–[73]. There are also multiple applications in cranio-maxillofacial surgery [61], [74]–[78]. Orthognathic surgery has highly benefited from the use of these techniques to improve accuracy and optimize the results [77], [79]–[81].

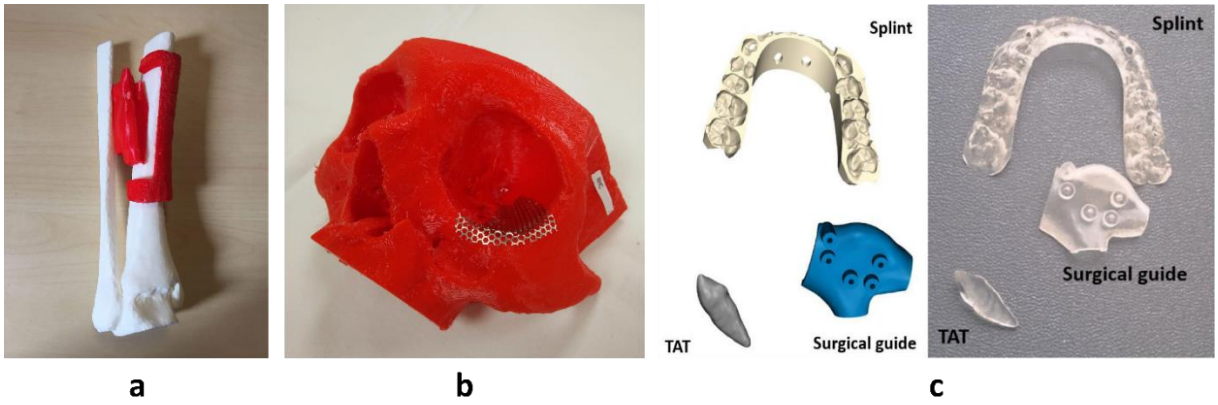

Figure 1.5. Examples of the use of 3D (three-dimensional) printing in medical applications: (**a**) biomodels, (**b**) modelling of surgical tools, (**c**) splints, surgical guides and tooth transplantation [82].

The cost of 3D printers has recently decreased thanks to the patent expirations [53]. Many companies offer 3D printing services, recommended if the printing volume is low, but the process can also be implemented in-house. Although prices range between $2,000 for the more basic printers to $900,000 for the most accurate, the associated cost of the printers is relatively low [83]. However, this also depends on the material used, where printing with metal is generally more expensive [65], [84]. Additionally, there is free, open-source software available [84], which can help in reducing the costs.

The time demanded from CAD/CAM highly depends on the task, although advancements in software and workflow automation are shortening the process. Also, preoperatively designing and printing surgical tools can reduce the operative time. A study concluded that a reduction of 10 minutes in the operating room is equivalent in cost to 1 hour dedicated to design and manufacture prior to surgery [85]. Beyond this, the benefits introduced by this technology, including the translation of the preoperative plan to the surgical field, with the consequent reduction of surgical time, anesthesia exposure or blood loss, and the improvement of surgical outcomes, are invaluable [72], [86], [87].

1.2.3. Surgical navigation

Surgical navigation, also known as image-guided surgery, allows the surgeon to display the position of the surgical instruments with respect to the patient's anatomy through virtual image overlays [30]. The surgeon can use these systems to localize and visualize the anatomical target with precision and decide the path to follow with the navigated instrument to reach the surgical site safely [88]. The position of the tracked instruments is projected onto the preoperative or intraoperative images. It can also be represented with respect to 3D rendered anatomical models, making visualization and guidance easier. This technology is often compared to a Global Positioning System (GPS), as it includes an element to be localized, which is the surgical instrument (GPS unit), a tracker to localize it (satellite), and an image over which the instrument's position is displayed (map) [89].

The navigation systems emerged to transform surgery into a safer and less invasive procedure. Not only do they indicate the surgical instruments' position, but they can also provide relevant information at the right time, such as measurements, distances to targets, or indicate the paths defined preoperatively during surgical planning, improving accuracy and surgical outcomes [88]. They open the way to minimally invasive procedures where only

small incisions are made to insert the instruments, and no direct line of sight with the target area and instrument's tip is maintained. They have also allowed the performance of more daring procedures, as less accessible structures can be reached.

The use of medical images to guide a surgical procedure came along almost simultaneously to Roetgen's discovery of X-rays in 1895. Soon after the first paper was published, a surgeon used an X-ray image to remove a sewing needle from a woman's hand [90]. A month later, it was used to remove a bullet from a patient's leg [91]. In 1905, Victor Horsley and R.H. Clarke introduced the first stereotactic frame, the basis for the first navigation systems [92]. They affixed a monkey's head to a frame and used external anatomical landmarks from the ears and eyes to define a Cartesian coordinates system. Navigation solutions based on stereotactic frames are still used today for some surgical procedures, mainly in neurosurgery. In fact, for almost a century, surgical navigation was confined to this field as the skull provides a rigid and stable frame compatible with this setup.

With the invention of CT scanners, the appearance of the first personal computer in 1981, and the improvements in computational power, neuronavigation increased, becoming the standard of care for certain procedures. With time, it expanded to other specialties such as trauma and orthopedic surgery. The first frameless stereotactic system was presented by Friets et al. in 1989 [93]. They used an ultrasonic rangefinder to localize the patient and an operating microscope where a single CT image was dynamically updated. Four years later, Galloway et al. presented a navigation system for neurosurgery based on an articulated arm with 6 degrees of freedom, where orthogonal views of the CT were displayed, enabling 3D navigation [94]. However, articulated arms can be intrusive, and soon other tracking alternatives were developed. Nowadays, the most common tracking devices are optical and electromagnetic tracking systems.

Optical trackers are composed of a camera and active or passive markers placed in the patient and surgical instruments to track their position (**Figure 1.6**). The passive markers are made of a material that reflects a near-infrared (IR) light emitted by the camera, while active markers include IR light-emitting diodes (LEDs). This technology presents high accuracy and a large working volume, being the preferred solution in most clinical applications [95]. However, they require a direct line of sight between the camera and the markers and are sensible to occlusions. An optical tracker widely extended for medical applications is the

Polaris® System (Northern Digital Inc., Waterloo, Canada). Other less expensive solutions are the OptiTrack V120:Duo or V120:Trio (Natural Point Inc., Corvallis, OR, US).

Figure 1.6. Surgeons using a passive optical tracking system for intraoperative guidance.

The electromagnetic tracking systems overcome some limitations of the optical trackers. They include a magnetic field generator (the transmitter) and sensors (solenoids) with three orthogonal coils on which the field induces a current [96]. The system measures the strength of the magnetic field at the location of the sensors to estimate their position. The greatest advantage of these systems is that they do not require a direct line of sight. Hence, they can be tracked inside a body cavity. Also, some sensors are designed with a reduced size and can be introduced in surgical instruments such as needles. However, one of the most significant limitations is that they are connected through cables that need to be covered to maintain the intervention area sterile. Also, they can suffer from artifacts introduced by ferromagnetic and conducting materials, affecting the measurements, and reducing the

accuracy. The most extended devices are Aurora and 3D Guidance TrakSTAR (Northern Digital Inc., Waterloo, Canada).

Surgical navigation systems require an alignment of the patient with the preoperative images so that the tracked instruments are represented in the correct location on the image. This process of aligning both coordinate systems is called registration. If the structures to register are rigid, a registration composed only of translations and rotations of the data sets can be performed. This procedure is called rigid registration. Non-rigid registration is required in surgeries involving deformable structures (such as the abdomen). However, in many cases, these registrations still lack robustness [97].

The most common method for registration of 3D data in surgical navigation is the paired point registration, where the same points are localized both in the patient and the preoperative image. These points can either be anatomical or fiducial landmarks [98]. The root-mean-square distance between the paired points measures the registration error. However, this does not necessarily reflect the errors in the target region [99], [100]. To ensure accuracy, it is essential to correctly choose the registration landmarks, using clearly defined points distributed surrounding the area of interest.

Surgical navigation is fully established in neurosurgery, where it has been adopted and incorporated successfully into clinical practice over the last two decades [88]. It guides biopsies, intracranial tumor resections and treatment of Parkinson's disease or epilepsy [101]–[103]. Because it is mainly performed on bones, orthopedic surgery is also an adequate setup for surgical navigation, improving pedicle screws placement [104], hip replacement [105], and tumor removal [106]. Surgical navigation is also gaining popularity in craniomaxillofacial surgery, enhancing accuracy in orthognathic [107] or craniofacial procedures [108]. It has also enabled safer surgery in head and neck cancer [109] when the tumor to be removed is located in deeper regions surrounded by delicate structures.

There are currently many navigation solutions available for specific clinical procedures. Companies such as Stryker (Freiburg, Germany) or Brainlab (Munich, Germany) have commercial navigation systems for neurosurgery (VectorVision from Brainlab [110]), spine (SpineMap® 3D from Stryker [111]), craniomaxillofacial (STN navigation system from Stryker [112]), or ENT (ear, nose, and throat) surgery (Scopis [113]).

There are also open-source platforms popular in the research community that allow sharing knowledge and reusing code, including software packages for implementing image-

guided surgery applications. The source code of these platforms is freely available and can be adapted to different applications. Some are under the Berkley Software Distribution (BSD) license, which allows users to develop software for any purpose without the need to share it, retaining their proprietary rights [114]. The most popular are Medical Imaging Interaction Toolkit (MITK) [115], Image-Guided Surgery Toolkit (IGSTK) [116], and 3D Slicer [117]. 3D Slicer is a free and open-source multi-platform from Brigham and Women's Hospital in Boston supported by a large community. It offers multiple functionalities useful in clinical and biomedical applications. The software comprises modules focused on different purposes, including medical image processing, visualization, segmentation, registration, or image-guided therapy (IGT). Developers can design customized modules to perform a specific task or work on a particular clinical case.

1.2.4. Augmented Reality (AR)

AR is the technology through which virtual (computer-generated) objects are overlayed on a user's view of the real world to enhance it [118]. These virtual objects appear to coexist in the same space as the elements from the physical world [119]. The projection of the virtual elements is usually achieved using cameras, displays, projectors, trackers, or special equipment [120].

The term "Augmented Reality" was defined for the first time in 1990 by T. Caudell and D. Mizell, researchers for Boeing working on a see-through display to help workers on the assembly of complicated parts for jetliners [121]. However, the idea emerged decades earlier, appearing for the first time in a novel written by L. F. Baum. It was not until 1968 that Ivan Sutherland, a computer science professor from Harvard, created the first prototype of an AR system consisting of a head-mounted display (HMD) [122]. The first developments appeared in the military sector [118] but soon translated to gaming and entertainment [123], and have grown remarkably since then. These days, the use of AR systems is becoming increasingly popular in multiple sectors, including the medical field, where it has been used for different applications such as training [124]–[126], preoperative planning [127], [128], and intraoperative guidance [129], [130].

AR in surgery has proved to be a helpful tool to improve safety and efficacy [120]. It is primarily used to visualize delicate and vital structures, such as major vessels or nerves, or target elements such as tumors or bones. These anatomical models are projected directly onto

the patient, and their visualization can be modified through interactive panels, buttons, gestures, or voice commands, depending on the device. One of the main advantages of this technology is the ability to visualize these elements without deviating the attention from the surgical field to look at an external screen. This behavior reduces time and makes it more intuitive than conventional visualization systems [131].

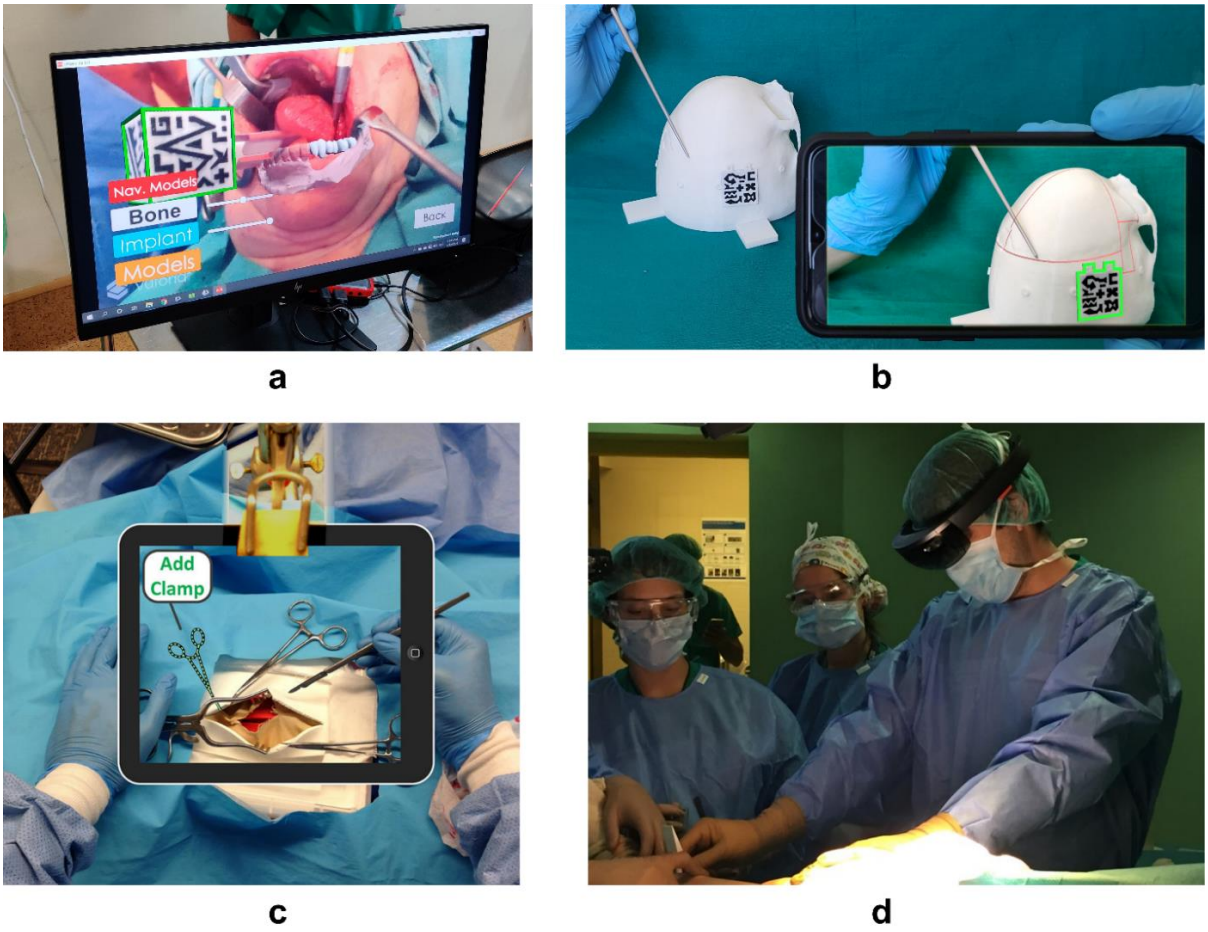

Figure 1.7. Augmented reality (AR) devices: (**a**) monitor, (**b**) smartphone, (**c**) tablet (figure reprinted with permission of the copyright holder, Springer Nature) [132], (**d**) head-mounted display (HMD).

The devices used for AR are typically based on the superimposition of the virtual models on the image captured by a camera. The resulting image can then be displayed on a screen from a PC [133]–[135], smartphone [130], [136] or tablet [137], [138] (**Figure 1.7**). Other common devices are the HMDs, also called "smart glasses". The holographic models are directly projected on the glasses of the headset using stereoscopic rendering, providing a more intuitive visualization without the need to hold any device. This is especially convenient in surgical setups to avoid breaking aseptic protocols. These AR devices commonly incorporate hardware and algorithms that track their position with respect to the environment,

so that the virtual elements can maintain their location in the physical world. Some of the most extended HMDs for surgery are the Microsoft HoloLens 1 and 2 (Microsoft, Redmond, WA, USA) [129], [139], [140], Google Glass (Google Inc., CA, USA) [141], nVisor ST60 or MH60 (NVIS Inc., Reston, VA, USA) [142], [143] and Magic Leap (Magic Leap, Inc., Plantation, FL, USA) [144].

The representation of the virtual elements aligned with the patient's anatomy is achieved by performing a registration step. Multiple solutions have been presented to achieve registration in these setups, going from manual to automatic techniques. Manual alignment is the simplest method but can be slow, imprecise, and requires constant refinement to compensate for movements [145]. Precise registration can be achieved by using trackers, which detect markers fixed to the patient and estimate the position of the camera or device with respect to them, displaying the holograms in the correct position. These markers can be infrared [146]–[149], fluorescent [150] or optical [129], [151]–[153]. There are also marker-less solutions based on RGB (red, green, blue) cameras [154], [155] or laser surface scanning [156], [157]. The main limitation of these camera-based systems is the required direct line of sight, so electromagnetic tracking systems have been proposed as an alternative [158], [159].

AR, as surgical navigation, is mostly useful in surgeries involving organs with minimum movements and deformations. This is why the most common applications are found in head and brain procedures [153], [160]–[162] and orthopedic surgery [142], [146], [163]–[165]. Their use is also extended for minimally invasive procedures, where it has proved to be a valuable tool to provide visual cues and improve hand-eye coordination [166], [167]. Apart from visualizing the anatomical structures of interest in the specific procedure [168], AR can translate the preoperative plan to the surgical room, displaying the incision or cutting planes, trajectories [169], or the optimal placement of surgical instruments [170].

Therefore, AR is an emerging technology with great potential in assisting surgeons by improving visualization of the surgical field and enabling an intuitive translation of the preoperative plan to the actual procedure. Although the precision provided for surgical guidance is lower than conventional navigation systems (around 2 mm compared to 0.5 mm) [131], the use of this technology in clinical applications is expected to increase in the upcoming decades together with the technological and computational improvements [171], [172].

2

MOTIVATION AND OBJECTIVES

2.1. Motivation

The role of CAS solutions in surgery is expected to continue increasing for the following decades, improving efficiency, safety, and cost, and enhancing training. Advances in this field have already made it possible to perform surgeries previously considered impossible or too risky. It has also enabled personalized treatments adapted to the specific case presented by a patient, from the analysis of the condition and the preoperative planning to the final surgery and posterior monitoring.

Cancer treatment is one of the surgical specialties that has mostly benefited from the introduction of these technologies. And not only because of the high cancer incidence or mortality, but also because surgical oncology presents scenarios where precision is crucial and often difficult to achieve using conventional methods. The margins between the tumor and healthy tissue are difficult to discern. For this reason, resections are frequently either too close to the tumor, leaving cancerous cells that can lead to relapse, or so extensive that they affect the functionality of the patients or their appearance. In these scenarios, CAS can provide the necessary assistance to effectively guide the resection, adhering to the optimal surgical margins defined during preoperative planning.

These systems are of particular interest in surgeries that present a certain complexity in their execution. Such difficulties may be caused by the size of the area to be treated, its anatomical complexity, limited access, or the proximity to vital structures that are at risk of being damaged. Two examples of surgical scenarios presenting a high complexity are the resection of tumors in the pelvis and resections in deep head and neck regions. In both cases, the interventions are hazardous due to their proximity to delicate anatomical structures such

as nerves or blood vessels. In the case of pelvic resections, the pelvic bone presents a complex morphology and a large size. On the other hand, resections in deep head and neck regions involve a reduced surgical area with limited access and line of sight.

Many studies have been published assessing the precision provided by these technologies in such complex procedures with promising results. However, it is crucial to ensure high guidance precision and a convenient and minimally invasive setup to achieve a correct integration of these systems in clinical practice. Surgeons should be capable of operating without any elements disturbing or interfering with the procedure. Also, using these tools should not imply exposing more surgical areas than in the conventional intervention. Another point to consider is the price of these systems. The technologies must present an affordable cost and be easy to apply to become accessible to all. In many cases, the proposed solutions are expensive, invasive, and entail a complex setup that increases operative time. All these criteria are often overlooked or undervalued. However, their consideration is crucial to promote the implementation of these systems in regular clinical practice.

Therefore, obtaining solutions based on precise methods, easy to implement, convenient, and non-invasive is of great interest in all surgical fields, especially in those procedures that present greater complexity.

2.2. Objectives

The objective of this thesis is to explore the possibilities of CAS techniques to optimize complex oncological procedures. We propose new solutions that present reliable, precise, convenient, and less invasive setups based on 3D printing, surgical navigation, and augmented reality. We test the use of these technologies separately or combined and assess their precision in experimental setups, with phantoms and cadavers, and in clinical situations with patients.

For this thesis, we focus on two surgical scenarios where CAS techniques represent a valuable tool: pelvic oncological resections and the resection of head and neck tumors. Specifically, we focus on tumors located in the palate. Our work has then the following objectives:

1. Evaluate the precision of less invasive patient-specific instruments (PSIs) with smaller sizes for the guidance of pelvic osteotomies in oncological procedures.

2. Combine the use of small PSIs with a surgical navigation system to reduce the invasiveness of conventional navigation setups while maintaining precision in pelvic tumor resections.
3. Use AR as a tool to guide the placement of small PSIs, overcoming one of the main limitations and sources of error for these surgical tools.
4. Explore the combination of 3D printing, surgical navigation, and AR for palate tumor resections to enable a conservative approach, providing precision with less invasive setups.

This work has been developed at Universidad Carlos III de Madrid in collaboration with the Orthopedic Surgery and Traumatology and Oral and Maxillofacial Surgery departments from Hospital General Universitario Gregorio Marañón in Madrid, Spain.

3

REDUCING THE SIZE OF PSIs FOR LESS INVASIVE PELVIC TUMOR RESECTIONS

3.1. Introduction

The use of 3D printing (3DP) has grown significantly in the last decade, and it is now a leading technique in healthcare [173]. Given the recent interest in centralizing 3DP within the hospital, access to this technology has been facilitated by offering cost-effective on-demand manufacturing [174]. Desktop 3D printers are commonly chosen for this purpose, as the associated cost is lower than that of industrial alternatives, and the printing quality is sufficient for most applications [175].

Surgical planning in orthopaedics and traumatology has benefited considerably from the emergence of 3DP and new image processing techniques, especially in surgical procedures involving complex anatomical regions [176]. 3DP enables not only to print fragments of the patient's anatomy but also to manufacture surgical tools. Since these tools can be customized to fit precisely in a specific position on the patient, they are known as patient-specific instruments or PSIs. Their design adapts to rigid anatomical structures (e.g., bone), thus making it possible to guide drills, saws, and other surgical tools towards a predefined path [177], [178].

Complex interventions in the pelvis, such as periacetabular osteotomy or pelvic ring tumor resection, can also benefit from PSIs. Solutions that improve negative resection margins are of particular importance, since experienced surgeons obtain satisfactory margins in only 52% of cases (95% CI: 37-67) [179]. More extensive resections should be avoided, as

they may cause significant functional deterioration if nerve roots, viscera, or blood vessels are damaged.

3DP models are subject to errors arising during the design and printing process that can lead to a mismatch between virtual planning and actual execution [180]. Brouwers et al. [181] identified several critical steps in the 3DP pipeline. The errors arising from these steps also affect the accuracy of the 3D-printed PSIs and, consequently, their placement. One of the limitations of PSIs compared to other techniques, such as surgical navigation, is the impossibility of verifying correct placement during the intervention, other than subjectively. For this reason, it is essential to be aware of possible sources of error in order to minimize them. A common solution is to design large PSIs covering a wide area to ensure correct placement. However, large PSIs require the surgical procedure to be modified, thus making it more invasive.

Some studies have measured the accuracy of PSIs in pelvic osteotomy by comparing the results with other approaches [177], [178]. While these studies showed promising results, they presented two main limitations: their PSIs were large, and the total number of surgical guides used, as stated by the authors, was too low. Furthermore, these studies addressed the deviations of the osteotomy from the virtual plan but did not report the actual placement errors of the PSIs.

3.2. Objective

Our work aimed to efficiently characterize the accuracy of PSI placement for four common pelvic osteotomies. An experimental cadaveric study was conducted in a large sample using small surgical guides fabricated with a desktop 3D printer. Translations and rotations were computed for each guide and osteotomy with respect to their planned position and represented in a local reference frame.

3.3. Materials and Methods

A total of nine cadaveric pelvises (four women and five men) were used for this experiment. We acquired CT images of the specimens (slice thickness 1 mm) and processed each study to obtain a 3D model of the pelvic bone with semi-automatic segmentation in the open-source software 3D Slicer [117]. The models were then saved in “Stereolithography”

(.stl) format and imported into Autodesk Meshmixer (Autodesk, Inc., USA), where we defined osteotomy cutting planes and designed their corresponding PSIs.

Four cutting planes were planned per hemipelvis, each one mimicking surgical practice for tumor resection. The location of anatomical structures such as nerve roots, blood vessels, and pelvic viscera was taken into account. Planes were defined in four regions: iliac crest, supra-acetabular, ischial, and pubic (**Figure 3.1**). A PSI was designed for each plane, matching the shape of the bone surface in that region, and following the curvatures to ensure correct insertion and fixation to the bone. The size of the guides was limited deliberately, as bulky PSIs should be avoided in clinical practice.

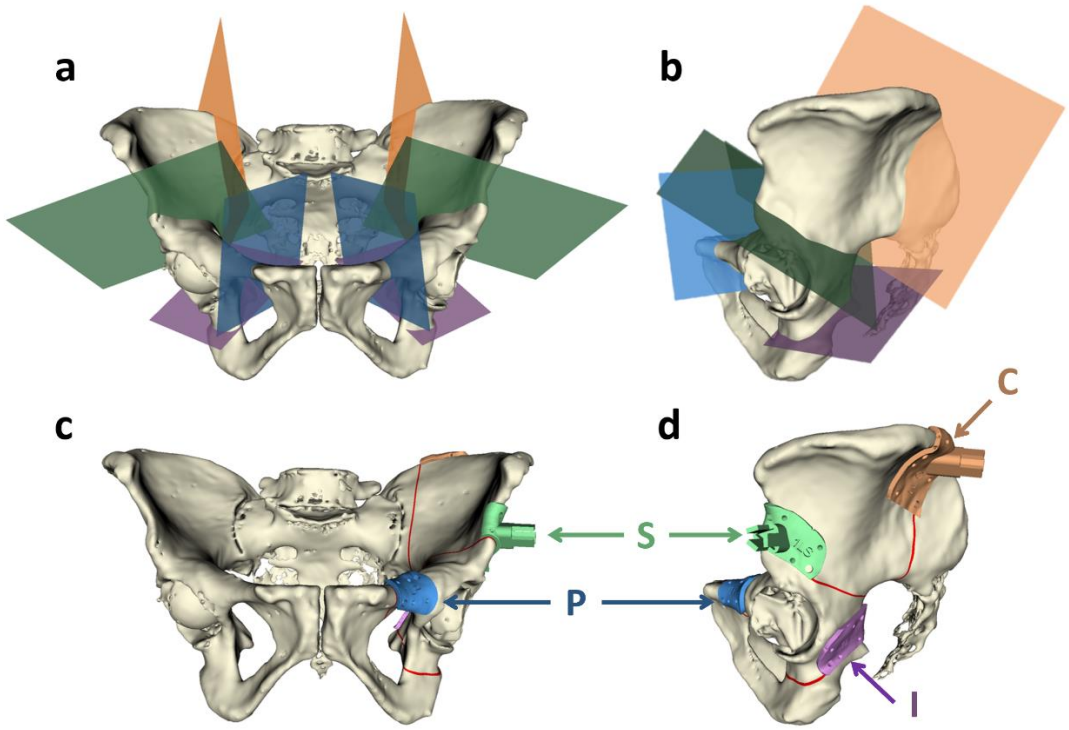

Figure 3.1. Definition of cutting planes in (**a**) frontal and (**b**) lateral view. Patient-specific instrument (PSI) placement in (**c**) frontal and (**d**) lateral view. The regions are iliac crest (C), supra-acetabular (S), pubic (P), and ischial (I).

The design process for PSIs consisted of the following steps (**Figure 3.2**):

a. Selecting the area in the bone where the surgical guide is to be fixed. The size of the area was limited to approximately 1200 mm^2.
b. Performing an extrusion of 2 mm, defining the thickness of the guide.
c. Generating two holes for placement of screws in opposite corners of the guide.
d. Adding an inscription with the PSI identifier (number, side of hemipelvis, pelvic area).

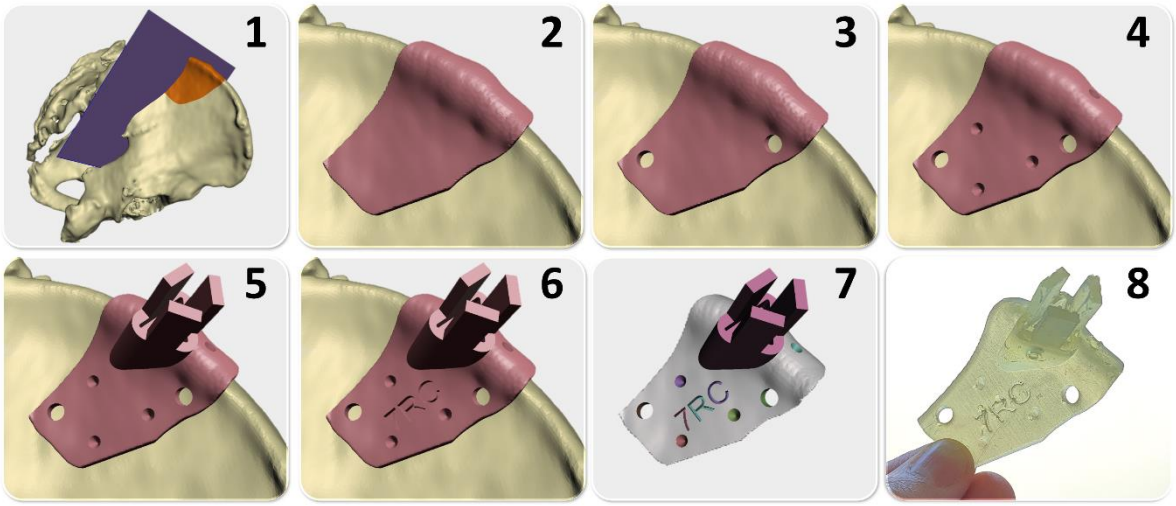

Figure 3.2. Steps for PSI design: (**1**) plane definition and area selection; (**2**) extrusion; (**3**) screwing holes; (**4**) creation of conical indentations; (**5**) addition of the socket; (**6**) inscription of the identifier; (**7**) final design; and (**8**) 3D printing.

In addition to these steps, we added four conical indentations to each guide and a prism-shaped socket in the iliac crest and supra-acetabular guides. These were used for surgical navigation. However, that step is not covered in this chapter.

PSIs were 3D-printed in a Formlabs Form2 3D printer using Dental SG resin, a Class I biocompatible material (ISO Standard from Formlabs Vertex-Dental BV resin: EN-ISO 10993-1:2009/AC: 2010, USP Class VI). Guides were cured to improve strength and stability and sterilized with ethylene oxide at 55˚C before the experiment.

The whole procedure could be applied to clinical cases since our hospital has obtained the corresponding local government license to manufacture these custom-made devices. This was possible after certifying the process following international standard ISO 13485 for Quality Management Systems for medical devices. Consequently, the in-house manufactured surgical guides can be used according to care needs.

During the experiment, five experienced surgeons (who were not involved in the design steps) placed the PSIs using pictures of the surgical plan for each case as reference (**Figure 3.1**). Bone surface exposure and cleaning were limited to resemble the real surgical scenario (**Figure 3.3**). Surgical guides were fixed to the bone using screws. From a total of 72 PSIs, two broke during drilling and other five were discarded due to time limitations. After the experiment, surgeons answered a questionnaire to collect their feedback (**Figure 3.4**).

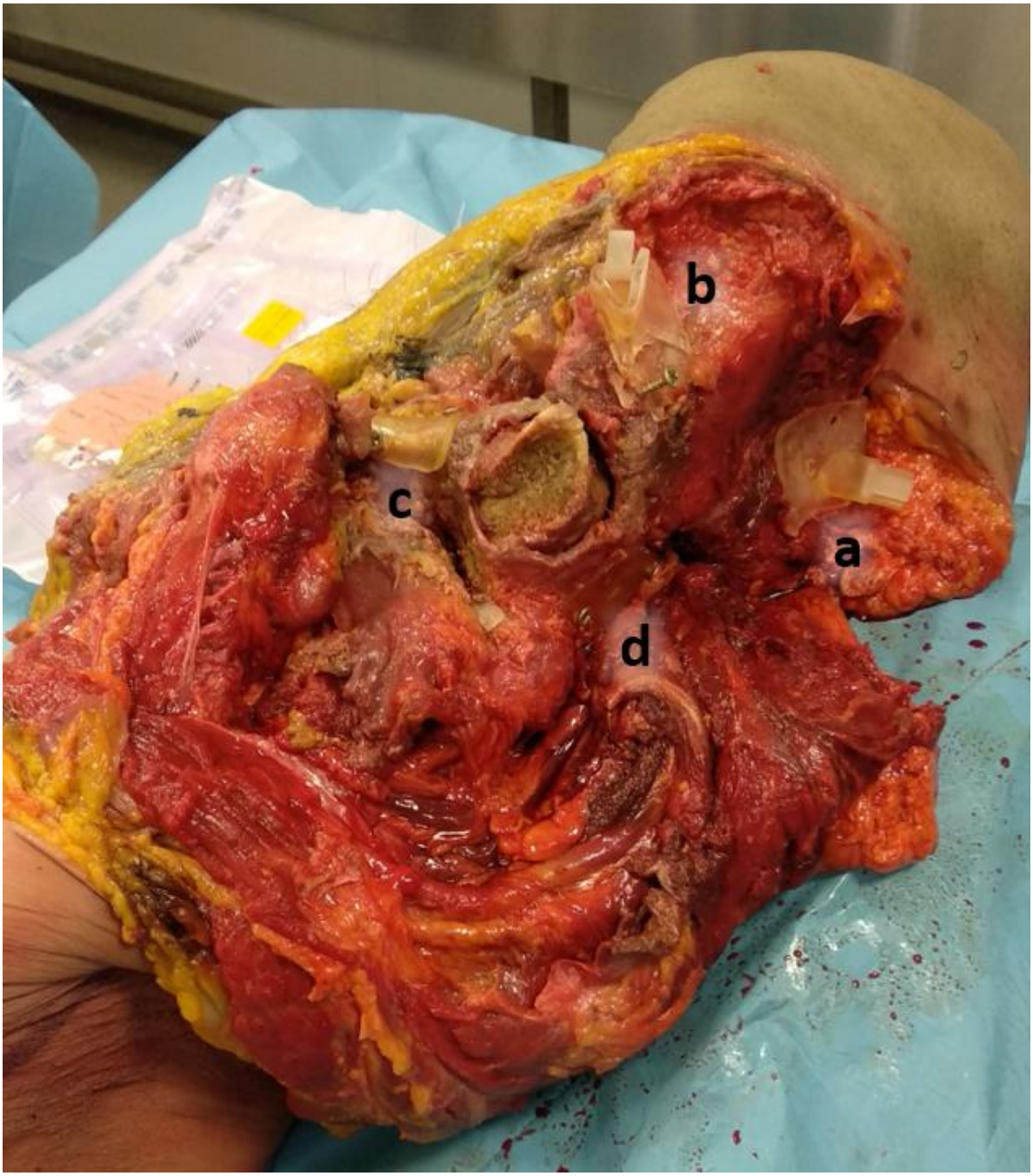

Figure 3.3. Placement of PSIs during the experiment: (**a**) iliac crest, (**b**) supra-acetabular, (**c**) pubic, and (**d**) ischial.

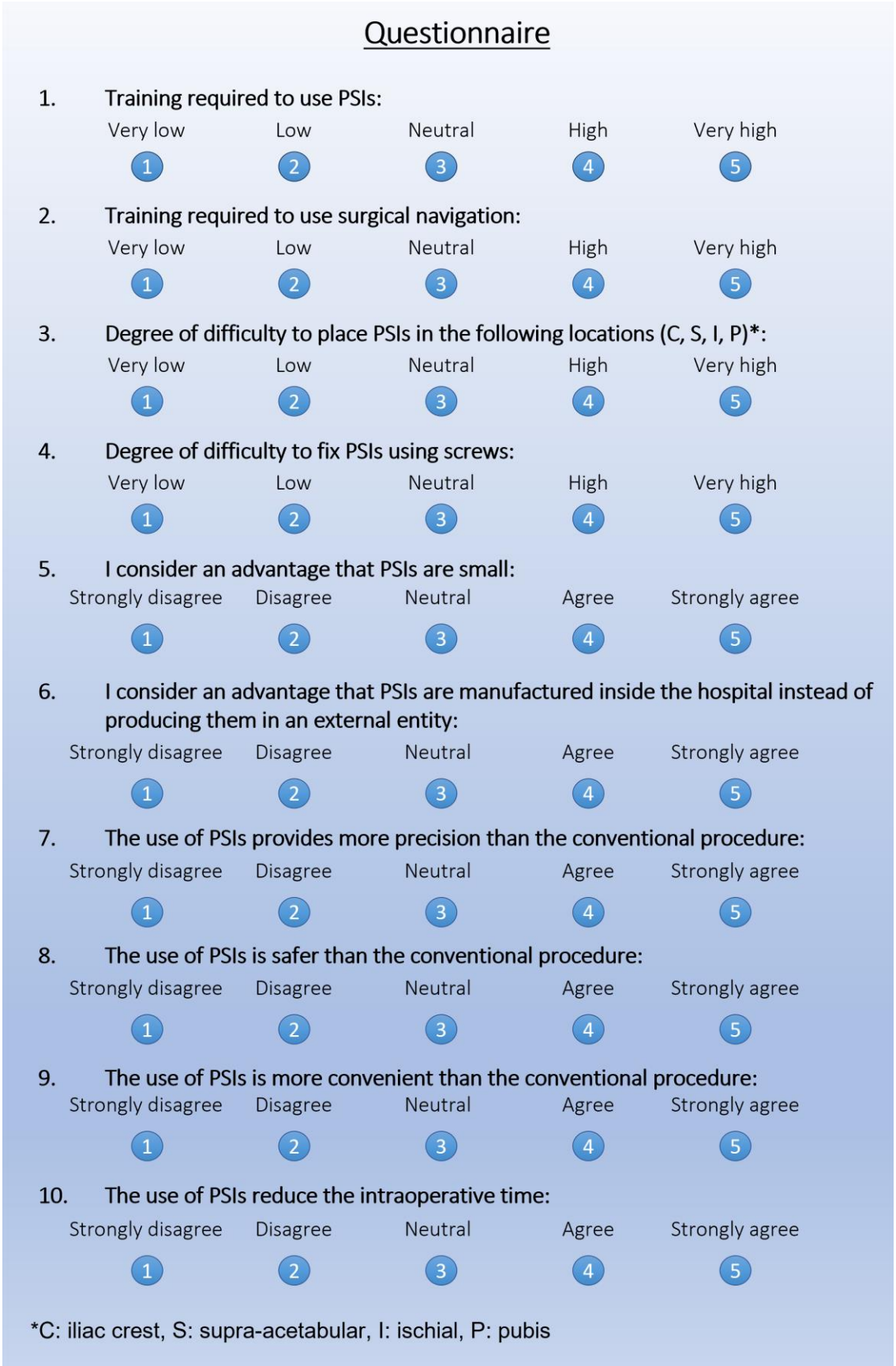

Figure 3.4. Questionnaire answered by surgeons.

Three days after the experiment, we acquired a CT image for each pelvis with the PSIs still attached. We generated a 3D model for each pelvis following the procedure described above for the preoperative CTs. Preoperative and postoperative models were registered using the iterative closest point algorithm [182]. Thus, the preoperative data (CT and 3D models of the pelvis and PSIs designed during planning) and postoperative data (CT and 3D models of the pelvis, PSIs, and screws placed during the experiment) were aligned and could therefore be compared.

We calculated a rigid transformation to characterize the displacement of the postoperative surgical guides with respect to their planning position. PSIs could not be fully segmented in the CT since the Hounsfield units for the resin were very similar to those of the surrounding tissue. Therefore, we computed the rigid transformation using point-based registration from landmarks manually selected on each guide after an initial rough segmentation. The registration points consisted of the screw positions (two for each guide) and additional characteristic landmarks. In the preoperative guides, the screw points were defined as the intersection of the longitudinal axis of the cylindrical hole for the screw and the surface of the bone. In the postoperative guides, the longitudinal axis was defined from two points in the CT: one on the centre of the screw head and one on the tip. As in the preoperative case, the intersection between this line and the bone was used to define the point.

Finally, we represented the transformation in a reference system defined locally for each preoperative surgical guide. This enabled the extraction of translations and rotations that had been decomposed along similar axes independently of the shape and size of the pelvis or the region where the PSI was placed. The steps for the new reference system definition were the following (**Figure 3.5**):

- X axis (v_plane): normal of the cutting plane.
- Y axis (v_normal): cross-product of the vector defined by the two screw points, S1 and S2, and v_plane.
- Z axis (v_edge): cross-product of v_plane and v_normal.
- Centroid: midpoint of S1 and S2.

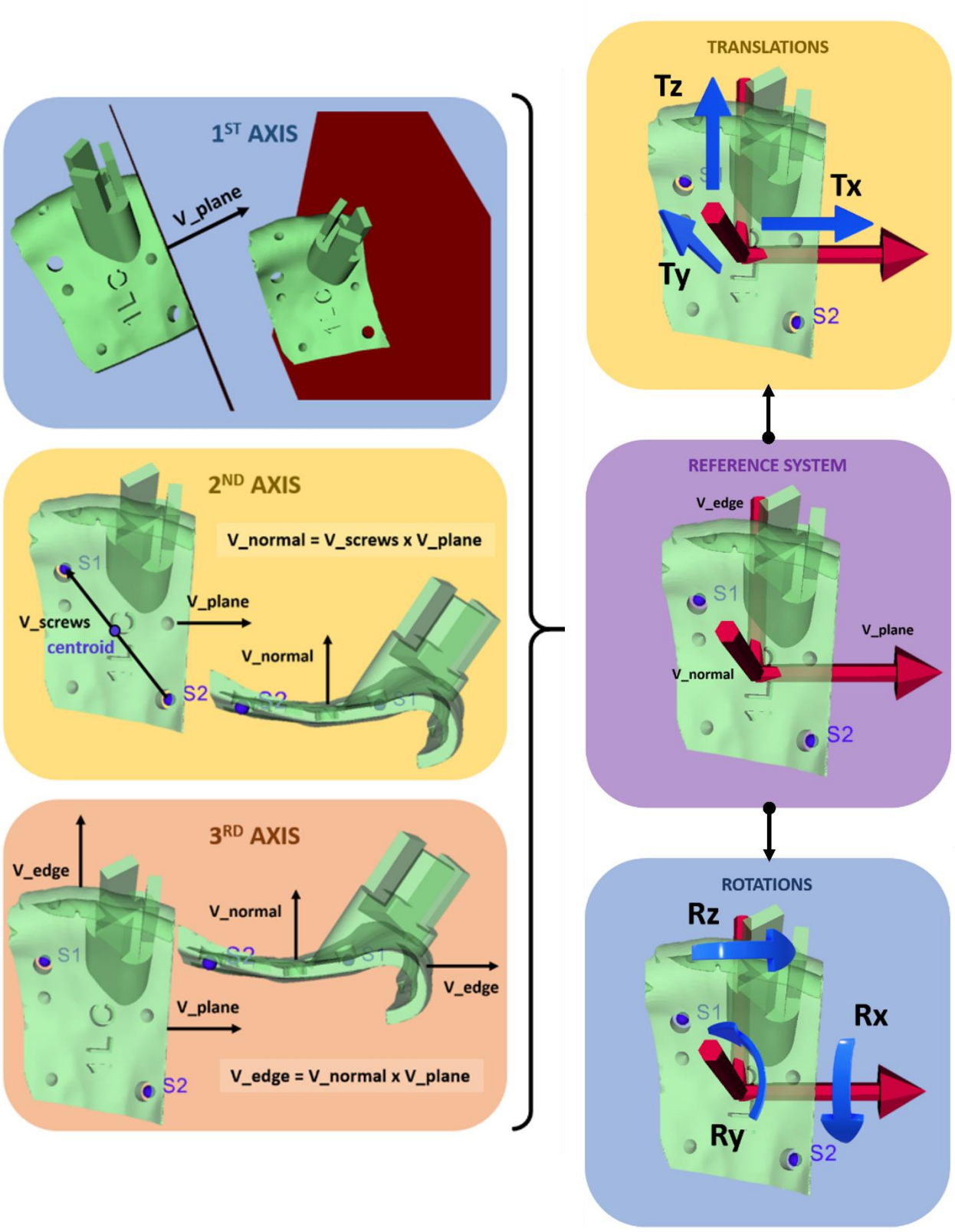

Figure 3.5. Reference system definition and translation (T) and rotation (R) axes.

The axes' signs were defined as shown in **Figure 3.6** to enable a similar interpretation for each guide regardless of the region and side.

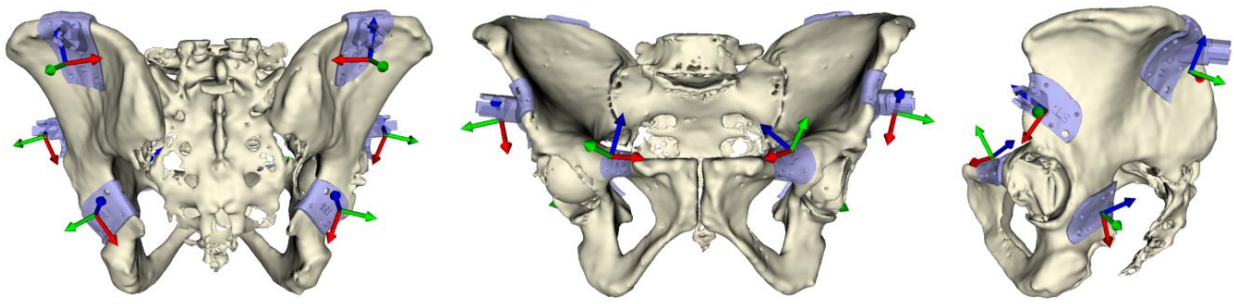

Figure 3.6. Reference system orientation for each region. Axes x, y, and z are shown in red, green, and blue, respectively.

Translations and rotations during PSI placement generate deviation errors along the whole osteotomy, reaching a maximum at the beginning or end of the cut. To identify these maximum deviations, the length of the cuts for each case was measured, and the deviation was computed from the sign and magnitude of the plane rotation (Ry) and translation (Tx).

In some interventions, only the upper section is removed during resections in the ilium. The osteotomies start in the iliac crest and supra-acetabular regions and meet at a midpoint on the ilium. In order to estimate the errors for these cases, we computed the maximum osteotomy deviations for half of the original cut length in these two regions.

3.4. Results

We extracted translation and rotation values from the rigid transformation, which was obtained after aligning postoperative surgical guides with their planned position. These values were represented in the reference system described in the previous section. Translation and rotation values from PSIs corresponding to the left and right hemipelvis presented similar behavior regarding magnitude and direction, where rotations generally showed opposite signs due to the symmetry of the reference frame definition (**Figure 3.7**). For this reason, the remaining results are presented with both sides combined and in their absolute value.

Table 3.1 and **Table 3.2** show the mean and standard deviation for translations and rotations on each axis. Maximum osteotomy deviations for each region are presented in **Table 3.3**. As the deviations caused by rotations are directly related to the length of the osteotomy, the mean osteotomy length (MOL) for each region is included in **Table 3.3**.

.

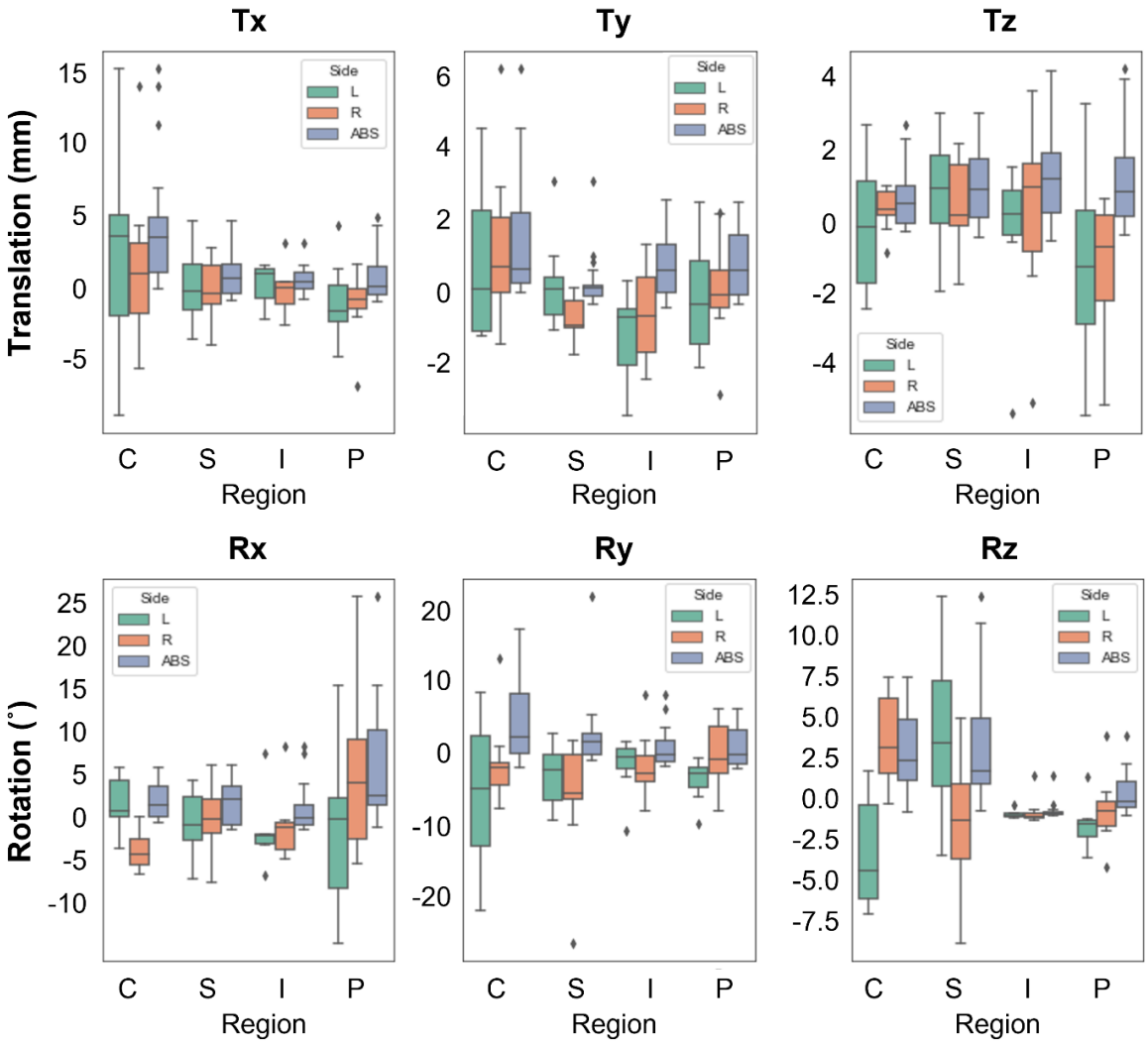

Figure 3.7. Data distribution of the translations and rotations on each axis (x, y, z) measured for each region (C, S, I and P). Values are divided into three categories: left (L) and right (R) side and combined data in absolute value (ABS).

Table 3.1. Mean and standard deviation of unsigned translations (mm) for each region and axis.

	Translation axis	C	S	I	P
Mean	x	5.3	1.8	1.5	1.8
SD		4.6	1.5	1.0	1.8
Mean	y	1.8	0.7	1.0	1.1
SD		1.6	0.7	0.8	0.9
Mean	z	1.2	1.5	1.8	1.8
SD		0.8	1.0	1.5	1.4

SD, standard deviation; C, iliac crest; S, supra-acetabular; I, ischial; P, pubic

Table 3.2. Mean and standard deviation of unsigned rotations (˚) for each region and axis.

	Rotation axis	C	S	I	P
Mean	x	3.2	3.1	2.6	7.7
SD		2.0	2.3	3.0	7.1
Mean	y	6.7	5.1	3.4	3.5
SD		6.1	5.4	3.1	3.1
Mean	z	3.7	4.2	0.3	1.3
SD		2.5	3.7	0.6	1.3

Table 3.3. Descriptive statistics for maximum osteotomy deviations (mm) in each region.

	C		S		I		P	
	Complete	Half	Complete	Half	Complete	Half	Complete	Half
MOL	90.8	45.4	77.3	38.7	47.6	-	25.9	-
Total cases	18	18	17	17	15	-	15	-
Mean	8.1	6.0	7.7	4.5	3.6	-	2.8	-
SD	5.4	4.4	7.1	3.2	2.3	-	2.5	-
Max	20.1	15.9	32.5	14.4	8.7	-	9.2	-
25%	4.1	2.6	3.5	2.5	2.0	-	0.6	-
50%	6.2	4.7	6.4	3.6	2.8	-	2.5	-
75%	11.8	7.8	7.8	5.5	5.5	-	3.7	-

MOL, mean osteotomy length

Mean translations were below 2 mm in all directions and regions except for the iliac crest, which presented more than 5 mm of error in Tx. Mean rotation errors were below 5˚ in all cases, except for the iliac crest and the supra-acetabular regions in the Ry direction and the pubic region in Rx, with values between 5˚ and 8˚.

Regarding the maximum osteotomy deviations, mean values were below 5 mm in the ischial, pubic, and short supra-acetabular osteotomies and between 6 and 8 mm in the iliac crest (long and short osteotomy) and long supra-acetabular osteotomies. Maximum deviations below 5.5 mm in ischial, pubic, and short supra-acetabular osteotomies were observed in 75% of cases. In the short osteotomy for the iliac crest and long osteotomy for the supra-acetabular region, the 75th percentile was 7.8 mm. Finally, this value was 11.8 mm for the long iliac crest osteotomy.

Table 3.4 presents the results from the survey answered by surgeons involved in the experiment. The results indicate that they rather have PSIs manufactured in the hospital than produced by an external entity. They agree that the reduction in the size of PSIs is an advantage considering that larger PSIs require modifying the surgical procedure and are less safe. They also agree that some training is required, but less than in surgical navigation. Regarding the experiment, they found the placement of the iliac crest PSIs the hardest one and agree that the fixation of PSIs using screws presented a low degree of difficulty. Finally, when compared to the conventional procedure, they consider that the use of PSIs reduces the intraoperative time, is more precise, safer, and more convenient.

Table 3.4. Results from the questionnaire.

		Individual scores (per surgeon)					
Question		1	2	3	4	5	Avg. score
1		4	3	3	4	3	3.4
2		5	5	3	5	5	4.6
3	C	4	1	2	5	5	3.4
3	S	3	1	4	3	4	3
3	I	5	1	4	3	3	3.2
3	P	4	1	4	3	3	3
4		2	2	1	3	2	2
5		5	4	5	4	5	4.6
6		5	5	5	5	4	4.8
7		5	5	5	5	5	5
8		5	5	5	5	5	5
9		5	4	5	5	5	4.8
10		5	4	5	5	5	4.8

3.5. Discussion

The anatomical complexity of the pelvis and its proximity to vital structures make tumor resection in this region very challenging. Pelvic cancer has a relatively high recurrence rate, which is associated with the difficulty of obtaining adequate resection margins [183]. Consequently, new solutions have been proposed to improve the outcome of pelvic procedures. Such is the case of surgical navigation [30] and PSIs [177], [178], which guide resection tools towards a predefined path decided during preoperative planning.

While surgical navigation is highly accurate, it usually increases intervention time, is expensive, and has a steep learning curve. PSIs, on the other hand, are more immediate, as they require less training and preparation in the operating room. However, while it is possible to check that the guidance is correct during surgical navigation, this cannot be verified when using PSIs other than visually. For this reason, it is essential to be aware of the accuracy provided by this technology. We addressed this issue by performing a thorough analysis of the placement errors when using PSIs for four common pelvic osteotomies. Our results demonstrate significant differences between regions that need to be addressed independently.

The region of the iliac crest where the corresponding PSIs were positioned is wide and has a homogeneous topology, thus making the selection of a point of placement for the PSI challenging. Consequently, the error rate was highest for this region, and the errors were mainly related to large translations along the bony ridge (Tx). Translation and rotation errors measured in the remaining axes were primarily a consequence of these translations, including the rotation of Ry, which can be explained by the curvature of the iliac crest. The high mean obtained for the maximum osteotomy deviations was a result of the length of the osteotomy and the high displacements in Tx and rotations in Ry.

Other studies present a different localization of the PSI for iliac crest osteotomy, placing it in the sacroiliac joint [177], [184] and obtaining deviations of around 5 mm. However, this location is not always the most convenient in terms of surgical approach. Jentzsch et al. [185] reported four clinical cases of pelvic sarcoma, where different osteotomies were performed depending on the tumor location. The osteotomies made in the iliac crest were freehand, obtaining deviations of 28 mm, which were significantly higher than those obtained in the present study using PSIs.

Supra-acetabular PSIs presented low displacements in all directions. However, rotations were around 5˚ in Ry and 4˚ in Rz, which are higher values than in other regions. These rotation errors were mainly a consequence of the curvature of the bone in this area. As the osteotomies were long, small rotations had a high impact on plane deviations. A wider design reaching the anterior superior iliac spine could reduce the rotation errors. Nevertheless, when used for osteotomies ending at the midpoint of the ilium, 13 out of 17 presented deviations below 5.5 mm. The mean deviation value was 4.5 mm (n = 17), which was very similar to the 4 mm (n = 5) obtained by Sallent et al. [177].

Ischial osteotomies were relatively short, and translation and rotation errors were low in all directions. Rotations in Rz were very close to 0 in most cases as the bone in the area is not curved. Maximum osteotomy deviations slightly above 5 mm were observed in only 2 out of 15 cases and were a consequence of rotations in Ry higher than 6˚. Sallent et al. [177] also measured the maximum osteotomy deviations for this region, although the PSI was placed at the anterior end of the cut. These authors obtained a mean error of 2.2 mm (n = 5), compared to our value of 3.6 mm (n = 15).

Finally, translations and rotations in the pubic region were low, except for the case of Rx, with values of around 8˚ owing to the cylindrical shape of the bone in this area. Since osteotomies in the pubic region were very short, rotations did not have a significant impact on the deviations. Only 3 out of 15 cases presented maximum osteotomy deviations slightly higher than 5 mm, and, in those cases, this was always a result of translation errors in Tx. These cases presented a PSI design that was too flat and small, which made it challenging to select the correct placement. We obtained a mean osteotomy deviation of 2.8 mm (n = 15) for this region, whereas Sallent et al. [177] obtained mean deviations of 0.8 and 1 mm (n = 5) using PSIs for biplanar osteotomies.

We performed an experimental study to measure the accuracy of PSIs following a realistic workflow in terms of subject selection, CT acquisition, and design and placement of PSIs. We used cadaveric specimens from elderly subjects; in most cases these were affected by osteoporosis, which hampered segmentation. CT acquisition parameters were similar to those of the clinical protocols in terms of slice thickness and radiation. The PSIs were designed small, as this is more indicative of clinical practice, and their location was chosen based on a realistic surgical approach. PSIs were sterilized before the experiment, as in clinical practice. Finally, the experiment was performed on a single day by surgeons who did

not participate in the PSI design process. In this study, we performed bone segmentation and PSIs design with free and open-source software. However, alternative platforms such as Mimics Innovation Suite (Materialise NV, Leuven, Belgium), which are validated for clinical applications, could be used to apply this workflow in surgical interventions.

Our experimental design was also subject to limitations. The use of cadaveric specimens enabled a more controlled scenario than real procedures. The time restrictions during the intervention resulted in some surgical guides being placed with a considerably high degree of error. In addition, the material used for the PSIs showed contrast similar to that of the surrounding tissue in CT. For this reason, we calculated the registration between pre- and postoperative PSIs based on manually selected points. This step may have contributed to the errors recorded during the procedure. The chosen material for printing can also be improved, as two PSIs broke while drilling during the experiment. Other similar biocompatible materials such as BioMed Clear resin may provide better results. This material presents better properties, as it is more rigid and non-brittle and can be used for non-dental purposes and long-term contact (USP Class VI). Also, a higher level of experience from the surgeons could reduce the risk of fractures. It is important to be aware that, when using PSIs or other helping tools during surgery, provisions should be made to revert the procedure to the conventional approach in case they break, fall, or do not behave as expected for any reason. Surgical protocol should be designed with this possibility in mind.

Our study presents interesting findings with respect to the manufacture of the PSIs and the analysis performed. PSIs were printed in resin using a desktop 3D printer, which, in this scenario, presents several advantages over industrial 3D printers. Their price is significantly lower than that of the industrial versions while the resulting PSIs are as accurate as the ones printed in other commonly used materials [177], [178]. Furthermore, PSIs can be designed and printed inside the hospital, without external support, providing faster and easier communication between clinicians and designers. This allows monitoring the end-to-end process (from design and validation to clinical use). However, the production inside the hospital also entails some limitations which need to be considered. You need specially trained biomedical engineers who know not only to design 3D models and control the 3D printers but also to interpret medical images and understand the clinicians' needs. The maintenance of the lab and workers is also an investment, so the demand must be studied to determine whether the in-house production is a better solution. Finally, the clinicians must be involved in the design process and their time is a limited resource.

Regarding the analysis, previous studies measured the accuracy of PSIs comparing the results with other approaches. In a cadaveric study, Sallent et al. [177] analysed osteotomies completed following the standard manual technique and those performed with PSIs. Similarly, Wong et al. [178] compared the accuracy of PSIs and navigation in periacetabular tumor surgeries. While the results from these studies were promising, the total number of surgical guides used was low (20 for the first study, 5 per osteotomy; and 12 for the second study, 6 per osteotomy). In our study, we increase the number of samples using a total of 72 PSIs (4 per hemipelvis in 9 specimens). Also, not only did we study the osteotomy deviations, but we also assessed the translations and rotations in all directions. Previous studies only focused on measuring mean or maximum osteotomy deviations [178] or presented the rotations of the osteotomy plane with respect to the anatomical axes, without considering the direction of the osteotomy or the shape of the local bone, thus hampering interpretation [177]. In our study, translations and rotations are presented in a reference frame defined considering the morphology of the bone, hence providing a more meaningful interpretation of the results. As the proposed analysis takes into account the shape of the bone in each region, it can be extended to other anatomical locations, such as the limbs, where PSIs are also commonly used. Moreover, the evaluation of placement errors in directions different from the cutting plane normal is relevant in cases where PSIs have purposes other than guiding the osteotomy (e.g. attachment of reflective [186] or augmented reality markers [129]).

3.6. Conclusions

To conclude, when designing PSIs, it is essential to study the shape of the target bone, as the accuracy provided by this technology is highly dependent on factors such as homogeneity and curvature. PSIs placed in the supra-acetabular, ischial, and pubic regions proved to be sufficiently accurate to guide short osteotomies. However, PSIs guiding longer osteotomies in the iliac crest and supra-acetabular region presented errors above 5 mm caused by incorrect placements. The novel analysis presented in this study provides a comprehensive tool for characterizing placement errors. In addition, the design and methodology proposed for manufacturing PSIs are as accurate as those of other technologies, yet more appropriate for real surgical procedures.

The content of this chapter has been published in the International Journal of Computer-Assisted Radiology and Surgery (IJCARS):

M. García-Sevilla, L. Mediavilla-Santos, M.T. Ruiz-Alba, R. Pérez-Mañanes, J.A. Calvo-Haro, J. Pascau. "Patient-specific desktop 3D-printed guides for pelvic tumour resection surgery: a precision study on cadavers". Int J CARS, vol 16, pp. 397–406 (2021).

4

COMBINING SURGICAL NAVIGATION AND PSIs FOR PRECISE AND LESS INVASIVE PELVIC TUMOR RESECTIONS

4.1. Introduction

As already mentioned in the previous chapter, pelvic tumor surgeries are challenging due to bone's morphological complexity and proximity to vital structures. In these interventions, achieving safe margins is essential as they present high local recurrence rates (70% in marginal resections and 90% in intralesional) [187], [188]. However, according to a study on simulated models of the pelvis, the probability of obtaining adequate margins following the conventional approach is only 52% (95% CI: 37-67) [179]. Consequently, several technologies have been introduced to improve resection accuracy and reduce the risk of recurrence.

Computer-assisted navigation has improved precision in complex surgical settings [30], [189]–[192]. Many studies have already proved its benefits in pelvic tumor resections [190], [191] [193], [194]. Thanks to the real-time visual feedback, tumor and adjacent anatomical structures can be identified and located accurately. The preoperative surgical plan can be easily translated to the operating room, increasing not only the resection accuracy but also the intra-operative confidence [190].

The use of navigation requires some preparation of the surgical field [189]. After the exposure of bone and tumor, a dynamic reference frame is attached to the patient's bone to account for intra-operative movements. It is then necessary to register preoperative images and patient's anatomy. This image-to-patient registration is usually performed through pair-

points and surface-points matching. These points are identified in the preoperative images and recorded during surgery on the patient using a navigation probe or pointer. The registration process is the most critical step to achieve optimal accuracy. If the software indicates an error above 1 mm, the process is generally repeated until a lower value is achieved. Additionally, correspondence between image and patient is visually verified by placing the pointer in anatomical landmarks. This verification is essential, as target registration errors can be high even if the fiducial registration error was low [99], [100]. Current registration approaches provide acceptable results, but there is still room for further improvements. Alam et al. [195] identify the need for registration methods providing higher efficiency, accuracy, and robustness in acceptable time frames. They also describe as a challenge the detection of reliable landmarks, either manually (which requires medical expertise and takes more time) or automatically (which requires large databases for training).

PSIs are considered an alternative to surgical navigation in some scenarios [177], [185], [196]–[198]. They provide similar accuracy [178] while guiding the surgeons towards a predefined path without diverting their attention from the surgical field. Also, they can be manufactured with a 3D printer at a low cost [174]. However, they do not offer the information provided by surgical navigation, such as real-time image guidance, which limits their use to osteotomy assistance. Besides, PSIs correct placement cannot be verified other than subjectively [178], and incorrect positioning can lead to positive resection margins. To overcome this limitation, PSIs are commonly designed with large sizes, covering more bone surface to ensure precise fitting into the bone and, thus, accurate osteotomy guidance.

Both techniques (computer-assisted navigation and PSIs) present better accuracy than conventional procedures, but they also show some limitations. Large PSIs alter the surgical approach as their sizes imply more bone exposure [177], [184], requiring extensive dissections that increase the surgical risks. Similarly, surgical navigation modifies the intervention as the registration anatomical landmarks, which are distributed all over the hemipelvis, require the exposure of bone regions not necessarily involved in the procedure. Furthermore, the rigid fixation of the reference frame becomes cumbersome, since the setup must ensure stability [199] and avoid interference in the surgical field [106]. Therefore, it is necessary to find less invasive solutions that preserve the surgical approach but, at the same time, ensure adequate resection margins.

4.2. Objective

In this paper, we propose combining both techniques to solve their limitations and benefit from the advantages they offer. We replace registration anatomical landmarks with artificial points included in the PSIs. These PSIs are designed with small sizes to limit bone exposure and manufactured with a desktop 3D printer at a low cost. The reference frame is also 3D-printed and fixed to the patient with a PSI, simplifying its installation. It is also detachable, avoiding surgical interference when not used for navigation.

We present a study to assess the feasibility of the proposed setup, the precision of the reference frame placement in PSIs, and the system's navigation accuracy for common scenarios in pelvic tumor resections. This study has been performed in cadavers, which provide a realistic surgical simulation. The results validate this setup and show the best configuration of PSIs placement for each resection type and the navigation accuracy expected in each scenario.

4.3. Materials and Methods

This section explains the methodology followed in the present study to validate each of the setup proposals. These include the design and manufacturing of PSIs and navigation reference frame with a desktop 3D printer, the reference frame's attachment to a PSI, and the use of navigation combined with small PSIs in a realistic environment. The last subsection explains the analysis performed, with data obtained from the cadaveric experiment, to evaluate the navigation system's accuracy in common surgical scenarios for pelvic tumor resection.

4.3.1. Design and validation of the reference frame attachment

We designed a reference frame in the shape of a prism and a socket for its insertion (**Figure 4.1**). The prism was designed with an isosceles triangular base to fit in a unique position in the socket and avoid possible rotations while presenting a simple shape. The frame included three branches with snap-fit posts for the attachment of spherical markers. We defined their positions considering the constraints for a correct localization with optical tracking (distance between markers of at least 40 mm, and differences of at least 3.5 mm between segments connecting each pair of markers) [200].

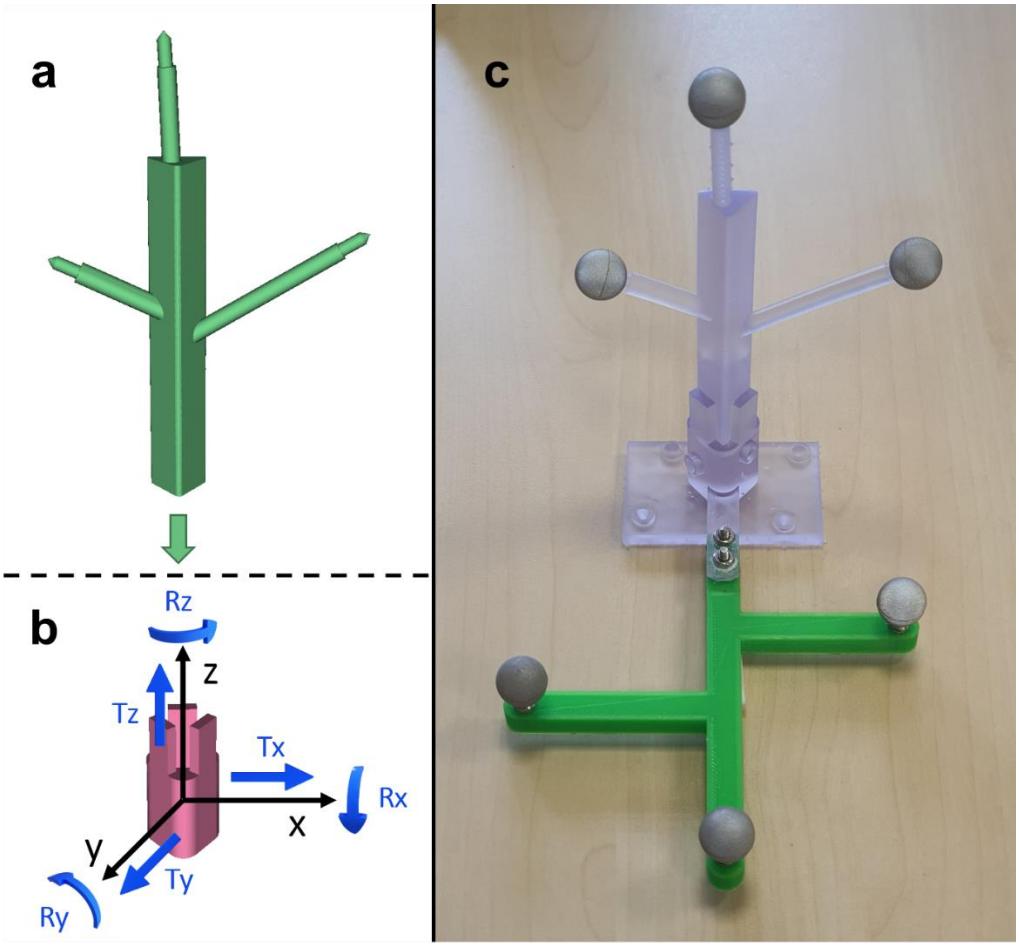

Figure 4.1. Design and validation of reference frame attachment: (**a**) reference frame; (**b**) socket and coordinate system used for the analysis; (**c**) setup for validation.

To reattach the reference frame during an intervention without the need to repeat the registration process, the reference frame's position should be maintained across insertions. To verify this assumption, we recorded the reference frame position with respect to the socket during 20 insertions. To track the socket position, we added to the design a platform with spherical markers attached. We computed the deviations of the reference frame's pose (position and orientation) in every insertion from the mean pose, decomposing these values into the translations and rotations present in every axis, defined as shown in **Figure 4.1**.

A Polaris Spectra (NDI, Waterloo, Canada) optical tracking system was used to track the position of the reference frame and the socket. Spherical optical markers attached to the tools reflect the infrared light emitted by the device, which is then captured by the cameras to estimate their position with a trueness of 0.170 ± 0.090 mm [201].

Both the socket and the reference frame were 3D-printed on a Formlabs Form2 (Formlabs Inc., Somerville, MA, USA) 3D printer in Dental SG, a Class I biocompatible

material, also used for PSIs (ISO Standard from Formlabs Vertex-Dental BV resin: EN-ISO 10993-1:2009/AC: 2010, USP Class VI). After printing, we followed three postprocessing steps: rinsing in isopropyl alcohol (Form Wash), removing supports, and post-curing (Form Cure) to maximize mechanical properties. When fabricating surgical guides, the surface in contact with the patient should be smooth. Hence, it is recommended to avoid the placement of supports in this area. Surgical guides can therefore be printed upside down to leave that surface free of supports. However, this means that they are placed inside the socket instead. So, it is essential to remove those supports after printing to ensure the correct insertion of the reference frame. The attachment of the spherical markers to the posts of the reference frame should also be verified after printing. In order to replicate this procedure for our experiment, the validation platform was 3D-printed upside down. Supports were thoroughly removed from the socket and the reference frame. A space of 0.115 mm between the reference frame and the socket walls was included in the design, considering the 3D printer's tolerance. This way, a static insertion was achieved.

4.3.2. Cadaveric experiment

To validate our setup's feasibility, we conducted an experiment with a total of 6 cadaveric pelvises (three female and three male). Specimens were scanned with a CT slice thickness of 1 mm, since this value is a good compromise between accuracy and radiation exposure. Previous studies present lower thickness values [177], [178], which can provide higher precision for 3D models reconstruction but are difficult to justify in clinical practice. A model of the pelvis was extracted for every specimen through a segmentation process using thresholding. Four planes were defined in each hemipelvis presenting common osteotomy locations: iliac crest (C), supra-acetabular (S), ischial (I), and pubic (P). A PSI was designed for each osteotomy plane, presenting a small size to preserve the surgical approach. Each PSI included four pinholes to perform point-based registration [26]. C and S PSIs also contained the socket to attach the navigation reference frame. A detailed description of the PSIs design can be found in chapter 3. The reference frame and PSIs were 3D-printed in Dental SG resin on a Formlabs Form2 3D printer. The NDI Polaris Spectra optical tracking system was used to obtain the real-time position of the reference frame and the pointer.

We developed a custom module in 3D Slicer [117], a free and open-source multi-platform software package widely used for clinical and biomedical applications. We used the SlicerIGT kit [202] to develop our customized graphical user interface for surgical navigation

and the PLUS toolkit [203] for communication with the tracker through OpenIGTLink. Our module allowed the visualization of the models for each case (pelvis, planes, PSIs, and reference frame) and recording points for analysis (**Figure 4.2**). The user could modify the models' visibility. The point of view could also be changed manually or by selecting one of the predefined views (lateral, superior-inferior, or anterior-posterior) shown on the left panel in **Figure 4.2**.

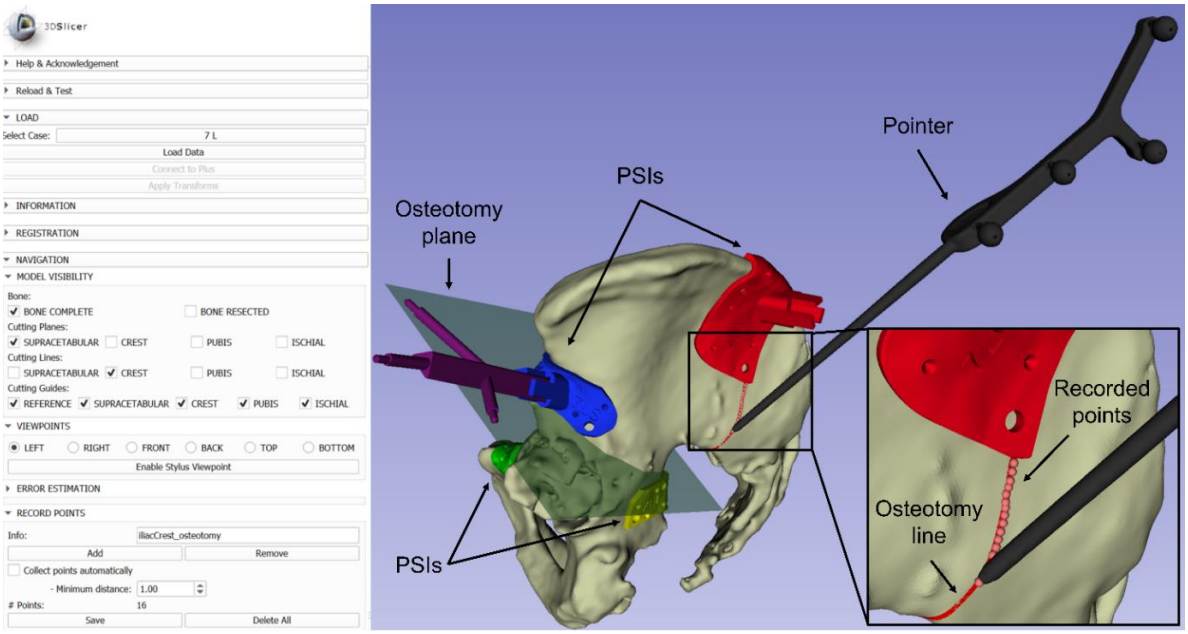

Figure 4.2. Module developed in 3D Slicer for surgical navigation of each hemipelvis.

Five experienced surgeons participated in the experiment placing PSIs. Surgical navigation was performed using the developed software. For each hemipelvis, the experiment consisted of the following steps (**Figure 4.3**):

1. PSIs placement and fixation with screws
2. Attachment of the dynamic reference in the C or S PSI
3. Point-based registration with the C or S PSI
4. Recording of pinholes from the four PSIs (C,S,I and P)
5. Navigation of the C or S osteotomy
6. Recording of points along the navigated osteotomy

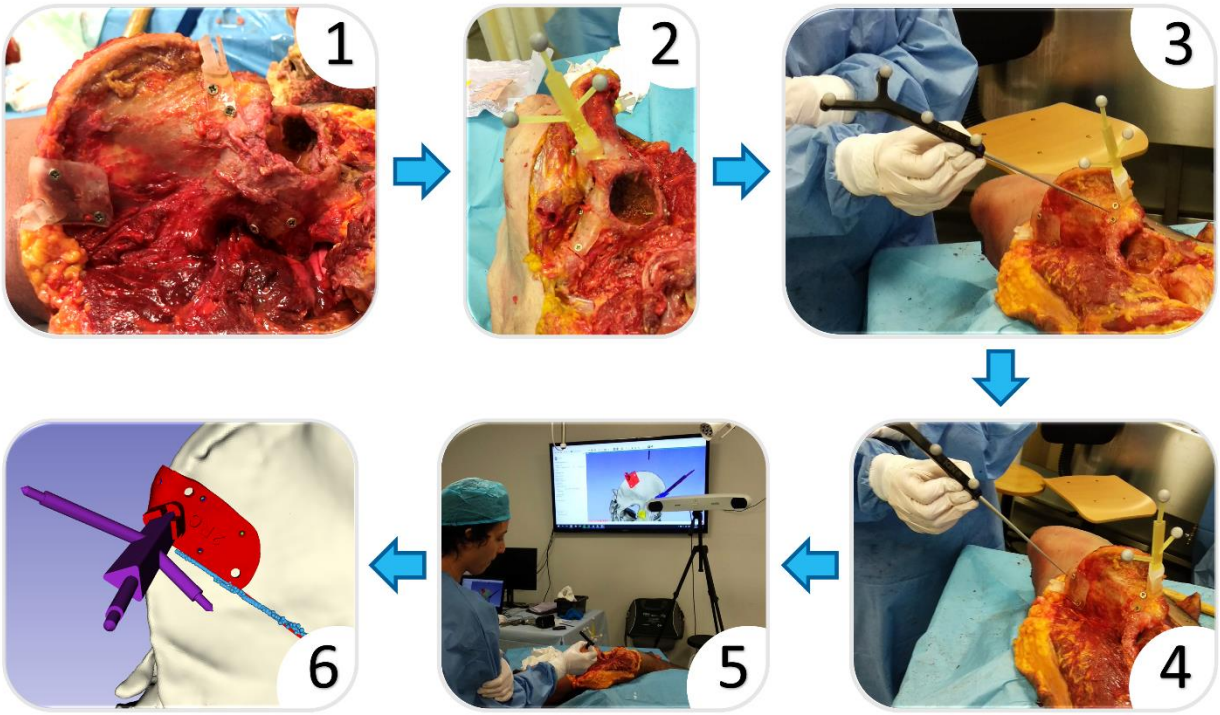

Figure 4.3. Steps followed for each case during the experiment: (**1**) PSIs placement and fixation; (**2**) reference frame placement; (**3**) registration; (**4**) recording of points in all PSIs; (**5**) navigation of osteotomy; (**6**) recording of points along the navigated osteotomy.

Osteotomies were navigated to validate our setup, and points were recorded along the osteotomy to visually compare them with the plane displayed in the virtual navigation scene. We developed a questionnaire to address the main contributions and possible limitations of the proposed setup (**Figure 4.4**). The survey included questions regarding the reference frame installation through the PSI, the use of small PSIs, and the registration with artificial landmarks located in the PSIs. We were also interested in the difficulty perceived by surgeons regarding the placement of each PSI and the use of surgical navigation and 3D-printed PSIs. The questionnaire was developed in Google Forms and sent to the surgeons after the experiment.

4.3.3. Analysis of navigation accuracy

During navigation, the only feedback provided by the system regarding accuracy is the fiducial registration error. However, as Fitzpatrick et al. [99] concluded, this value is a poor indicator of the error found in the target region. Errors in the target area can only be verified visually by comparing the position of the tool in the patient and its position in the image or 3D model. Similarly, the placement of the PSIs can only be checked visually. Our

work studies the error distribution in the target area using the data collected intraoperatively and a postoperative CT, that allowed obtaining the real locations of the PSIs.

The postoperative CT was acquired for each pelvis with the PSIs still attached. The position of the PSIs was extracted from the CTs as well as the bone models. Preoperative and postoperative data of the same case were aligned using a model to model registration (based on iterative closest points algorithm [182]) between the bone models. We extracted the transformation between preoperative and postoperative PSIs as explained in chapter 3. These transformations allowed us to characterize the displacement with respect to the planning position.

The data collected during the experiment (recorded points in all PSIs), together with the pre and postoperative data, were used to analyze the accuracy provided by the navigation system. Our analysis considered different scenarios, defined according to the pelvic tumor resection classification by Enneking and Dunham [204] (**Figure 4.5**). In each scenario, the PSIs and the reference frame are placed in different locations. **Figure 4.6** presents the resulting configurations considered for each of these scenarios.

All these configurations could be analyzed for every specimen by performing the following procedure. As the landmarks for all PSIs were collected in every hemipelvis, we can choose the points from one (or more) PSIs to simulate a specific scenario where those points are used for registration with the virtual plan. The virtual scene will then show the osteotomy planes at a particular position, and those planes would be used to guide the osteotomies. However, this position displayed by the navigation scene may not correspond to the correct one due to registration errors. These registration errors can arise from navigation inaccuracies, fiducial localization errors, and incorrect positioning of PSIs. As we have the real position of the PSIs from the postoperative CT (which represents the real scene), we can register the navigation scene with the real scene using the collected landmarks from all PSIs. That way, we can compare the position of the osteotomies according to that particular navigation scene with their real position. Therefore, we can quantify the navigation error for that scenario. **Figure 4.7** represents these steps graphically. The diagram uses as an example the scenario where registration is performed using only the landmarks from the S PSI.

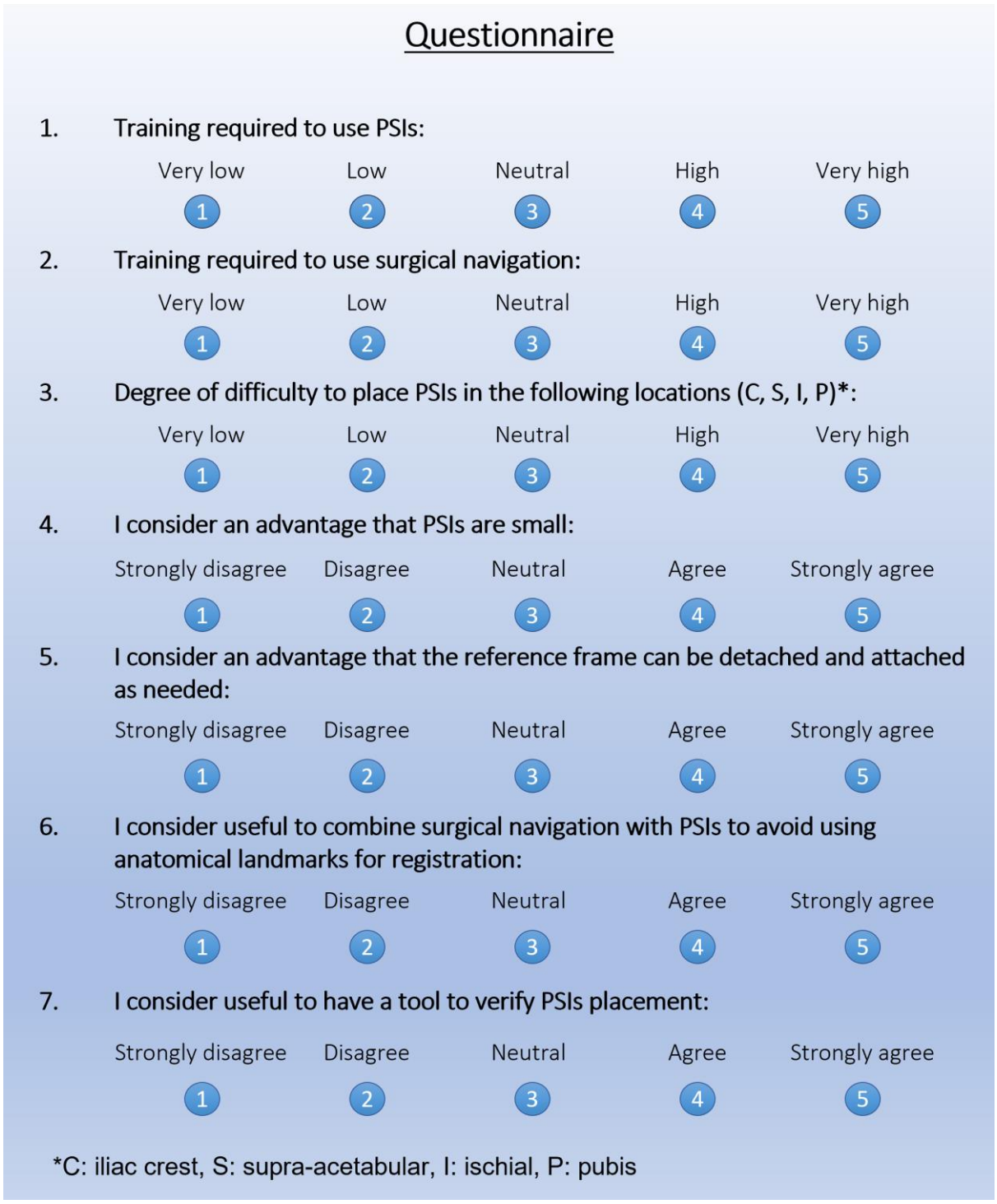

Figure 4.4. Questionnaire answered by surgeons.

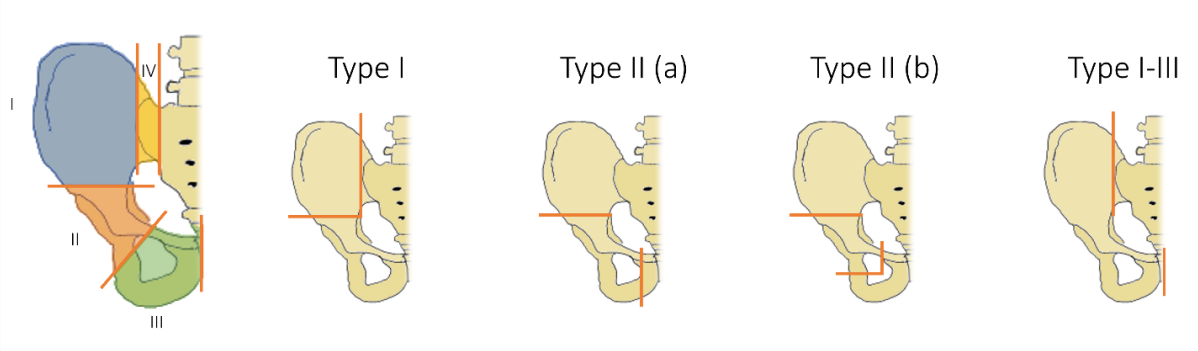

Figure 4.5. Pelvic tumor resection classification by Enneking and Dunham.

Following this procedure, we analyzed the errors in every configuration. As mentioned earlier, we can identify two sources of error in each scenario: PSI placement and navigation. As placement errors have already been analyzed in chapter 3, here we focus on the errors introduced only by navigation and the ones resulting from the combination of both sources (total error). Total errors result from navigation errors (inaccuracies introduced by the tracking device or the user when recording the registration points) and incorrect placement of the PSIs, making the virtual plan differ from the real scene. In order to extract the navigation errors separately, we can assume PSIs were correctly placed. Therefore, we can take the real scene as the virtual plan. **Figure 4.7** represents the steps for the extraction of the two error types. The diagram shows how virtual and real scenes coincide when computing the navigation error but differ for the computation of the total error.

We measured the maximum osteotomy deviation (MOD) for each configuration. That is the maximum distance between the osteotomy that would be performed based on the navigation scene and the osteotomy defined in the virtual plan. To compute this distance, we first extracted the intersection of the osteotomy plane in the virtual plan with the bone, generating a 3D model (point cloud). Then we transformed that osteotomy plane to the real scene to place it where the cut would be performed in that specific scenario. Once again, we extracted the intersection of that plane with the bone. Finally, we computed the maximum distance between both models. For that, we computed the distance of every point in one intersection model to its closest point in the other intersection model. The MOD was defined as the maximum distance obtained from this computation. **Figure 4.8** includes a graphical representation of the procedure.

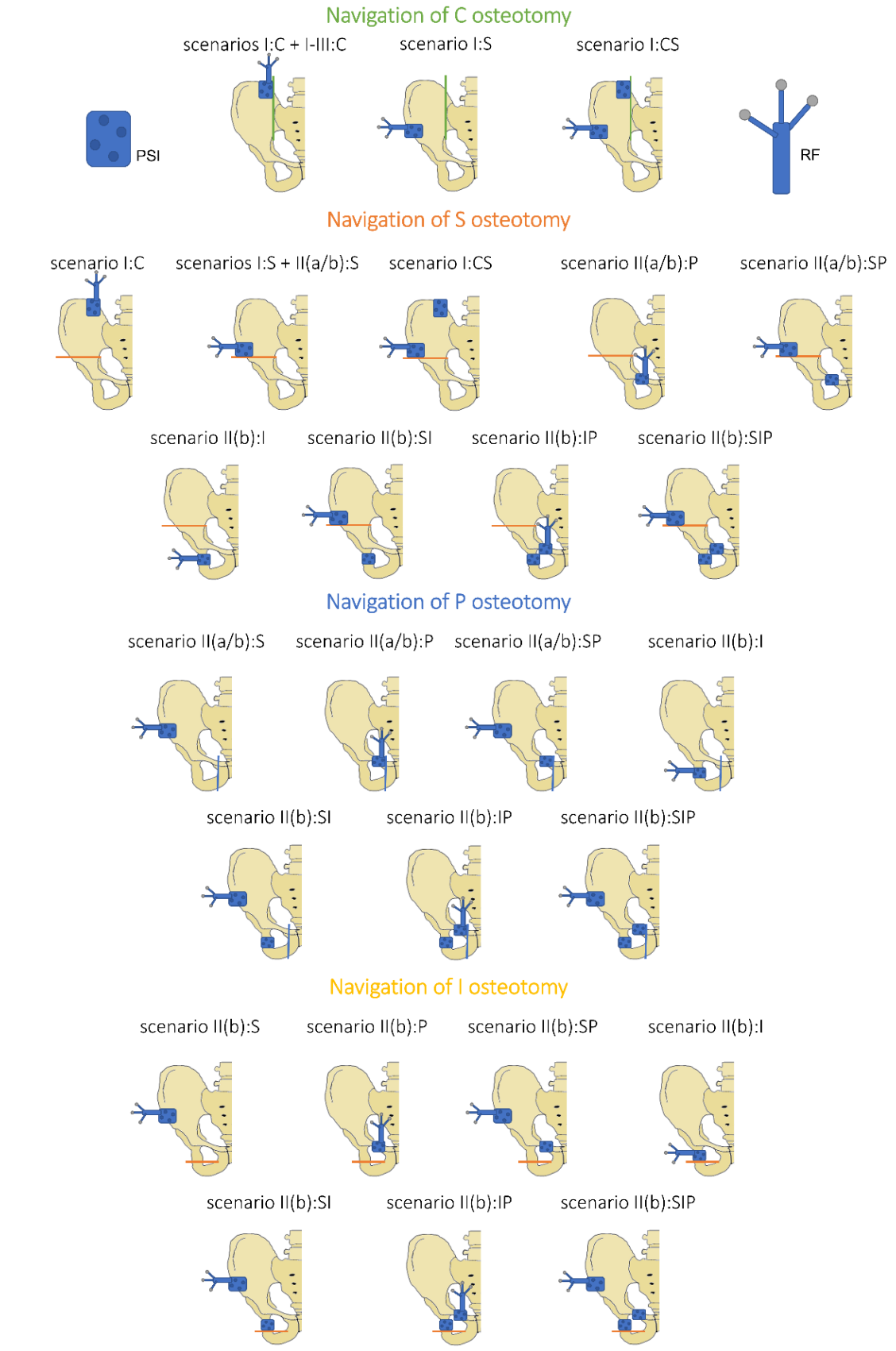

Figure 4.6. Configurations of PSIs and reference frame (RF) for each scenario considered in the analysis. The colored lines indicate the osteotomies involved in each configuration.

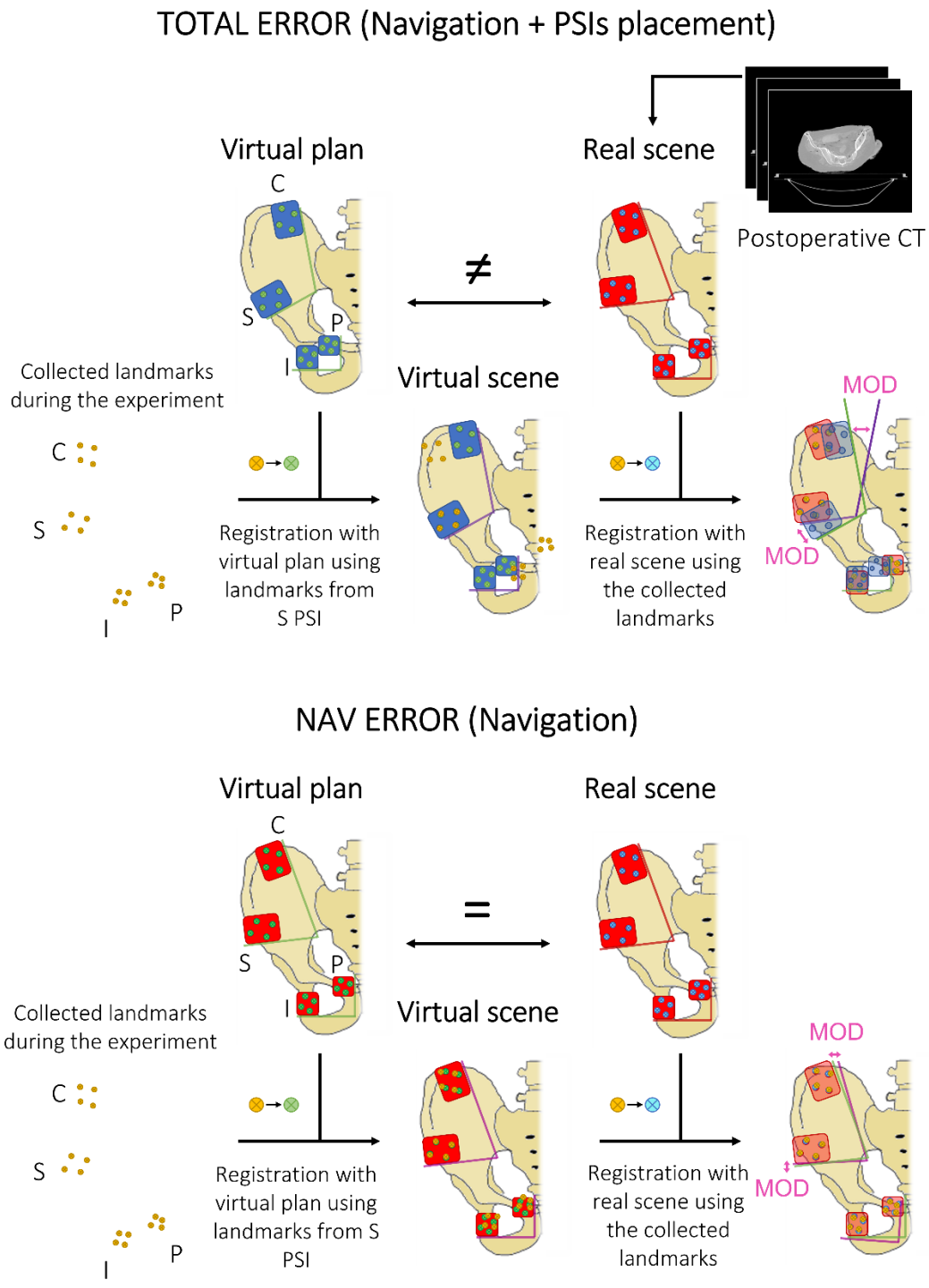

Figure 4.7. Representation of the steps followed to analyze total and navigation errors in every configuration of PSIs, illustrated with the scenario in which only S PSI is used for registration.

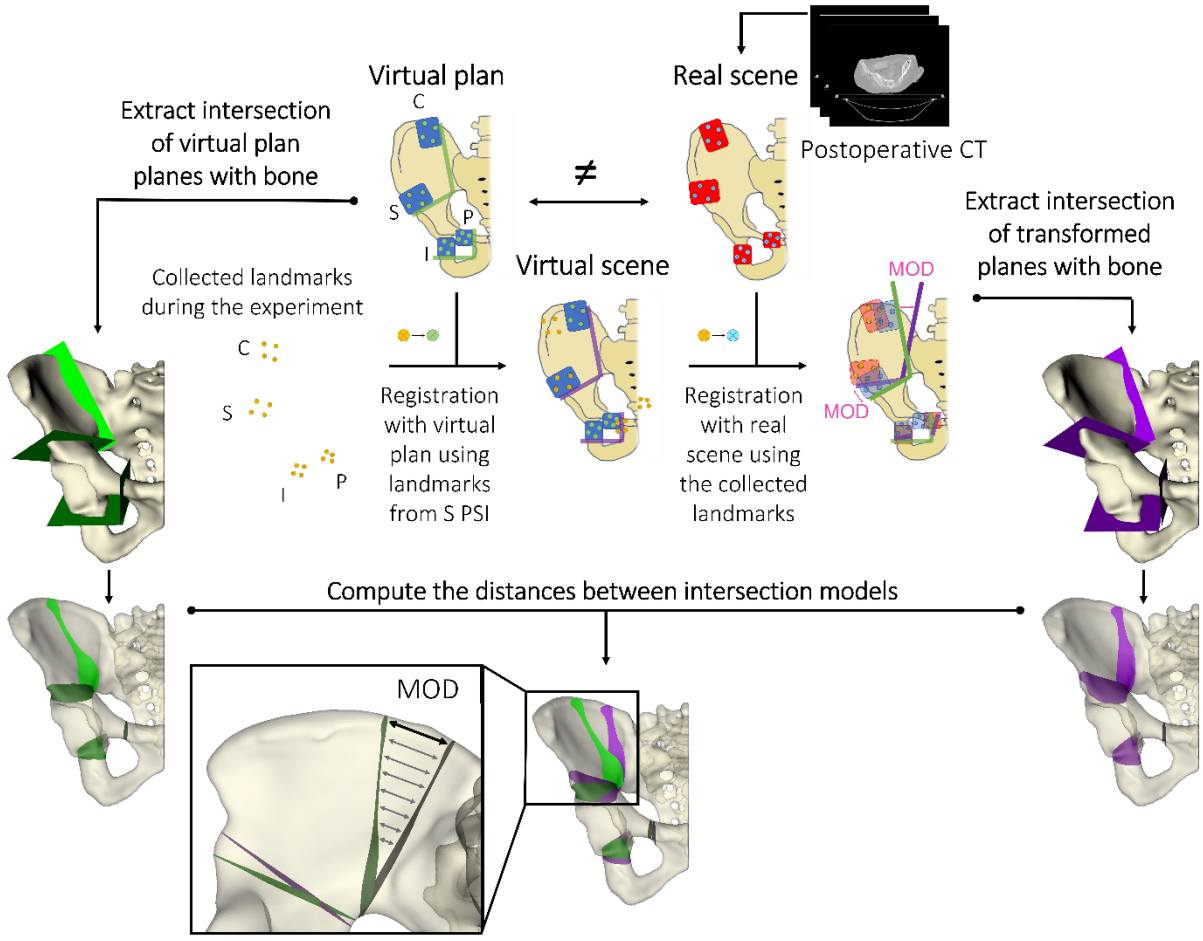

Figure 4.8. Workflow for the computation of maximum osteotomy deviation (MOD).

As navigation can be used for other purposes apart from guiding the osteotomies (for instance, to identify the tumor and other anatomical structures), we also computed the error distribution across the bone surface. First, all data was centered and aligned with the RAS (Right, Anterior, Superior) coordinate system. Then, we extracted the transform between virtual and real scenes for every case and applied it to a pelvis model used as a reference. We measured the distances between corresponding points of the original and the transformed models. Finally, we computed the mean error of every surface point for each configuration.

4.4. Results

4.4.1. Design and validation of the reference frame attachment

The reference frame was inserted 20 times in the socket. We recorded the pose for each insertion and computed the deviations from the mean (calculated from the 20 repetitions) to report the placement precision. The resulting mean, standard deviation, and maximum deviation values for translations and rotations are presented in **Table 4.1** for each axis defined in **Figure 4.1**.

Table 4.1. Descriptive statistics of translation (T) and rotation (R) errors in every axis (x, y, z) for the insertion of the reference frame in the socket.

	Tx	Ty	Tz	Rx	Ry	Rz
Mean	0.02	0.02	0.02	0.15	0.22	0.07
SD	0.01	0.02	0.02	0.12	0.14	0.04
Max.	0.05	0.05	0.09	0.50	0.57	0.20

Translations present a mean deviation of 0.02 mm and a standard deviation of 0.02 mm or lower in all axes. Maximum deviations in translations are below 0.10 mm. Mean rotations are below 0.25˚, with a standard deviation below 0.15˚ and maximum rotations below 0.6˚. The direction of the insertion (z-axis) presents the highest translation and the lowest rotations.

4.4.2. Cadaveric experiment

PSIs were rigidly fixed to the bone with screws, and the navigation was performed successfully. The reference frame was easily inserted in all PSIs, and it was correctly tracked during the experiment without interfering with the procedure. The surgeons were able to navigate the osteotomies using the tracked tools and the navigation system.

Table 4.2 collects valuable feedback from the surgeons involved in the experiment. Surgeons agree that the use of both techniques requires training but presents an advantage due to the reduced sizes of PSIs, the ability to attach and detach the reference frame, and the substitution of anatomical with artificial landmarks for registration. They also agree that having a tool to verify PSIs placement would be very valuable.

Table 4.2. Results from the questionnaire.

		Individual scores (per surgeon)					
Question		1	2	3	4	5	Avg. score
1		4	3	3	4	3	3.4
2		5	5	3	5	5	4.6
3	C	4	1	2	5	5	3.4
3	S	3	1	4	3	4	3
3	I	5	1	4	3	3	3.2
3	P	4	1	4	3	3	3
4		5	4	5	4	5	4.6
5		5	5	5	5	5	5
6		5	5	5	5	5	5
7		5	5	5	5	5	5

4.4.3. Analysis of navigation accuracy: maximum osteotomy deviation

For every hemipelvis, we extracted the MOD in each region (C, S, I and P) with every configuration presented in **Figure 4.6**. **Table 4.3** shows the mean and standard deviation values in each osteotomy plane for the different combinations of PSIs used for registration. The results are divided into "Total" errors (which result from placement and navigation errors) and "Nav" errors (which are only a result of navigation errors).

The results demonstrate how using multiple PSIs for registration improves navigation accuracy, providing the lowest deviation errors. For the total errors in C and S osteotomies, using both PSIs for registration gives MODs with a mean value of 5.90 mm in C and 1.65 mm in S. For navigation errors, we can observe the same behavior, where registration with C and S PSIs gives a mean error of 1.29 mm in C and 0.76 mm in S. Therefore, when performing type I resections, it is best to use both PSIs. For type I-III resections, deviations depend only on the correct placement in C, where the mean error is 8.18 mm.

Using S and P PSIs shows the highest accuracy for type II(a) resections, with mean values of 3.46 mm in S and 2.47 mm in P for total errors and 2.86 mm and 0.83 mm for navigation errors. For type II(b) resections, MODs present the lowest values when using S, I, and P PSIs for registration. The mean values for the total errors are 3.44 mm in S, 1.88 mm in I, and 1.97 mm in P. For navigation errors, these values are 1.32 mm, 0.72 mm, and 0.66 mm, respectively.

Table 4.3. Mean and standard deviation of the maximum osteotomy deviations in each configuration (values are in mm). The lowest values for each osteotomy are presented in bold.

			PSIs used for registration								
Osteotomy	Error Type	Metric	C	S	I	P	CS	SI	SP	IP	SIP
C	Total	Mean	8.18	7.48			**5.90**				
		SD	4.01	4.79			3.84				
	Navigation	Mean	2.58	5.64			**1.29**				
		SD	2.23	2.50			1.17				
S	Total	Mean	9.03	4.73	4.95	6.12	**1.65**	4.48	3.46	9.70	**3.44**
		SD	7.67	4.37	3.64	6.62	0.93	3.15	1.90	9.31	2.33
	Navigation	Mean	4.57	2.60	4.60	6.19	**0.76**	1.45	2.86	2.06	**1.32**
		SD	3.56	1.29	3.14	4.57	0.33	1.03	0.74	1.46	0.75
I	Total	Mean		4.27	3.47	9.83		2.12	3.64	4.17	**1.88**
		SD		1.80	2.34	6.09		0.83	1.67	2.26	0.64
	Navigation	Mean		1.58	1.36	8.99		1.02	2.95	1.44	**0.72**
		SD		0.59	0.65	6.10		0.91	1.72	0.87	0.48
P	Total	Mean		2.29	4.48	3.13		4.18	2.47	2.48	**1.97**
		SD		1.36	4.96	1.60		3.63	1.41	1.62	1.16
	Navigation	Mean		1.10	4.02	1.37		2.22	0.83	0.93	**0.66**
		SD		0.81	3.68	0.57		1.85	0.56	0.70	0.45

When using multiple PSIs, high patient-image registration errors can be indicative of incorrect placements. In these situations, PSIs can be repositioned until a lower error is achieved. As navigation accuracy highly depends on the correct positioning of the PSIs, low registration errors can be used to ensure precise navigated osteotomies. To determine which registration values are acceptable for navigation, we have selected from total and navigation data those scenarios using multiple PSIs for registration. In particular, we have chosen those cases presenting the optimal configuration in each resection (registration with C and S PSIs for type I, with S and P PSIs for type II(a), and with S, I, and P PSIs for type II(b)). From this data, we have extracted those cases where MODs are below 2 mm, and we have analyzed their corresponding registration errors. We have also obtained cases with registration errors below 2 mm to identify their MOD. The results for each analysis are presented in **Table 4.4**.

Table 4.4. Registration errors for maximum osteotomy deviations (MODs) below 2 mm and MODs for registration errors below 2 mm. The table presents the number of cases used, mean, standard deviation, and 75th quartile for each resection type with their optimal registration configurations.

		Type I C & S	Type II (a) S & P	Type II (b) S, I & P
Registration errors for MODs < 2 mm	Number of cases	11	12	7
	Mean	1.90	2.54	2.46
	SD	0.99	1.32	1.40
	75%	2.38	3.67	4.07
MODs for registration errors < 2 mm	Number of cases	9	8	7
	Mean	1.73	1.23	1.32
	SD	2.46	0.97	0.99
	75%	2.01	1.56	1.70

In cases with MOD below 2 mm, most registration errors are between 1 and 4 mm. Mean values are lower than 2 mm in type I resections and below 2.6 mm for type II. 75% of the cases in type I resections present registration errors below 2.38 mm, and below 3.67 mm and 4.07 mm in type II(a) and type II(b), respectively. Registration errors below 2 mm present MODs of 2 mm or lower in 75% of the cases.

Therefore, in these configurations, registration errors lower or equal to 2 mm ensure a precise navigated osteotomy in most cases, with maximum deviations below 2 mm.

4.4.4. Analysis of navigation accuracy: error distribution

Apart from measuring the MOD, we analyzed the navigation error distribution across the bone's surface for each configuration. The results are presented in **Figure 4.9**, where one of the hemipelvis from the study is used to represent the distances computed with the data from all cases. These values indicate the errors we would find in all the hemipelvis, assuming a correct placement of PSIs.

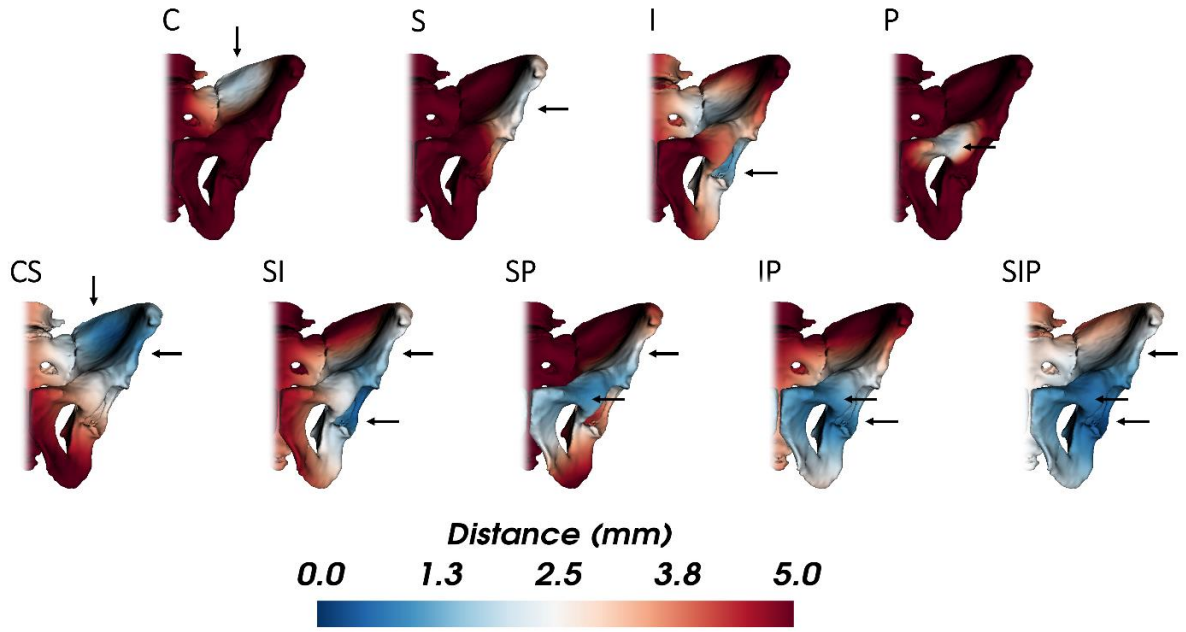

Figure 4.9. Navigation error distribution for every configuration of PSIs considered for the analysis. Arrows indicate the position of the PSIs.

The results show how the error is lower in the areas close to the PSIs used for registration. When using multiple PSIs, errors are reduced not only in the PSIs location but also in the area between them. The configuration CS (registration with C and S) presents the best navigation results in the ilium region with errors below 2 mm. As for the acetabular region, the SIP configuration presents errors below 2 mm, and below 5 mm in all the hemipelvis.

4.5. Discussion

The resection of tumors located in the pelvis becomes very challenging due to the complex morphology of the bone and the proximity to vital structures. Tools such as surgical navigation or PSIs have shown improvements in precision, but they also result in more invasive approaches. In this study, we introduce a new, less invasive solution combining both tools. The proposed setup has been tested and validated in a realistic environment with cadavers.

As an alternative to the fixation to the patient's bone, we propose using PSIs for an easier and more convenient installation of the navigation's reference frame, which can be attached only when necessary. Our study has evaluated the repeatability of its placement,

which avoids performing the registration for every new insertion. The identified placement error was below 0.1 mm in translation and 0.6 in rotation. These values are negligible considering the error introduced by the optical tracking system [205].

PSIs also become a valuable tool for registration since artificial landmarks included in the PSIs replace anatomical landmarks and surface points, reducing bone exposure and solving some of their limitations [106], [190], [206]. Besides, they are easier to identify, reducing intra- and interobserver variability in the registration process. Previous studies have also replaced anatomical landmarks with bone-mounted fiducial markers improving registration results [108], [193]. However, these solutions usually require the implantation of titanium pins prior to the preoperative CT and are more invasive. Nevertheless, if registration relies on artificial landmarks located in the PSIs, the navigation accuracy is highly dependent on their correct placement, which is challenging to ensure as presented in chapter 3. If registration is computed from a single PSI, low registration errors can be misleading. However, when using multiple PSIs, high registration errors may indicate incorrect placements that can then be rectified. Hence, low registration errors can ensure precise navigation. We have identified the registration errors associated with precise osteotomies when using multiple PSIs. The results show that, in most cases, 2 mm or lower registration errors ensure MODs below 2 mm.

PSIs positions depend on the surgical scenario and the planned osteotomies, but thanks to a novel methodology, we could analyze different PSI and osteotomy combinations in a single specimen. During the experiment, PSIs were placed in the four most common osteotomy regions (C, S, I, and P). We recorded the position of all the artificial landmarks present in the PSIs. From the data collected during the experiment with the six cadaveric specimens, we analyzed the system's precision when performing registration with different combinations of PSIs for type I, type II, and type I-III resections [204]. The results presented in **Table 4.3** and **Figure 4.9** demonstrate how using multiple PSIs for registration always offers the highest precision in the area of interest. These results align with previous studies from Fitzpatrick et al. [99] and West et al. [100], who studied how the configuration of the landmarks used for registration affects the error distribution in the navigated surgical field. They found that low errors can be achieved in the target region if fiducials are widely spread and surrounding the area. Ideally, the target would be placed in the centroid of the markers. Hence, using multiple PSIs (composing a set of landmarks spread and surrounding the navigation area) presents lower errors. When using a single PSI for registration, as all

registration landmarks are distributed in the PSI, the errors in that area are low. Inaccuracies in the localization of fiducials can result in small translations and rotations close to the landmarks. However, these errors increase with distance, so we obtain high errors far from the PSI used for registration.

Therefore, if we consider the scenarios presented in **Figure 4.6**, both C and S PSIs should be used for type I resections, S, I, and P should be combined for type II or, if the ischial osteotomy is not performed, only S and P. For type I-III resections, as the PSI in C is the only one used, incorrect placement can cause high navigation errors. Therefore, in this case, it would be advisable to use additional PSIs in the iliac crest or the symphysis to reduce errors and verify correct placement. In this and any other scenarios, PSIs can be used exclusively for registration, avoiding their fixation to the bone.

The proposed setup was tested in cadavers following a realistic surgical approach, where surgeons successfully placed PSIs and navigated the osteotomies. Overall feedback from the surgeons was very positive. They all agreed that the setup proposal, including the reduced size of PSIs, the reference frame's installation, and the use of artificial landmarks, presented an advantage compared to conventional procedures or using either technology independently. They also concurred that navigation requires more training and experience than PSIs. However, there were some discrepancies regarding the difficulty in PSI placement for each region. Although C PSIs are the ones presenting higher placement errors followed by S PSIs [207], some surgeons found the placement more challenging in other regions whereas others considered all regions equally tricky. These incoherent results highlight the difficulty of identifying erroneous placements, a significant limitation of PSIs. Surgeons agreed on the usefulness of a verification tool for PSIs placement, which would avoid high errors during guidance. In our setup, registration errors can be used for this purpose.

The MODs obtained considering placement errors are similar to those obtained in other studies using only surgical navigation or PSIs. Wong et al. [178] studied the mean MODs in supra-acetabular and partial-acetabular resections with both techniques, obtaining errors of 3.6 mm with surgical navigation and 2.6 mm with large and multiplanar PSIs. Sallent et al. [177] used PSIs in 5 cadaveric specimens obtaining mean MODs of 5 mm in the sacroiliac joint, 4 and 3.6 mm in the supra-acetabular region, 2.2 mm in the ischial osteotomies, and 0.8 and 1 mm in pubic osteotomies. Fehlberg et al. [106] obtained a median deviation of 3.3 mm in a series of 13 patients.

Our setup can be replicated by following the indications given for the design of the surgical guides [207] and the fabrication of the 3D-printed tools. If Dental SG resin is used for 3D printing, it should be stored following the manufacturer's indications (a cool, dry place out of direct sunlight in containers at 10 – 25 ˚C). The orientation of the surgical guides during printing should be carefully studied to ensure smoothness in the surface in contact with the patient. Supports added inside the socket or in the reference frame should be thoroughly removed, and the correct insertion of the reference frame in the socket and the optical markers in the posts should be verified before use. Models of the reference frame and socket are available at https://dx.doi.org/10.21227/zcbr-k673.

During navigation, it is essential to ensure adequate lightning conditions in the surgical field. Materials presenting similar properties to the optical markers could reflect the infrared light emitted by the optical tracker and result in tracking errors.

4.6. Conclusions

To conclude, we have proposed and validated a new setup for pelvic tumor resections using surgical navigation and PSIs. The novelty of our study relies upon the fact that both techniques, 3D printing and image-guided surgery, are combined to provide a less invasive setup. This invasiveness is reduced by using small PSIs, which also act as artificial landmarks.

We have also presented a new and more convenient installation of the dynamic reference frame using a socket included in the PSI. This installation has demonstrated repeatability, which allows the removal of the reference frame without the need to repeat the registration step every time it is reinserted.

A realistic experiment on cadavers allowed us to describe the optimal PSIs configuration in three different resection scenarios. We computed the MODs for all cases and identified the registration errors minimizing these deviations. Additionally, we studied the distribution of the navigation error in the target regions, which to our knowledge, has not been previously analyzed. We can conclude that the best results are achieved when at least two PSIs are used surrounding the area of interest. Our results show how, with our setup, correct PSI placements lead to low navigation errors and high accuracy while providing a less invasive surgical approach.

The content of this chapter has been published in IEEE Access:

M. García-Sevilla, L. Mediavilla-Santos, R. Moreta-Martinez, D. García-Mato, R. Pérez-Mañanes, J.A. Calvo-Haro, J Pascau. "Combining Surgical Navigation and 3D Printing for Less Invasive Pelvic Tumor Resections". IEEE Access, vol. 9, pp. 133541-133551 (2021).

5

USING AR TO GUIDE PSIs PLACEMENT IN PELVIC TUMOR RESECTIONS

5.1. Introduction

The use of PSIs for surgical guidance is widely extended [177], [185], [196], [197]. These 3D-printed tools are designed to fit in a particular region of the patient's bone and guide the osteotomies. In contrast to surgical navigation, PSIs do not provide real-time visual feedback, but they have reported similar accuracy [178] and allow surgeons to focus on the surgical field rather than looking at the navigation display. They are also easier to use, more convenient, and faster.

However, the accuracy of PSIs is subject to the correctness of their placement, which highly depends on PSI shape and bone morphology. Finding the correct position in smooth and homogeneous regions becomes challenging, and tissue covering the bone can also hamper their installation. Moreover, the placement cannot be verified objectively during the intervention [178], increasing the risk of high osteotomy deviations resulting from incorrect positioning. In the pelvis, the ilium presents a large and homogenous shape, and thus the installation of PSIs for tumor resection is more prone to errors [177], [207], [208]. Therefore, additional tools assisting PSI placement would be of great value in these surgical scenarios.

Another technology that is gaining popularity in surgical procedures, including orthopedic surgery, is AR [209], [210]. It displays computer-generated elements which augment and enrich the visualization of the physical world. Devices such as smartphones or head-mounted displays are commonly used for this purpose. Inside the operating room, AR mainly focuses on visualizing the tumor and other anatomical structures [129], [136], [147], enhancing guidance during resections. The virtual models can be displayed in accordance

with the patient's anatomy by performing a registration step, which is either calculated manually [211], using tracking systems [212], [213], through advanced algorithms for surface registration [214], or by markers detected with pattern recognition techniques [215]. A recent study presented a solution consisting of a 3D-printed pattern that can be detected by an RGB (red, green, blue) camera [129]. This pattern is attached to a PSI, whose position in the patient is known, and therefore the virtual elements are displayed in place. Several studies have proved this solution evaluating feasibility, convenience, and accuracy in different surgical scenarios [129], [130], [136].

Studies focused on estimating the accuracy provided by these technologies are performed in a living subject [194], a cadaver [177], [178], [207], [216], or a phantom [136], [179], [197]. Although phantoms provide a less realistic environment, they present several advantages apart from avoiding patient risks. They are readily available and can provide more consistent results as they offer a controlled environment where the anatomy is maintained. It is more difficult to compare results between cases in real surgical settings, as the anatomy and other factors change and need to be considered for the analysis. Depending on the application, phantoms can be designed replicating the anatomical structures or the composition of human tissue in more or less detail. Also, thanks to 3D printing, patient-specific phantoms can be generated more easily for personalized measurements [217]. Several studies have used phantoms to report the accuracy results from CAS, PSIs, or AR in pelvic tumor resections [179], [197]. These phantoms consist of a replica of the bone, usually made of plastic. However, when evaluating PSIs placement, as the smoothness and homogeneity of the bone's surface and the presence of tissue are essential factors, the results provided by these phantoms may not be realistic enough.

5.2. Objective

In this study, we propose to use AR as a tool to guide PSIs placement in pelvic tumor resections, overlying virtual models of the PSIs on the patient to indicate their planned position to surgeons. These models are displayed in place thanks to a 3D-printed AR marker attached to a PSI. We assess the accuracy provided by the system on two phantoms, a conventional one consisting only of the plastic pelvic bone and a realistic version including a layer of silicone simulating tissue. Six pairs of PSIs were designed representing six different scenarios for tumor resection in the ilium. Four users placed the PSIs in both phantoms

following three different methodologies: freehand, AR with a smartphone, and AR with a head-mounted display (HoloLens 2). The results prove the value of using AR to minimize placement errors, showing how simulated tissue in the phantom complicates placement and underlying the importance of the area where PSIs are installed.

5.3. Materials and Methods

We designed a phantom based on the CT image of a patient (**Figure 5.1 a**). The bone model was extracted with the 3D Slicer platform [117] through a segmentation process using thresholding and divided with a sagittal plane to keep only the right hemipelvis. Using Meshmixer software (Autodesk, Inc., San Rafael, CA, USA), we designed a base for the phantom to place it in a similar position to that found in an actual surgery ("floppy lateral" [218]). A reference frame was added to the design for navigation. Finally, the bone phantom was 3D-printed using the Ultimaker 3 Extended (Ultimaker B.V., Utrecht, Netherlands) desktop 3D printer in polylactic acid (PLA).

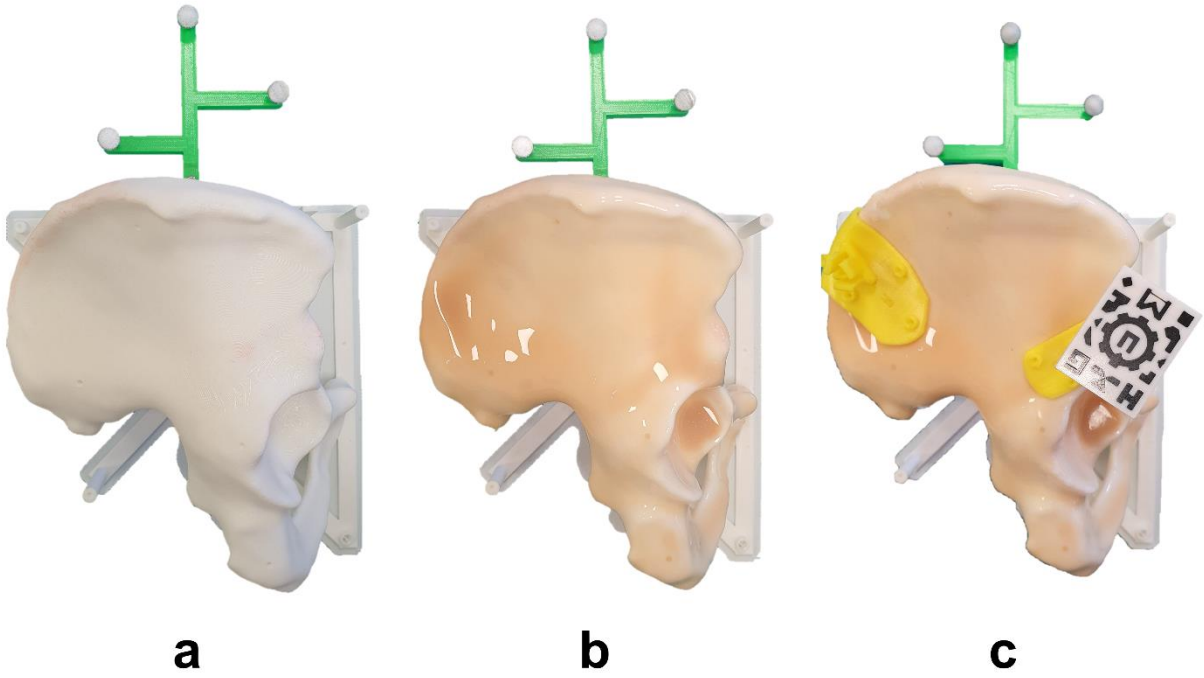

Figure 5.1. (**a**) Conventional bone phantom and (**b**) realistic phantom including a silicone layer. (**c**) PSIs and AR marker placed on the phantom.

Six scenarios were designed for tumor resections in the ilium (type I according to Enneking and Dunham's classification [204]). Each scenario was composed of two PSIs

indicating the osteotomies, one in the supra-acetabular region (S) and one in the iliac crest (C). The designed PSIs presented different sizes, shapes, and locations inside the target region. All PSIs were created in Meshmixer following the steps described in chapter 3 and 3D-printed in PLA (**Figure 5.1 c**).

Since PSIs are designed based on the bone model, they easily fit into the phantom, adapting to the surface like a puzzle. Only imperfections introduced during printing can hinder their placement. However, in a real scenario, there are other factors to consider that affect placement. As previously mentioned, there is frequently tissue in contact with the bone that has not been completely removed. Additionally, errors in the segmentation process can generate discrepancies between the virtual model and the patient's bone. Consequently, the surface of the PSIs would no longer match the bone seamlessly. Therefore, to better reproduce that real scenario, a silicone layer (Ecoflex^{TM} 00-10) was overlaid on the phantom, simulating the tissue, and adding complexity to the placement (**Figure 5.1 b**). The silicone was extended across the surface with a brush and cured within 4 hours.

An AR marker similar to the one described by Moreta-Martinez et al. [129] was used to display the virtual models overlaid on the phantom (**Figure 5.1 c**). This marker presented a unique black and white pattern that an RGB camera could recognize. It was 3D-printed in PLA with the Ultimaker 3 Extended 3D printer using the dual extruder functionality. We added a prism-shaped pillar to the design. Thus, the marker could be attached to the surgical guides by inserting it in a socket included in the PSIs. The position of the marker in the PSIs and the bone can be known with precision, as this attachment has demonstrated repeatability in previous studies [208].

Two software applications were developed to display the virtual models with AR, one to be deployed in a smartphone (**Figure 5.2 a**) and a similar one for the Microsoft HoloLens 2 device (**Figure 5.2 b**). Both applications were implemented on Unity platform (version 2019.3), using the Vuforia development kit (Parametric Technology Corporation Inc., Boston, MA, USA) for pattern recognition. Details regarding the development of an AR app for these purposes have been previously described by Moreta-Martinez et al. [219]. The applications included a menu to select the case and buttons to change the visibility and opacity of each model. In the smartphone app, this interaction was done on the screen. For the HoloLens 2, an interactive panel was shown in front of the user. The applications included the visualization of virtual models of the PSIs for that specific case, as well as a

model of the bone. The idea was to adjust the placement of S PSIs using the bone model as a reference. Once fixed, the planned position of C PSI would be displayed and used as guidance. The steps followed for AR guidance are therefore the following:

1. Placement of S PSI
2. Placement of AR marker in S PSI
3. Detection of marker with the AR device and visualization of the virtual models
4. Adjustment of S PSI so that virtual and physical bone models are visually aligned
5. Placement of C PSI so that it overlaps the overlayed virtual C PSI

We designed an experiment to assess the accuracy provided by the system. Four users without clinical background placed the PSIs for each of the six cases following three different methodologies: freehand, AR guidance with a smartphone, and AR (or Mixed Reality) guidance with the HoloLens 2 (**Figure 5.3**). In order to replicate the setup we would follow in the operating room, users held the smartphone with one hand and used the other one to place the PSIs. This setup allowed them to move the smartphone freely and change their point of view. As the smartphone can be introduced in a sterile case, the surgeons could hold it in the same way inside the operating room and maintain asepsis. Users repeated the process with the conventional phantom (without silicone) and the realistic phantom version (with silicone). We wanted to compare the results for each method and detect whether the addition of silicone significantly increased the placement difficulties. We were also interested in analyzing how the different shapes and locations of the PSIs affected the results. Additionally, we measured the time required for each user to place the PSIs for each scenario.

To record the position of the PSI during the experiment, we used the Polaris Spectra (NDI, Waterloo, ON, Canada) optical tracking system and the SlicerIGT [202] module for navigation included in the 3D Slicer software. The reference frame with spherical passive markers included in the bone phantom allowed to track its position (**Figure 5.3**). This reference frame was attached to the phantom using screws. Therefore, although the position of the reference frame can be known from the design, depending on how well the reference frame is fixed, small rotations or translations can be present. Hence, we performed a registration step to ensure that the target registration errors were minimized. Initial point-based registration was calculated from artificial landmarks recorded on the bone with a tracked pointer. To ensure an accurate registration, the result was then refined with the iterative closest point algorithm (ICP) [182] calculated on points recorded across the surface.

The registration was only performed once at the beginning and before adding the layer of silicone to ensure an accurate surface registration. This way, the registration used was maintained for all cases, methods, and phantom versions. The ICP registration error obtained was below 0.1 mm.

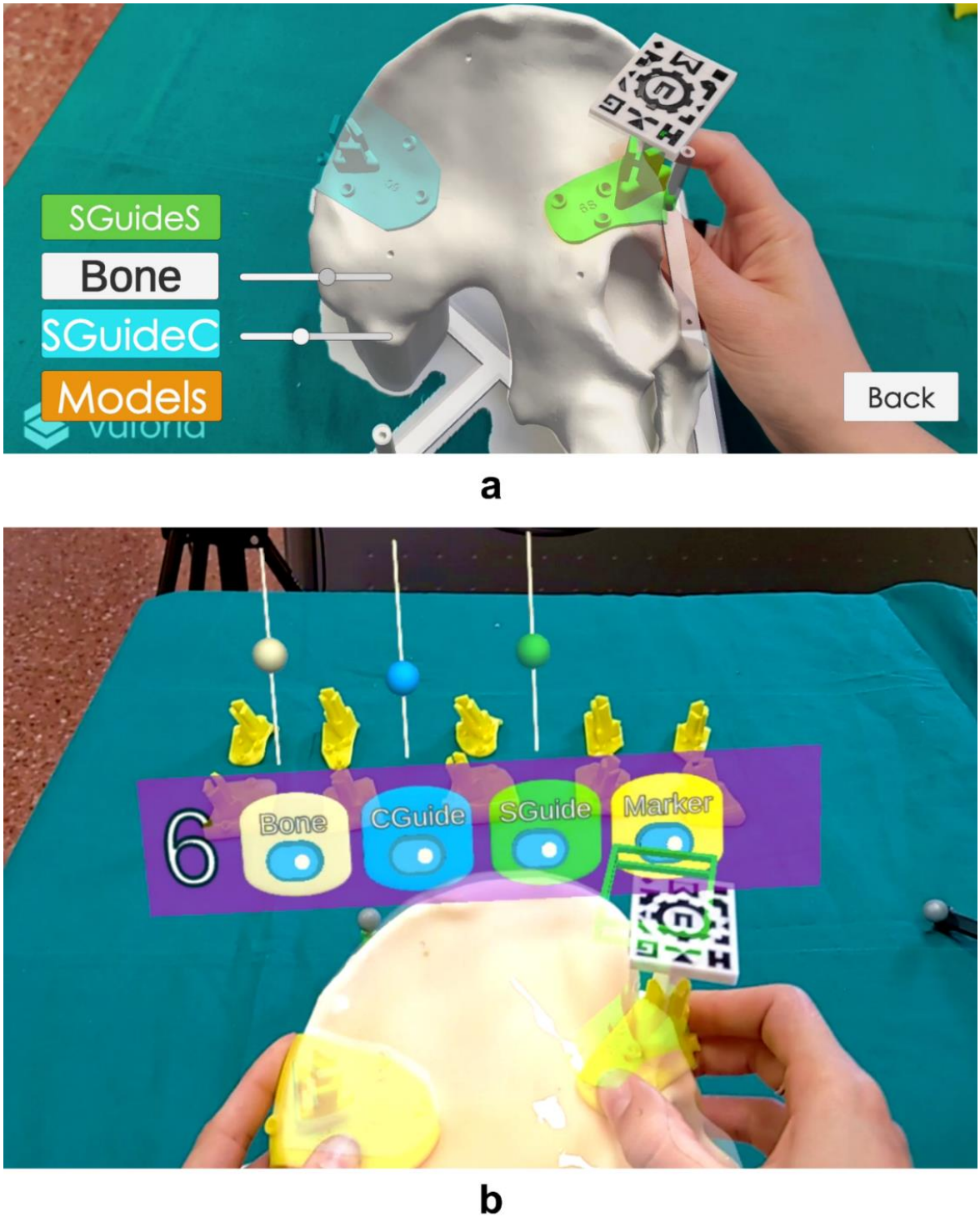

Figure 5.2. Screenshots of the AR visualization with the (**a**) smartphone and (**b**) HoloLens 2 during PSIs placement. Specific interactive panels of each device are shown, containing visibility and opacity buttons and sliders.

During the experiment, we obtained the position of four pinholes present in every PSI with the pointer. These points were later used to obtain the transformation of the PSI from its planned position to the actual one (planToReal). **Figure 5.4** represents the steps followed in each scenario for the assessment.

Figure 5.3. Setup for the assessment using (left) the HoloLens 2 and (right) the smartphone. The setups include the following elements: (**a**) optical tracker, (**b**) reference frame, (**c**) AR marker placed in PSI, (**d**) conventional, and (**e**) realistic phantom versions, (**f**) HoloLens 2, (**g**) smartphone, and (**h**) pointer.

When using PSIs, we are interested in minimizing the errors or deviations from the planned osteotomy. Hence, we extracted the maximum osteotomy deviation (MOD) for each PSI to measure the system's accuracy. For that, we first found the intersection of the planned osteotomy planes with the bone in S and C for each case. Then, we applied the corresponding planToReal transform to the planned osteotomy planes and extracted their intersection with the bone, obtaining a 3D model (point cloud). Finally, we computed the distances between every point in the planned intersection model to its closest point from the actual intersection

model. The maximum distance obtained for that case was defined as the MOD. These steps are represented graphically in **Figure 5.5**.

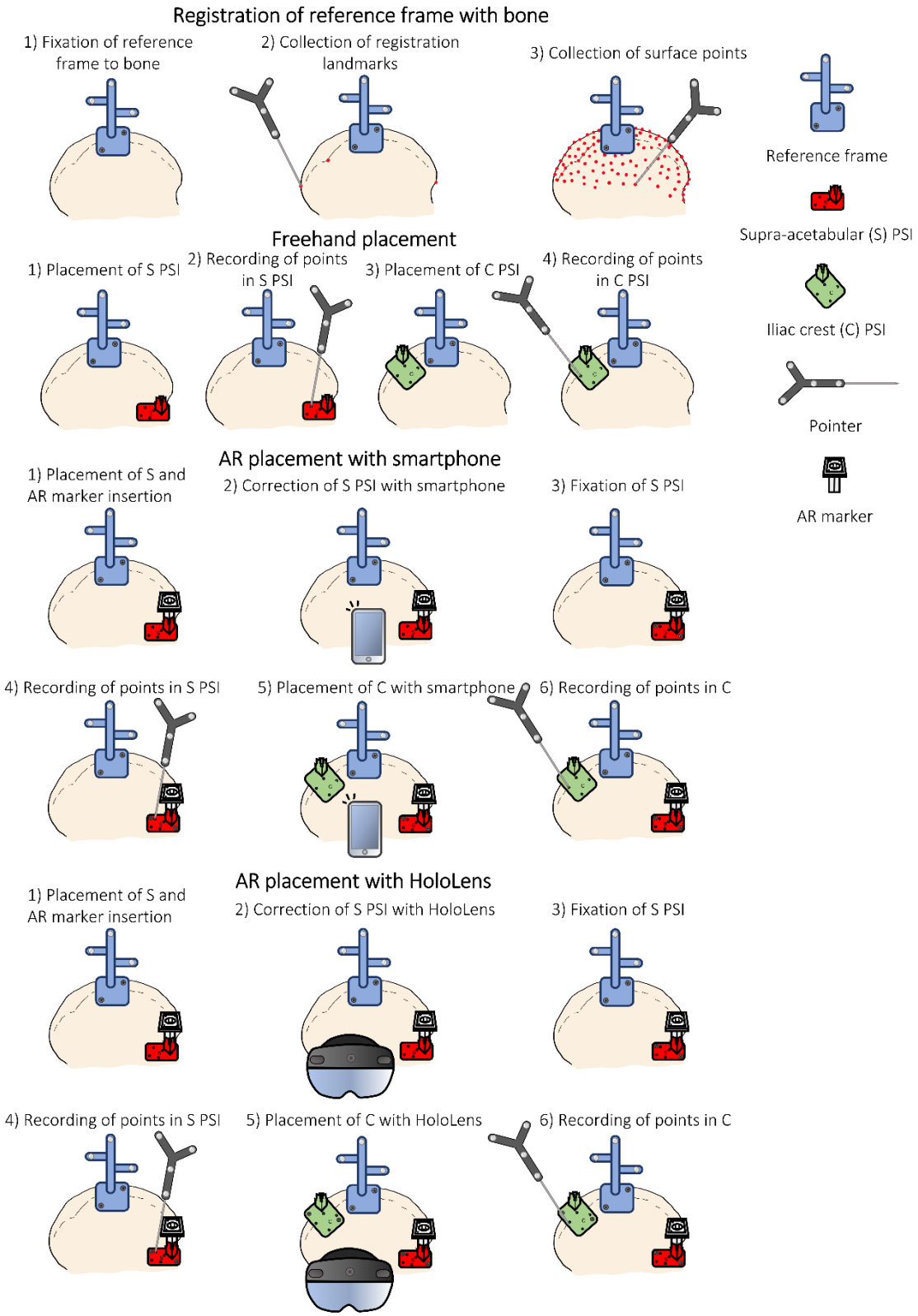

Figure 5.4. Steps followed during the experiment for registration and to record PSIs placements in each methodology.

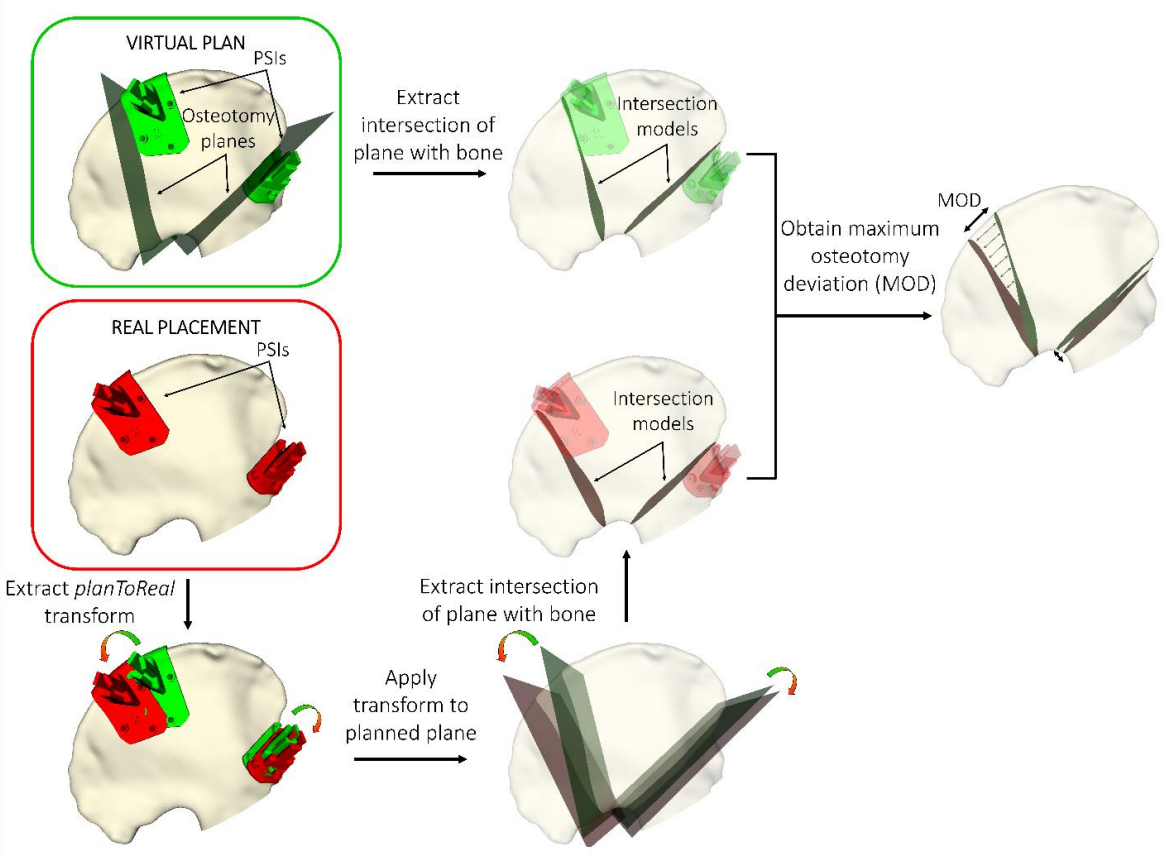

Figure 5.5. Computation of the MOD between planned and real osteotomy planes. The real osteotomy is defined by the PSI placement performed by the user.

Finally, we analyzed the statistical difference between the MODs obtained for each method (freehand, AR with smartphone and AR with HoloLens 2), phantom (conventional and realistic) and case, obtaining the median (Mdn) and interquartile range (IQR).

5.4. Results

We computed the MOD for all cases with the conventional and the realistic phantom. **Table 5.1** presents descriptive statistics of these measurements, where the results for each guidance method are presented divided by regions (C and S) and combined.

The results obtained using the smartphone or the HoloLens 2 present median values for MOD below 2 mm in the realistic phantom and below 1 mm in the conventional one. These deviations are below 1.6 mm in 75% of the non-silicone cases and below 2.7 mm in 75% of those with silicone. Without silicone, errors are slightly higher for the C region, while they are lower than S when using silicone. The maximum errors recorded are 3 mm in the conventional phantom and 5 mm in the realistic phantom.

Table 5.1. Descriptive statistics of maximum osteotomy deviations for each phantom. Q25 and Q75 represent the 25th and 75th percentile. Mdn represents the median.

		Freehand			Smartphone			HoloLens		
		C	S	Total	C	S	Total	C	S	Total
Conventional phantom (no silicone)	Min	0.27	0.47	0.27	0.28	0.38	0.28	0.45	0.34	0.34
	Q25	1.02	0.96	1.01	0.78	0.77	0.77	0.83	0.83	0.83
	Mdn	1.48	1.81	1.70	1.15	0.95	1.04	1.12	1.01	1.06
	Q75	2.64	2.56	2.56	1.38	1.42	1.42	1.60	1.39	1.54
	Max	7.27	3.45	7.27	2.20	2.52	2.52	2.87	3.00	3.00
Realistic phantom (silicone)	Min	0.79	0.41	0.41	0.33	0.54	0.33	0.51	0.92	0.51
	Q25	2.37	2.09	2.10	0.94	1.36	1.07	1.01	1.66	1.13
	Mdn	3.70	3.24	3.37	1.22	2.21	1.54	1.40	2.50	1.84
	Q75	10.02	4.13	6.13	2.12	3.01	2.55	2.04	2.89	2.68
	Max	54.03	9.83	54.03	5.00	4.89	5.00	3.89	4.13	4.13

When PSIs are placed freehand, the median value for MODs is 1.70 mm with the conventional phantom and 3.37 mm with the realistic one. The C region presents the highest deviations, with maximum errors of 7.27 mm without silicone and 54.03 mm with silicone. The 75th percentile in C presents an error of 10.02 mm with the silicone phantom, which is considerably higher than the 2.64 mm on the non-silicone one.

We conducted a statistical analysis to identify significant differences between methods, cases, and phantoms. The results for each analysis are presented in the following subsections.

5.4.1. Methods comparison

A Kruskal-Wallis test showed that the method chosen significantly affects the results, $H(2) = 25.80$, $p < 0.001$. The freehand method presented higher maximum deviations (Mdn = 2.22, IQR = 1.23 – 3.63) than using the smartphone (Mdn = 1.20, IQR = 0.85 – 1.86) or the HoloLens 2 (Mdn = 1.33, IQR = 0.97 – 2.11). Post-hoc Dunn's test was used to compare all pairs of methods. The difference between HoloLens and the smartphone was not significant ($p = 0.47$). However, the differences between using the freehand method and using either

HoloLens or the smartphone were significant ($p < 0.001$ in both cases). Taken together, the results suggest that placing the PSIs freehand affects MODs, increasing the risk of high errors considerably.

We also recorded the time taken by each user to place the PSIs in every scenario. The Kruskal-Wallis test proved significant differences among methods ($H(2) = 10.19$, $p = 0.006$). The time required with the freehand method (Mdn = 48.5 seconds, IQR = 30.50 – 48.50) was significantly lower than using AR guidance with the smartphone (Mdn = 75, IQR = 68.25 – 110.25) or HoloLens (Mdn = 78.5, IQR = 62.25 – 106). However, these time values are negligible compared to the intraoperative surgical time for these procedures.

5.4.2. Cases comparison

Deviations were also compared among cases for the C and S regions. A Kruskal-Wallis test was calculated, obtaining not statistically significant differences in S, but significant differences in C, with $H(5) = 33.50$ and $p < 0.001$. The Dunn's test indicated significant differences between cases 1 (Mdn = 2.07, IQR = 1.48 – 5.00) (**Figure 5.6 c**) and 4 (Mdn = 1.73, IQR = 1.49 – 2.58) **(Figure 5.6 d**) with cases 3 (Mdn = 0.97, IQR = 0.64 – 1.15) (**Figure 5.6 a**) and 5 (Mdn = 1.11, 0.73 – 1.37) (**Figure 5.6 b**). If we analyze the results from C considering their size and position, we can observe how the highest errors correspond to smaller PSIs placed in smoother regions. In comparison, the best results are obtained for larger PSIs covering less homogeneous regions. The S region is narrower than C, and therefore there are fewer variations in position among PSIs.

5.4.3. Phantoms comparison

Finally, we compared the results obtained using the realistic phantom with those from the conventional phantom by conducting a Kruskal-Wallis test. Significant differences were obtained for the freehand method ($H(1) = 18.07$, $p < 0.001$), the smartphone ($H(1)= 14.07$, $p < 0.001$) and the HoloLens ($H(1) = 17.12$, $p < 0.001$). Errors were higher in all cases when using the phantom with the layer of silicone.

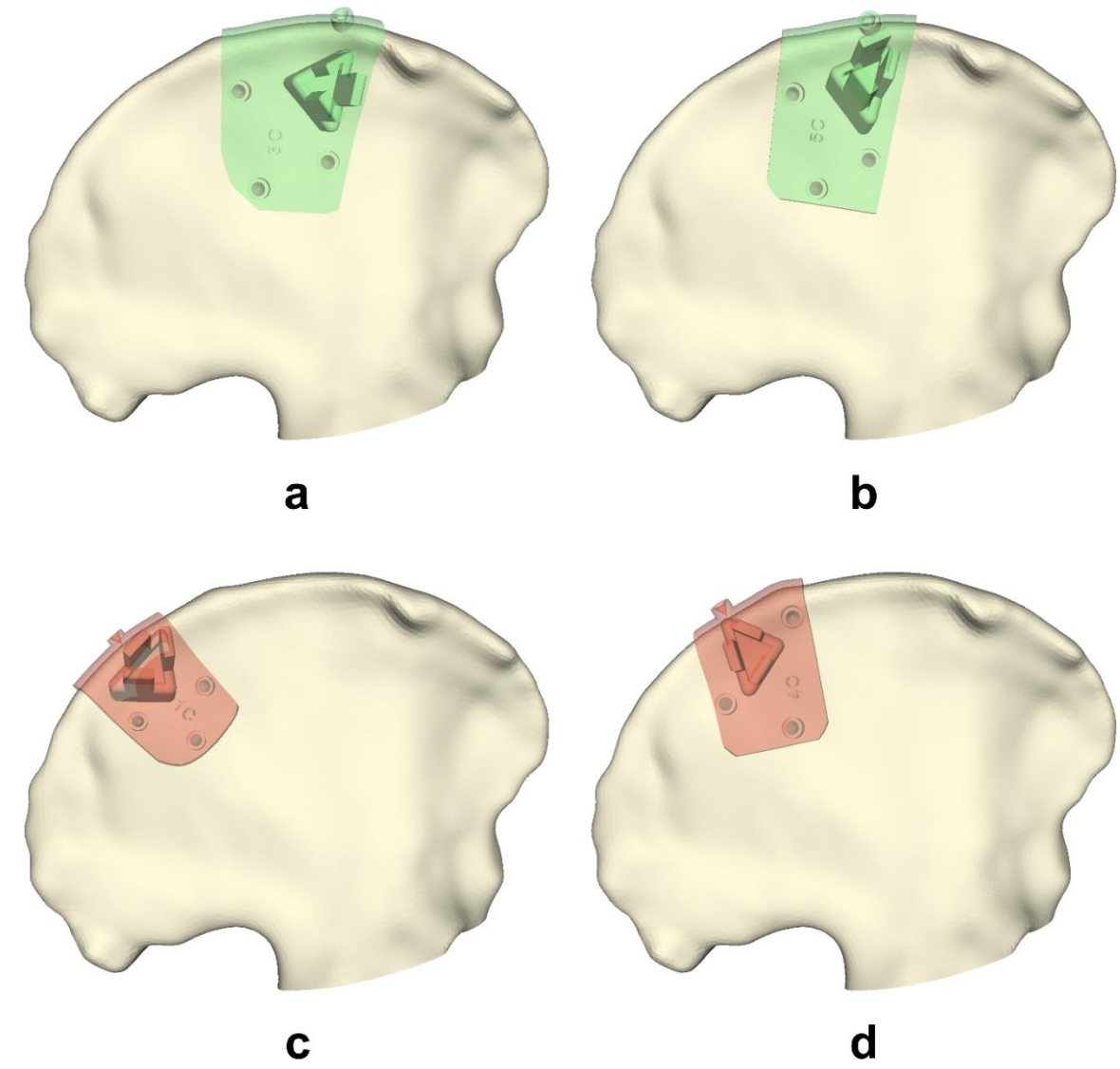

Figure 5.6. Cases with C PSIs presenting significant differences with each other. The figures represent the cases with (**a**, **b**) lower and (**c**, **d**) higher errors.

5.5. Discussion

The correct placement of PSIs in pelvic tumor resections is a critical step that conditions the results obtained in surgery. However, there is no current solution to guide their installation, and surgeons can only rely on their intuition and verify their placement visually. External devices providing guidance and allowing an objective verification can therefore represent a significant improvement in using PSIs, minimizing errors and increasing precision.

In this work, we propose the use of AR to guide and verify this placement. Our setup is based on 3D-printed AR markers that snap into the PSIs at a particular position. By visualizing the bone model and the relative position between PSIs, surgeons can guide their placement in the patient. We focus our study on the ilium, the region of the pelvis presenting more placement difficulties. Our setup includes two PSIs, one in S and one in C. The AR marker is placed in the S PSI since placement errors in this area are lower due to its small and characteristic shape. The bone model is used to correct S PSI placement. After this adjustment, the planned virtual model of the C PSI is displayed to guide the placement.

We designed an experiment with four users who placed the PSIs on a phantom following three different methods: freehand, AR with a smartphone, and AR with HoloLens 2. Then, we computed the MOD between the cutting planes defined by the placed PSIs and the cutting planes obtained from the preoperative plan. The results demonstrate that placing PSIs with AR guidance significantly reduces MOD errors. Specifically, it avoids placements far away from their planned position. AR methods presented median values below 2 mm and MODs below 5 mm in all cases, while the freehand method recorded higher median values (1.70 mm and 3.37 mm) and maximum errors of 54 mm. As for the AR methods, both devices presented similar results. Therefore, selecting one over the other is more dependent on the surgeon's personal preferences and convenience. The smartphone can be easily inserted into a sterile bag or case such as CleanCase (Steridev Inc., Lansing, MI, USA) [136], but it requires the surgeons to hold it, leaving only one hand free. On the other hand, the HoloLens 2 does not require holding, but it can generate discomfort in long-term use and is more expensive.

Our study was performed on two phantoms, a conventional one consisting only of a plastic replica of the bone and a second one including a layer of silicone to simulate tissue and add difficulty to placement. The results obtained show higher errors in all methods when using the realistic phantom. In the case of AR methods, this may be a consequence of a thicker layer of silicone present in some areas, specifically in S. This explains why, with AR methods, the realistic phantom presented higher errors in S, while similar values were maintained for both phantoms in C. Nevertheless, the differences between both phantoms are especially remarkable in the freehand method, where the median error is duplicated, going from 1.70 mm in the conventional phantom to 3.37 mm in the realistic one. This increase can be noted in both regions, S and C. Therefore, the results obtained reinforce the idea that using

plastic phantoms without any material simulating tissue makes the placement easier and does not resemble the real scenario correctly.

Although the silicone coating served its purpose by adding difficulty during placement, the phantom's design can be further improved. When we poured the silicone, the entire surface was covered smoothly. However, in a real setting, the tissue is not evenly distributed. Therefore, future studies could improve the design of the phantom to make it more realistic by adding small fractions of silicone with different thicknesses unevenly distributed.

A tumor model could also be added to the phantom to provide more realistic measurements, as it is used as a reference for placing the PSIs in surgical settings. The surgeons can notice that the direction of the osteotomy crosses the tumor or is too deviated from it and correct the PSI placement accordingly. However, to simulate this with a phantom, the tumor should be included with enough realism to resemble the surgical scenario, where tumor margins are not clearly defined. Therefore, we believe including a 3D-printed tumor would not be realistic enough and could result in lower deviations than in real surgical settings. Additionally, in our study we wanted to measure and compare the deviations of the osteotomies with different methodologies and scenarios. In order to minimize the possible factors introducing variations in the assessment, the same phantom and reference frame registration was used for all the experiments, and the scenarios were simply modified by changing the target positions of the PSIs. The introduction of a tumor for each case would have implied designing and printing a different phantom for each scenario. Therefore, 3D printing inaccuracies would cause variations among phantoms, and registrations errors would not be the same, modifying the conditions in all scenarios. Hence, we consider our setup to be adequate, although it must be noted that the reported deviations in the freehand method could be reduced in a clinical setting. Changes in dimensions and form of the tumor from the acquisition of the preoperative image to the moment of the intervention are factors that can affect the surgical outcomes when using surgical guidance based on preoperative planning. Therefore, it affects similarly when using surgical navigation or PSIs. This is a known limitation that can only be solved by using intraoperative imaging. However, these changes do not affect the registration step for AR guidance, as it is based on the position of the PSIs in the bone. Only changes in the target bone area can prevent from using PSIs. In that case, the procedure could be performed following the conventional approach without any guidance.

The shape, size and location chosen during PSIs design have shown to be highly relevant factors to consider for minimizing placement errors. In our study, those cases presenting both small size and homogeneous target area exhibited significantly higher errors than those with larger sizes and a more distinct target surface. However, the available target area may be limited depending on the surgical case, leaving no choice but to choose a homogeneous surface. Regarding size, although larger designs are easier to install in the correct location, they are also more invasive [177], [184]. Hence, a trade-off between ensuring precision and reducing invasiveness should be found.

Further testing should be performed in a clinical setup to analyze the placement accuracy and validate the system in a real scenario. Nevertheless, using PSIs combined with AR inside the operating room has already been tested in previous studies for other purposes [129], [136], obtaining satisfactory results. The use of a smartphone or HoloLens does not significantly modify the surgical procedure, neither requires additional installation of devices or tools inside the OR, unlike other systems such as CAS with an optical tracking system.

5.6. Conclusions

In this study, we have presented a guiding tool for PSIs placement based on AR. The system has been validated in a phantom designed to provide a more realistic setup than conventional ones. The results obtained from this study are promising and demonstrate that using AR for guidance can significantly reduce the risk of high placement errors and ensures an accurate installation close to the target. We believe that the presented system can overcome the current limitations of PSIs — the impossibility of verifying their placement objectively — conveniently and effectively.

The content of this chapter has been published in Sensors:

M. García-Sevilla, R. Moreta-Martinez, D. García-Mato, A. Pose-Diez-de-la-Lastra, R. Pérez-Mañanes, J.A. Calvo-Haro and J. Pascau. "Augmented reality as a tool to guide PSI placement in pelvic tumor resections". Sensors, vol. 21(23), pp. 7824 (2021).

6

3D PRINTING, SURGICAL NAVIGATION, AND AR FOR PRECISE AND LESS INVASIVE PALATE TUMOR RESECTIONS

6.1. Introduction

Salivary gland tumors account for approximately 5% of head and neck cancers [220] and are, in most cases, benign. Only 20% of these neoplasms are malignant, although this rate varies depending on the gland of origin [221], [222]. Unlike most head and neck cancers, which are squamous cell carcinomas, salivary gland tumors comprise multiple histologic entities, each presenting a different clinical behavior [223]. Mucoepidermoid carcinoma is the most frequent malignancy, followed by adenoid cystic carcinomas, representing less than 1% of all malignancies in head and neck cancers [224]. These tumors can appear in both minor and major salivary glands. Most major salivary tumors occur in the parotid glands, while the palate is the most common location for minor salivary gland tumors [225].

Tumors located in the palate are often diagnosed in advanced stages of the disease due to indolent growth during early stages, with vague and unspecific symptoms [224], [226]. In some cases, this phenomenon leads to extensive involvement of surrounding structures, such as the nose, paranasal sinuses, orbits, and even the middle cranial fossa, with the subsequent implication of vital structures such as the internal carotid artery, the jugular vein, and cranial nerves.

Regardless of whether it is followed by radiotherapy, surgery is the treatment of choice for midface tumors. To date, the surgical management of these tumors consists of radical maxillectomies combined with transfacial approaches, which are usually associated

with significant functional and aesthetic sequelae. However, achieving safety margins is a therapeutic challenge. This is due to the complexity of the anatomical region, the reduced field of vision, the restrictive surgical field hindering the access and maneuverability of surgical instruments, and the risk of complications (bleeding, nerve injuries, or even cerebrospinal fluid leaks) [227]. In addition, middle third tumors are frequently irregular in shape and invade neighboring structures. Consequently, it is not uncommon to set suboptimal cutting trajectories, which results in a high rate of positive margins.

In these scenarios, tools facilitating local control during surgical resection and confirming adequate margins while minimizing morbidity are capital [228].

6.1.1. Computer-assisted surgery in oral and maxillofacial surgery

In recent years, intraoperative navigation in craniofacial surgery has become an effective tool, improving results and safety while minimizing the risk of injuries [25], [229]. Surgical navigation initially involved rigid fixation of the region to be treated, a situation that, on many occasions, entails significant mechanical limitations for the surgeon. Hence, navigation was initially confined to neurosurgery as it provides a rigid and stable frame [30]. However, technical advances in image processing and computed tomography allowed the development of frameless stereotaxy devices over the years, enabling its use in maxillofacial surgery without the need for rigid fixation.

One of the most critical steps in surgical navigation is image-to-patient registration. In oral and maxillofacial surgery, a paired points registration is usually performed using either anatomical landmarks or artificial fiducials, including skin stickers [230], dental splints [231], or bone-implanted screws [232]. Surface-points matching is also widely applied by collecting points in the facial skin surface and aligning them with their corresponding landmarks in soft tissue models obtained from preoperative images [230], [233], [234].

The progressive evolution of intraoperative navigation systems has led to the use of this technology almost routinely in the field of neurosurgery (skull-base surgery, vascular lesions), otorhinolaryngology (endoscopic sinus surgery, lateral skull-base surgery, cerebrospinal fluid leaks), and, recently, orthopedic surgery (hip and knee arthroplasty, spinal procedures) [30]. However, the extended application of this technology has not been widely evidenced in maxillofacial surgery [235], [236]. In 2015, Dubois et al. [237], [238] presented the benefits of surgical navigation for accurate implant positioning secondary to orbital

trauma by performing a cadaveric study. Four years later, Wu et al. [239] demonstrated the feasibility of using surgical navigation for zygomatic implant placement. Many other studies found in the literature have proved the benefits of surgical navigation, especially for complex procedures where a personalized approach is required.

Some applications of CAS have been described in this field, including intraoperative navigation for orbital reconstruction [240], [241], and CAD/CAM for orthognathic [242] and implant surgery [243]–[245]. Surgical navigation has also been used in tumor removal to delineate surgical margins and achieve safe and accurate resections [26], [229], [246], [247]. The results are promising, but the clinical adoption is still reduced. The main limitations of this approach include complexity, technical support, cost, steep learning curve, or the rigid fixation of navigation references [246], [248], which are perceived as an entry barrier. Nevertheless, several commercial solutions exist in the market for oral and maxillofacial surgery [112], [247], [249]–[254]. Although some studies have presented AR-based surgical navigation systems for oral and maxillofacial surgery applications [130], [255], [256], no commercial systems are available.

The application of CAS in the midface, specifically in resections involving the maxilla and the middle cranial fossa, can become a valuable tool in complex procedures. Additionally, the presence of bone structures that do not modify their contours and volumes during the intraoperative process due to surgical maneuvers is an essential advantage for navigation [257]. Therefore, these interventions provide an adequate scenario for navigation and can highly benefit from this technique.

6.1.2. Adenoid Cystic Carcinoma

Adenoid Cystic Carcinoma (ACC) is a rare malignant tumor accounting for 1% of head and neck cancers and 10% of salivary gland tumors [258]. It is commonly found in palate small salivary glands, from where it spreads slowly but aggressively. These tumors settle in the upper palate and maxillary region and tend to local infiltration and perineural spread. Consequently, they may behave in an indolent and silent manner until late diagnosis, appearing as destructive masses that can even involve intracranial structures. In addition, this histologic type is characterized by a high predisposition to systemic dissemination, mainly hematogenous (lung, liver, brain, and bone) and lymph nodes. They present a high propensity to local recurrence and distant metastasis [224]. The primary treatment consists of surgical

removal with clear margins and complementary radiotherapy when needed. Data on the efficacy of systemic therapy or radiotherapy in recurrent or metastatic salivary gland tumors are limited, with some benefits described in proton-based radiotherapy [259]–[261] or the recent systemic use of Lenvatinib [262]. Consequently, an effective primary surgical treatment with adequate margins is the best prognostic factor for these patients.

However, this intervention is highly challenging due to the occasional centrofacial tumor location, complex elective surgical approach, limited line of sight, and the need for immediate reconstruction. Additionally, the tumor boundaries are difficult to discriminate from the normal surrounding tissue.

In this type of intervention, where complex anatomy is present and high accuracy is needed, surgical navigation becomes a valuable tool to improve clinical outcomes. It provides guidance that can help achieve accurate safety margins and protect vital structures. However, despite its great potential in these clinical applications, there are currently limited studies using CAS for midfacial tumor resection. Wei et al. [229] tested surgical navigation in patients who underwent surgery near the skull base, including five patients with adenoid cystic carcinoma at minor salivary glands of the palate. Their approach was limited by the invasive attachment of a reference frame to the patients' forehead and an image-to-patient registration based on non-precise anatomical landmarks, which can significantly reduce the navigation accuracy. Tarsitano et al. [246] followed a similar setup for maxillary tumors resection, screwing a dynamic reference frame to the patient's skull.

6.2. Objective

The aim of this study is to present and assess the accuracy of three different alternatives for surgical navigation in head and neck tumors based on 3D printing, surgical navigation, and AR visualization. These alternatives are less invasive than previous solutions [229], [246] and more convenient for these procedures than conventional registration solutions used in other disciplines such as neurosurgery, as they do not involve fixation of the patient's head. A 3D-printed patient-specific phantom was used for validation and assessment of the three navigation systems. One of the proposed solutions was then used to guide the tumor resection of a patient presenting a central palate carcinoma invading the nasal fossa floor and septum.

6.3. Materials and Methods

6.3.1. Clinical case

A 62-year-old woman was referred to the Oral and Maxillofacial Unit at our center for treatment. The patient presented an exophytic tumor of approximately 3x2 centimeters in the middle of the hard palate with normal oral mucosa (**Figure 6.1 a**). Endoscopy showed a nasal extension of the lesion, and biopsy results confirmed an adenoid cystic carcinoma. A CT scan showed hard palate bony erosion, invasion for the nasal septum and floor of the right fossa, and an intact ipsilateral inferior turbinate (**Figure 6.1 e** and **f**).

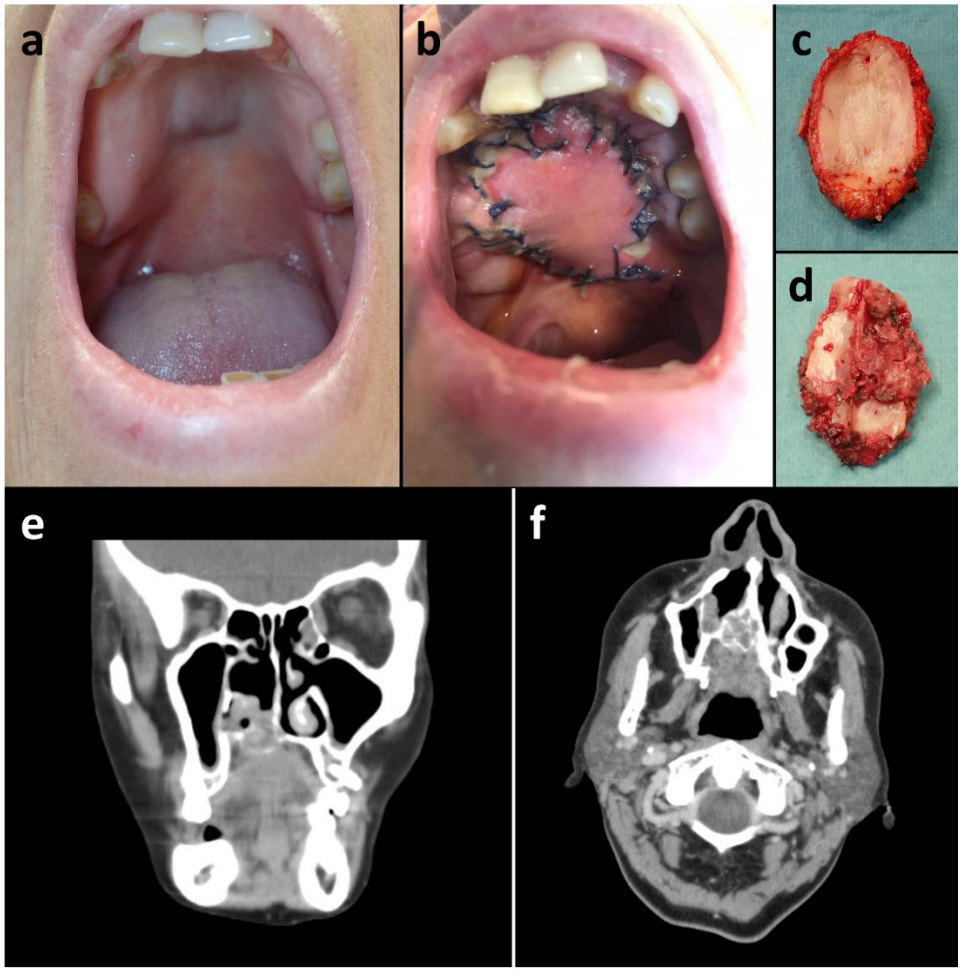

Figure 6.1. (**a**) Hard palate midline submucous bulging lesion and (**b**) palate reconstruction with radial forearm free flap (3 weeks after surgery). Resected specimen from (**c**) palate and (**d**) nasal view. (**e**) Coronal and (**f**) axial views of the CT image.

The chosen procedure consisted of an endoscopic nasal approach, a navigated transoral resection of the central palate with at least 2 cm margin (**Figure 6.1 c** and **d**), and

immediate reconstruction of the central hard and soft palate with a radial forearm free flap (**Figure 6.1 b**). Alternative surgical approaches considered were a Le Fort I osteotomy (downfracture of the whole maxilla and resection of the central part) or a IIb maxillectomy (Brown classification, sacrificing the intact alveolar process and denture) reconstructed with a fibula free flap. Our purpose was to achieve functional rehabilitation, including a tight palate seal and maintaining the whole alveolar process of the maxilla. The proposed solution presented a more straightforward reconstruction involving only soft tissue, as bone reconstruction is not needed in horizontal class a defects.

The preoperative CT scan was used to extract the 3D anatomical models (bone and tumor) and perform the preoperative plan, defining the desired tumor margins for the resection. Using Autodesk Meshmixer software (Autodesk, Inc., San Rafael, CA, USA), we increased the size of the tumor model 1 cm. The intersection of this model with the bone in the palate determined the surgical margins (1 cm margin with a thickness of 1 mm). Before image acquisition, five screws were attached to the maxilla above the upper teeth under local anesthesia as proposed by Zavattero et al. [263]. This procedure provides unobtrusive, rigid, and exact landmarks that are clearly visible on virtual data sets (CT images) as well as during the navigation procedure. The position of these screws was identified in the scan for later use during intraoperative image-to-patient registration.

6.3.2. Surgical navigation: simulation

Based on the anatomical models of the patient, we designed and manufactured a phantom in polylactic acid using the desktop 3D printer Ultimaker 3 extended (Ultimaker B.V., Utrecht, Netherlands). The phantom was used to simulate the intervention and to test the precision of three different solutions for surgical guidance (**Figure 6.2**).

The first solution consists in using an optical tracking system (NDI Polaris Spectra, CA) for computer-assisted navigation (**Figure 6.2 a**). We attached a 3D-printed dynamic reference frame to a silicone jig fabricated to fit on the patient's upper left teeth. The dynamic reference frame is used to compensate for head movements. This silicone jig consists of a mass given the shape of the patient's teeth during its malleable state. The image-to-patient registration is performed using the screws described in the previous section as artificial landmarks.

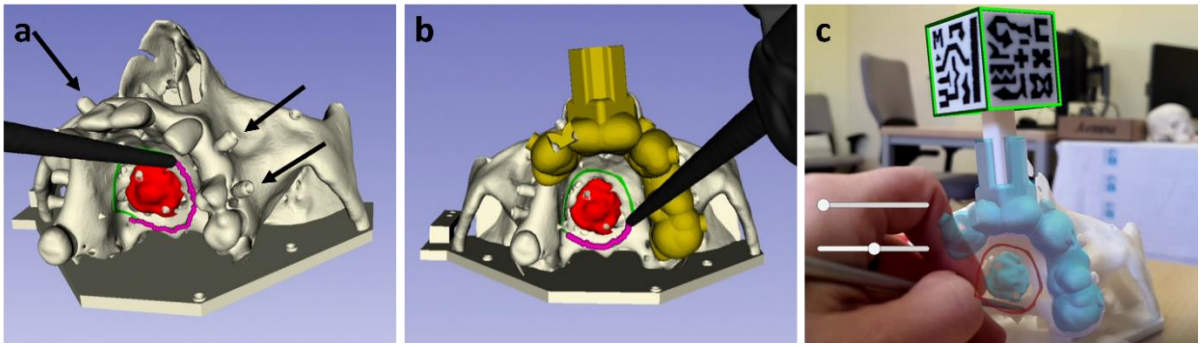

Figure 6.2. Solutions for surgical navigation tested on the patient's anatomical model: (**a**) navigation with an optical tracking system and registration with screws (black arrows); (**b**) navigation with an optical tracking system and registration with a splint; (**c**) navigation with an AR application and registration with a cubic marker.

A second solution involves the same tracking device, but the reference frame is installed by means of a splint (**Figure 6.2 b**) instead of using a silicone jig. This splint is designed from the 3D models of the teeth obtained from the preoperative images, and 3D-printed in a biocompatible resin (Biomed Clear), using the Formlabs Form2 (Formlabs Inc., Somerville, MA, USA) 3D printer. In contrast to the first method, the registration in this case is computed with artificial landmarks added on the splint during the design process.

Finally, the third solution uses AR for surgical navigation **(Figure 6.2 c**). We developed a specific smartphone app to visualize the patient's anatomy and the tumor margins. The application was implemented on the Unity platform (version 2019.3), using the Vuforia development kit (Parametric Technology Corporation Inc., Boston, MA, USA) for pattern recognition. The application displays the 3D models of the bone, tumor and surgical margins (obtained from the preoperative image and planning) and includes buttons to change the visibility of the models (modify opacity or hide). In order to display the virtual models in the correct position with respect to the patient's phantom, we attached a 3D-printed marker to the splint in a fixed and known position. This AR marker contains a unique black and white pattern printed using the double extruder functionality of the Ultimaker 3 extended 3D printer. The smartphone's camera detects this marker and displays the virtual models on the screen on top of the patient. **Figure 6.2 c** shows the appearance of the developed AR application.

The three configurations were tested on the phantom. After performing the corresponding registration, each navigation system displayed the position of the surgical margins defined preoperatively. Using the optical tracker and the pointer, we collected points

(with distances of 1 mm between each other) following the indicated surgical margins. The process was repeated three times for each configuration, including the registration step. A similar number of points was recorded for each sample (around 100 points).

Inaccuracies in the registration step would generate errors in the displayed margins. Therefore, the collected points would present deviations from the position of the real surgical margins. In order to assess the accuracy for each configuration, we computed the distances between the collected points (following the margins indicated by each navigation system) and the real position of the tumor margins. For that, we obtained the closest point of the resection margins (a 3D model or point cloud) to every recorded point and stored the distance. Then, we computed the median and quartiles for each solution. Finally, we conducted a statistical analysis to identify significant differences in accuracy between methods.

The surgical margins used as ground truth for evaluating the three methodologies were the ones defined during preoperative planning with the preoperative CT (1 cm margin). The real position of the tumor margins was obtained during assessment thanks to the rigid attachment of a reference frame to the phantom and a registration performed with landmarks distributed all over the surface to ensure accurate registration. These landmarks were added as conical holes in the bone region and the base of the phantom and differ from those used for registration on each configuration.

6.3.3. Surgical navigation: setup

Apart from tracking the patient with the 3D-printed dynamic reference frame (**Figure 6.3 b),** two different instruments were tracked during surgery: a pointer tool to record points and a piezoelectric handpiece for tumor resection. We designed and 3D-printed an adaptor with optical markers to fit in the handle (**Figure 6.3 c**) for handpiece tracking. An additional tool was also designed and 3D-printed to fit the instrument at a specific position. This tool included six small conical holes for registration. Finally, as the handpiece is composed of an interchangeable saw with a non-fixed rotation around the longitudinal axis, we added an extra step in the registration procedure. This step consists in recording the position of the saw tip and automatically finding the rotation that corrects the orientation of the saw in the navigation scene. That is the rotation that minimizes the distance between the virtual tip point and the recorded point. The pointer and all 3D-printed tools, including the dynamic reference frame, were sterilized before the intervention to maintain the asepsis of the surgical field.

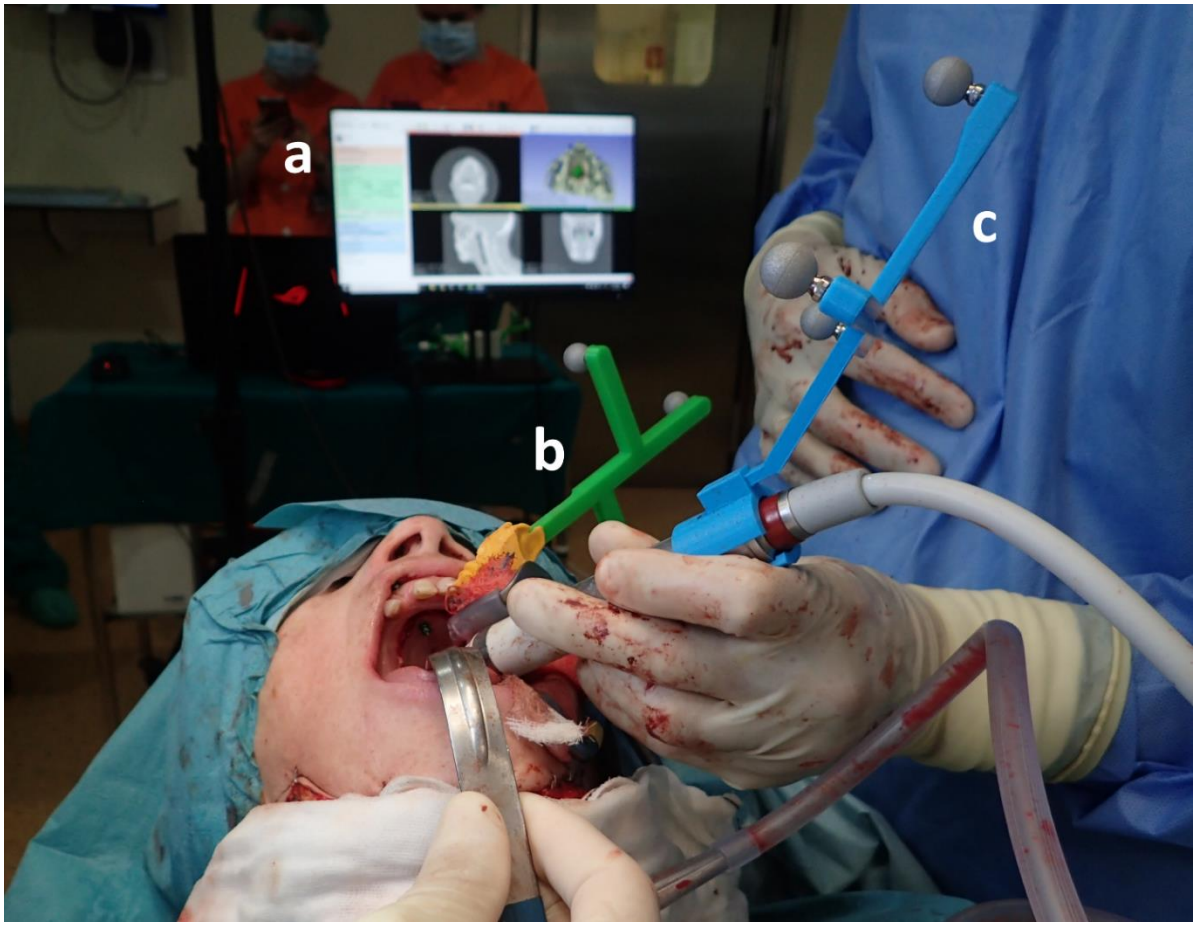

Figure 6.3. Surgical navigation setup during the intervention: (**a**) surgical navigation software; (**b**) 3D-printed patient's dynamic reference frame; (**c**) 3D-printed adaptor for tracking of the piezoelectric handpiece.

We developed a custom module for surgical navigation in the 3D Slicer platform [117], a free and open-source software package for clinical and biomedical applications. We used the SlicerIGT kit [202] and the PLUS toolkit [203] to define the graphical user interface and manage the transforms sent by the optical tracker through the OpenIGTLink protocol. Intraoperative imaging was not used during the procedure. However, our software allowed the visualization of the preoperative CT image and the 3D models obtained of the patient (bone, tumor, and surgical margins) and the position of the instruments (**Figure 6.3 a**). The three views of the CT (axial, sagittal, and coronal) could be updated in real-time to match the position of the instrument's tip for better guidance. The software also included other functionalities, such as modifying the point of view in the 3D view or recording points.

6.3.4. Surgical navigation: intervention

Resection margins were controlled in real-time using the developed software through constant visual feedback displayed on a screen adjacent to the surgical field. During the intervention, we increased the surgical margin 1 cm from the preoperative segmentation to ensure adequate en bloc resection with 2 cm of tissue free of disease. The final resection margins were recorded using the pointer. While not used for surgical guidance, AR was tested on the patient to validate the AR setup using the splint (**Figure 6.4**). The smartphone was introduced in a sterile case (CleanCase, Steridev Inc., Lansing, MI, USA) so that surgeons could hold it close to the patient.

Figure 6.4. Use of the AR app during the intervention.

After resection, a radial forearm free flap was harvested and placed to reconstruct the palate with an adequate seal. A postoperative CT scan was performed a week after surgery to assess the surgical outcome. Navigation accuracy was measured as the absolute distance between the points recorded intraoperatively and the real resection margins identified in the postoperative CT. A secondary CT scan was acquired 15 months after surgery for the patient's follow-up.

6.4. Results

6.4.1. Surgical navigation: simulation

We analyzed the accuracy provided by each navigation solution on the 3D-printed phantom by computing the distances between the collected points during guidance and the real resection margins. The results for each configuration are presented in **Table 6.1**.

Table 6.1. Mean and standard deviation of the distances between the tumor margins and the collected points with each navigation solution.

Navigation solution	Median	Q1	Q3
OTS (registration with screws)	0.57	0.34	0.81
OTS (registration with surgical guide)	0.61	0.30	0.98
AR	0.40	0.14	1.29

OTS: optical tracking system, Q1, Q3: first and third quartiles (25^{th} and 75^{th} percentile)

All methods presented median values below 0.7 mm. Most of the points recorded using the optical tracking system for guidance presented deviations from the surgical margins below 1 mm. The results obtained when using AR for guidance presented the lowest median value (0.4 mm). However, they also presented the highest variation, with an IQR of 0.89 mm compared to the ones obtained with optical tracking, where the IQRs for the screws and surgical guide configurations were 0.24 mm and 0.37 mm, respectively.

A Kruskal-Wallis test was performed to explore the differences between each configuration proposed for this study. No statistically significant differences were obtained ($H(3) = 4.27$, $p = 0.12$). Therefore, we can conclude that the three configurations present similar accuracy. The configuration using screws for registration was the one presenting lower error. Thus, it was the one chosen for the intervention.

6.4.2. Surgical navigation: intervention

The selected navigation system (optical tracker with screws for registration) was successfully used for guidance during the resection. Surgical instruments were accurately tracked with respect to the patient's anatomy, providing valuable feedback to the surgeons.

The registration step was repeated three times during the intervention, obtaining a fiducial registration error of 0.77, 0.93, and 0.81 mm.

The points collected along the surgical margins with the navigation system were compared with the real surgical margins identified in the postoperative CT by measuring their absolute distance. We separated the analysis into four regions divided by left and right sides and posterior and anterior locations. **Figure 6.5** displays the results.

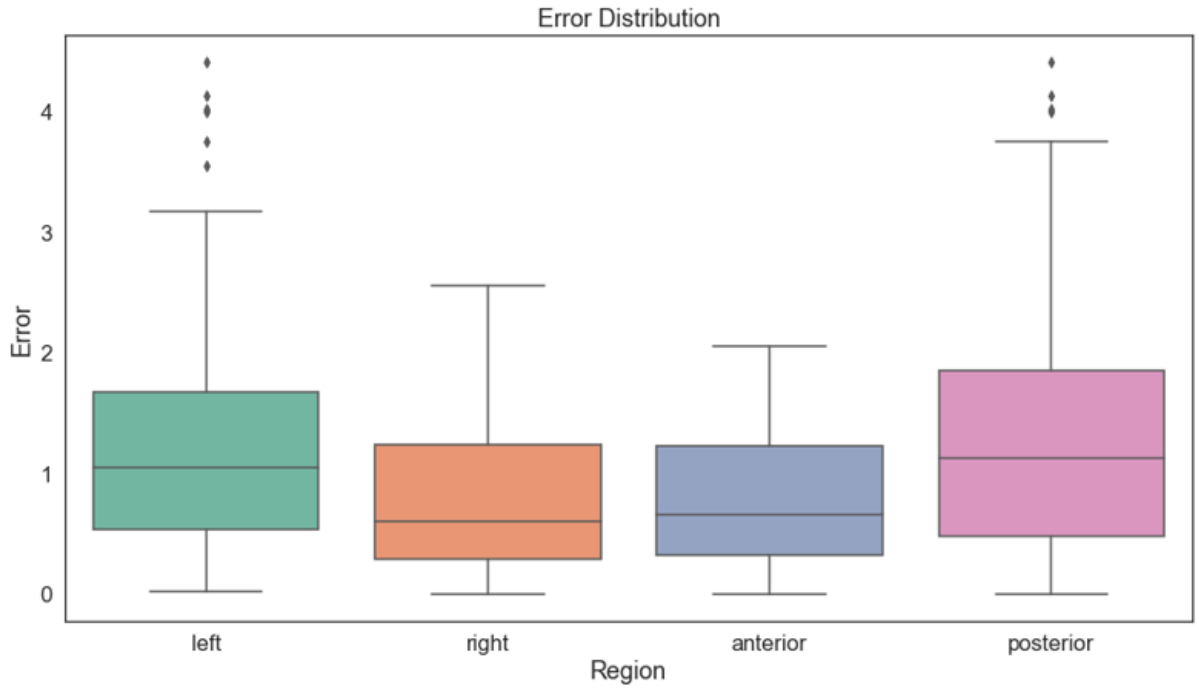

Figure 6.5. Distances between the resection margins collected intraoperatively with the navigation system and those identified in the postoperative CT.

The mean distances were around 1 mm and below 2 mm in 90% of the samples. The posterior region presented higher errors compared to the anterior. The left side showed higher deviations than the right one. However, this deviation appears to be caused by the jig, which was still in place during the points collection and limited the pointer movements (**Figure 6.6**).

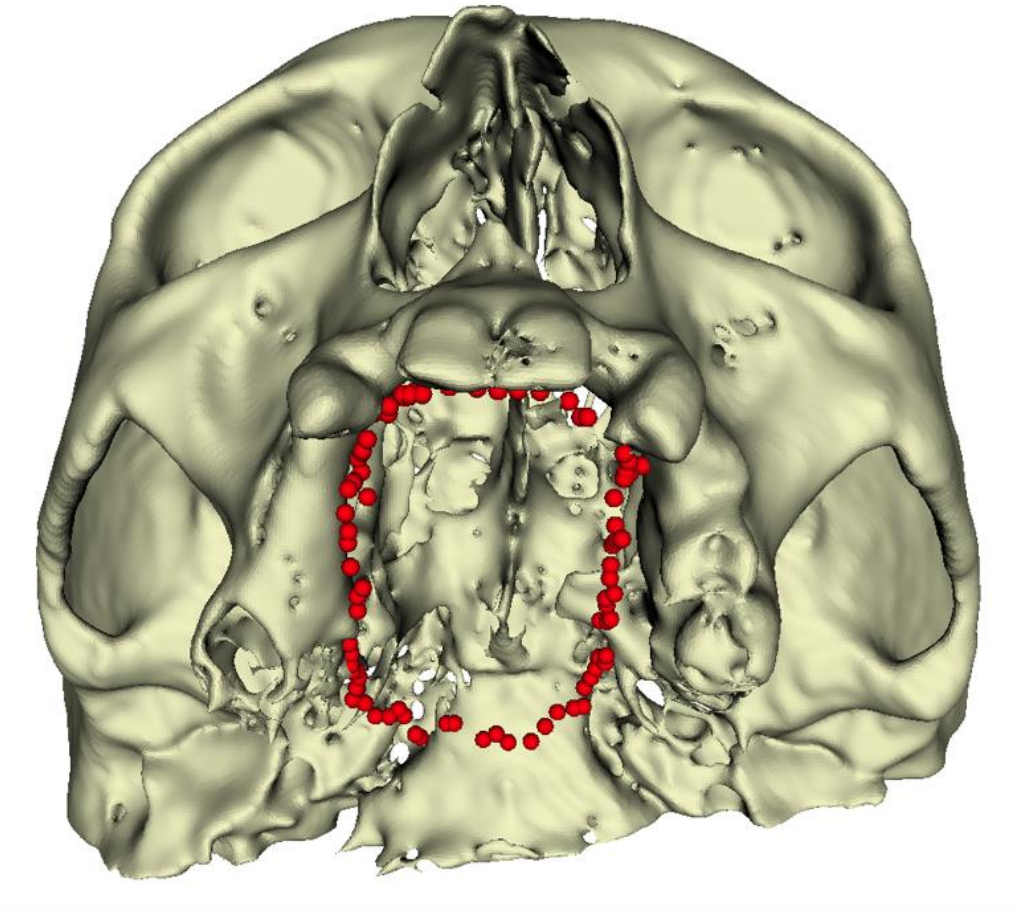

Figure 6.6. Points collected intraoperatively along the resection margins.

The AR app was also used inside the operating room, where surgeons visualized models of the patient's anatomy overlayed on the camera's image of an iPhone 6 (Apple Inc., Cupertino, CA, USA). The splint was inserted correctly and enabled AR display, where virtual models were represented aligned with the patient's anatomy.

6.5. Discussion

The resections of head and neck tumors in deep and less accessible regions represent complex surgical scenarios requiring extreme dexterity, as the field of view and instruments maneuverability is limited. For middle third tumors such as palate ACCs, the preservation of normal bony tissue and surrounding soft tissues should be maximized. Tel et al. [264] advocate an open "box resection" where the tumor is resected within a three-dimensional volume of healthy tissue. In these scenarios, CAS represents a valuable tool to plan [265], guide [266] and verify [246] the resection margins.

Although surgical guidance for tumor resections is a routine procedure in neurosurgery, the reports in the maxillofacial middle third tumors are scarce. The existing CAS applications mainly focus on virtual planning, intraoperative guidance for the free flap defect reconstruction, or validation of the reconstruction after trauma, not on the ablative procedure. Moreover, most existing commercial systems for surgical navigation use a three-point clamp (Mayfield clamp or similar) to fix the patient's skull and prevent head movements. Then, a dynamic reference frame is attached to the clamp to define a reference system for the patient and perform the image-to-patient registration. This setup is suitable for neurosurgery, and it can help achieve high accuracy. However, in the resection of middle third tumors, surgeons need free movement of the head to adjust the line of sight with the surgical field and enable proper angulation of the saw and surgical tools. Therefore, other solutions for tracking and registration need to be found for these procedures.

Some studies have presented alternative setups for tracking and registration. Malham et al. [111] use the SpineMask (Stryker, Leibinger, Freiburg, Germany) to track the patient's back and perform an automatic registration. This device is non-invasive, as it is an adhesive surgical tracker designed to be placed on the patient's back. The device contains markers for automatic registration, which are placed surrounding the surgical field. Other studies remove the dynamic reference frame from their setup and use conventional optical cameras to detect fiducial markers and constantly update the registration. These setups are usually based on computer vision algorithms for the detection of adhesive skin markers [267] or anatomical features in the bone [268]. Other frameless systems use different devices such as hyperspectral cameras to detect skin features [269] or advanced methods such as 3D digital image correlation (also called stereo DIC). This last solution presents precise real-time tracking at a lower cost and based on small markers. Xue et al. [270] tested it for tracking the maxilla after a Lefort I osteotomy. However, it was not evaluated in a clinical setup where light conditions and external factors such as blood or saliva can compromise the tracking and accuracy of the system.

Most of the existing alternatives focus on anatomical regions presenting deformations, where installing a dynamic reference frame and performing a rigid registration becomes inaccurate. Others are designed for specific applications, such as SpineMask, and are not applicable for reduced regions like the mouth. Also, we consider the systems based on skin markers not adequate for an open transfacial approach. Registration markers must be placed

surrounding the surgical field to ensure an accurate registration, but in our scenario, the space is limited and a rigid position between markers is difficult to maintain.

Tarsitano et al. [246] presented a surgical navigation setup for the resection of maxillary tumors in a study with twenty patients, obtaining promising results with clear margins in 91% of cases. In their setup, a dynamic reference frame was screwed to the patient's skull. The registration was performed first with a point-to-point registration based on anatomical landmarks, obtaining a mean error of 2 mm, followed by surface matching for refinement. They computed the errors in preoperatively defined target points, finding values between 0.30 and 1 mm, and a mean error of 0.47 mm. Wei et al. [229] also used a similar setup in 15 patients with tumors involving the skull base, five of them presenting an ACC in the palate. In their case, they also installed the dynamic reference frame in the patient's skull but used bony skull landmarks and tooth cusps for registration. The registration errors and the resection accuracy in this study were not reported. Although these studies present a feasible setup for ACC resection, the installation of the dynamic reference frame is invasive. Moreover, the use of anatomical landmarks and surface matching with points in the face presents a suboptimal registration for ACC resection. Points used for registration should be close to the surgical area and surround it to provide accurate results. Anatomical landmarks and tooth cusps are not clearly defined and subject to intra- and inter-observer variability, leading to higher errors.

In our study, we have explored two different configurations for tracking and registration in ACC resection. They provide a non-invasive installation of the reference frame allowing for head movements and a registration based on artificial landmarks located close to the surgical field. The dynamic reference frame is fixed to the patient's teeth either through a silicone jig molded with the shape of the teeth or by means of a splint. The registration landmarks for the first solution (jig) consist of screws placed preoperatively. For the second solution, registration is performed through conical holes included in the splint. Both configurations were evaluated in an anatomical phantom providing equivalent accuracy results with no significant differences, and with deviations from the planned surgical margins of 0.57 and 0.61 mm respectively. These results are similar to those obtained by Tarsitano et al. [246].

The jig and screws configuration was finally used in a surgical scenario of ACC resection, obtaining deviations from the surgical margin around 1 mm and below 2 mm in

90% of the collected points along the surgical margins. Errors were higher in deeper regions. This behavior was expected, since accuracy usually decreases in areas further from the registration landmarks [99], [100]. The splint was also placed in the patient during the intervention for testing. Although the installation of screws in the maxilla has been previously described in other works as an unobtrusive and precise method for registration (70), we believe that using a splint could provide similar results while presenting a straightforward and less-invasive approach.

We have also proposed an alternative guiding method based on AR. A splint was again used for registration, to fix an AR marker in a known position and display virtual models of the patient. The precision of this system has been evaluated in a previous study, obtaining visualization errors below 3 mm [136]. This solution was also considered in our phantom study, where we obtained a 0.4 mm (IQR = 0.89) median deviation from the planned surgical margins.

Previous studies have reported other registration methods for AR visualization. Gibby et al. [271] displayed the CT and virtual models indicating trajectories for pedicle screw placement in a lumbar spine phantom. They used the OpenSight software for the HoloLens to automatically register the data with the phantom. However, a manual adjustment was needed to correct the alignment. The pedicle screws were placed with deviations between 1.3 and 1.53 mm from their planned trajectory. Other studies rely only on manual alignment for registration [211] or use additional instruments like electromagnetic or optical tracking systems [212], [272].

Although all configurations are feasible, we found the AR app to be less convenient for this procedure, as the limited line of sight of the surgical field also restricts the movements and visibility with the smartphone. The sterilization of the smartphone was easily solved by introducing it in the sterile case. However, the need to hold the smartphone, leaving only one hand free, can present a limitation. The use of head-mounted displays such as HoloLens offers an alternative to the smartphone, although the possible points of view are as limited or more than with the phone. Therefore, AR can complement conventional navigation by allowing an inspection of the margins before or after surgery but is not adequate for resection guidance. The accuracy of the system depends on the quality with which the camera sees the AR marker. This factor is highly dependent on lighting conditions and the pose of the camera with respect to the marker. The detection is optimal when the camera is close to

the marker and looks at it from the front. However, when the camera moves and detects the marker from a different angle, some inaccuracies can arise. This inherent holographic instability has already been noted by Gibby et al. [271] with the HoloLens.

6.6. Conclusions

The resection of an ACC in the palate is very challenging due to the limited visibility and the proximity to vital structures. Surgical navigation becomes a valuable tool to ensure adequate margins in such complex scenarios while performing a conservative approach. This study proposes and evaluates three different navigation setups for ACC resection. All configurations aim to provide accuracy with a non-invasive surgical procedure, improving the solutions proposed in previous studies [229], [246]. Apart from providing a less invasive solution, the novelty of the proposed setups relies on the fact that all configurations, including AR guidance, are based on 3D printing to fabricate tools that enable navigation of the patient and surgical instruments. The splint, dynamic reference frame, AR marker, and adaptor for tracking the surgical instrument are all 3D-printed with desktop 3D printers at a low cost. The three solutions were evaluated in an anatomical phantom, where they provided similar results, and tested in a surgical case. The configuration using an optical tracker and screws for registration was chosen for resection guidance during the procedure.

Surgeons combined the transoral navigated surgery with a nasal endoscopic approach, performing an optimal resection while preserving the whole alveolar process of the maxilla and upper teeth. The postoperative CT scans showed adequate resection margins. The pathological result was low-grade adenoid cystic carcinoma cribriform type, invading the mucosa, hard palate, nasal septum, and nasal floor with clear margins and perineural invasion. Head and neck tumor board established surveillance without adjuvant radiotherapy and a close follow-up. After two years, the patient is free of disease.

The results obtained from this surgery showing the accuracy and convenience of the proposed setups are promising. Navigation provided the confidence needed to undertake a more conservative approach and avoided the complete removal of the maxilla. The proposed navigation setup allowed a less invasive procedure compared to previous studies. We believe that image-guided surgery and 3D printing can provide a personalized, safe, and conservative en bloc resection minimizing the need for reconstruction.

The content of this chapter has been published in Frontiers in Oncology:

M. García-Sevilla, R. Moreta-Martinez, D. García-Mato, G. Arenas de Frutos, S. Ochandiano, C. Navarro-Cuéllar, G. Sanjuán de Moreta, J. Pascau. "Surgical Navigation, Augmented Reality, and 3D Printing for Hard Palate Adenoid Cystic Carcinoma En-Bloc Resection: Case Report and Literature Review". Front. Oncol., vol. 11, pp. 5327 (2022).

7

DISCUSSION

Late advancements in imaging techniques and computational power have boosted the introduction of CAS inside the operating room to improve precision and safety in surgical interventions [88]. Initially, the application of these technologies was restricted to neurosurgical procedures. In these interventions, accuracy is crucial to obtain satisfactory surgical outcomes and minimize the risks. Also, the surgical field is surrounded by the skull, a rigid structure that can be fixated to provide a well-defined and reliable reference frame, necessary for precise surgical navigation [30].

In the last decades, these tools have been translated to other disciplines such as orthopedic [106], [191], and maxillofacial [109] oncology. However, this translation requires an adaptation to each surgical scenario. These procedures mainly involve rigid bony structures, facilitating the translation of the preoperative plan. However, these structures are mobile or cannot be fixed due to the surgical approach. Consequently, new solutions have been introduced involving dynamic reference frames and new registration methods.

Although many solutions have been proposed adapted for each surgical scenario, there is still room for improvement. We have to pursue feasible and convenient setups that do not impose a more invasive procedure and are accessible. Additionally, more studies should be performed to analyze their accuracy and define the optimal setups to ensure precision. The aim of this thesis was to tackle the limitations of current solutions and present new alternatives that meet these criteria, analyzing the accuracy provided and comparing the results with conventional methods.

We first focused on using 3D-printed PSIs as surgical guides for orthopedic oncology procedures. Their application is increasing as they are easily introduced in the surgical room

and do not require extra hardware [177], [178], [185], [197], [198]. However, they are designed with large sizes to ensure an adequate installation, requiring additional bone exposure and, therefore, increasing intraoperative time and invasiveness [177], [184]. Their use in the pelvis is of significant interest due to its large and complex shape, with adjacent delicate structures [176], [194]. However, no study measures the accuracy they provide in realistic scenarios with a sufficiently large number of cases.

In this thesis, we performed an experimental cadaveric study with a large sample to characterize the accuracy of PSIs in the four most common locations for pelvic osteotomies. We followed a realistic workflow for preoperative planning and intraoperative procedure. To minimize the invasiveness of previous solutions, we reduced the size of PSIs, limiting the bone exposure. Additionally, PSIs were fabricated in a biocompatible material with a desktop 3D printer to make them more accessible, as they present a significantly lower price compared to industrial 3D printers. We analyzed the placement errors, computing translations and rotations with respect to the planned position. These errors were represented in a local reference frame to improve their characterization and interpretation. We also measured the osteotomy errors resulting from PSIs incorrect placements. The results demonstrate similar accuracy in short osteotomies to previous studies with lower samples, performed with larger PSIs in less realistic setups. However, we recorded errors higher than 5 mm for larger osteotomies located in the ilium, which are not acceptable for oncologic resections.

An alternative to the use of PSIs in pelvic oncology is surgical navigation. It allows not only to guide osteotomies but also to identify other anatomical structures during the procedure, which can also enhance guidance and avoid damaging vital structures [30], [190], [191], [193]. However, it introduces additional and expensive devices in the operating room. The patient-to-image registration step requires exposure of bone areas not necessarily involved in the procedure as anatomical landmarks and large surfaces are used, becoming more invasive and increasing intraoperative time [190], [195], [206]. Also, installing a dynamic reference frame fixed to the patient's bone increases the operative time and can be obtrusive [106], [199].

To overcome these limitations, we propose the introduction of the small PSIs presented in our previous work to use them as artificial landmarks, limiting bone exposure. We also simplify the reference frame installation by including a socket in the PSIs design to introduce the dynamic reference frame, allowing to attach and detach it on request. This

solution reduces the invasiveness, as well as the time and the obtrusiveness. We tested the accuracy and feasibility of the proposed setup in a cadaveric study. The installation of the dynamic reference frame demonstrated repeatability, which allows removing it without the need to repeat registration every time it is reinserted. We also analyzed the errors introduced by the PSIs and the navigation system combined and separately, defining the optimum configurations of PSIs for three common surgical scenarios to achieve high accuracy in the surgical area following a non-invasive setup. We concluded that adequate navigation accuracy and osteotomy errors below 2 mm could be achieved when at least two small PSIs are placed surrounding the target region. The highest errors measured with the data collected from the experiment were again a consequence of incorrect placements of PSIs located in the ilium.

The ilium region presents an extensive and regular shape that hinders the correct placement of PSIs and can lead to high deviations from the planned position. Whether PSIs are used independently or as a tool for surgical navigation, this uncertainty in their placement is the most critical source of error [207], [208].

To prevent this, we proposed to use AR as a tool to guide PSIs placement. The planned position can be displayed on top of the patient's bone, indicating the surgeon where to install the PSI. We developed an AR application based on detecting a 3D-printed optical marker placed on a PSI and tested it with four users who placed six pairs of PSIs in the ilium (one in the iliac crest and the other in the supra-acetabular region). Users placed the PSIs freehand, using a smartphone, and the HoloLens 2. The results demonstrate how AR can significantly reduce the risk of high placement errors, ensuring placements close to the target. Both devices present similar results, and the selection of one over the other is more subject to surgeons' preferences. Additionally, we performed the experiment in two phantom versions, where one was the traditional version 3D-printed in PLA, and the other included a layer of silicone simulating tissue to provide realism. The results demonstrated that PSIs are easier to place in the non-realistic phantom, which should be considered for further studies focused on measuring the precision of these devices. We also studied the differences among cases where smaller PSIs located in smoother regions presented higher errors than those with larger sizes or placed in more distinct regions. Hence, there exists a trade-off between reducing invasiveness and ensuring precision for the design of PSIs.

Finally, with the same objective of optimizing the current technique, we wanted to apply these same technologies to another discipline where surgical guidance is also of great value to achieve an accurate oncological resection with low risks. This is the case of tumor resections in deep regions of the mouth where the visibility and access are limited, and vital structures are close to the affected area [227], [265], [273]. In these interventions, the patient's head cannot be fixed as surgeons need to move it to access the surgical region. Therefore, alternative setups based on dynamic reference frames or new registration techniques need to be applied. Some studies have presented solutions based on dynamic reference frames screwed to the head [229], [246]. However, these setups are invasive and use non-precise registration points.

For this thesis, we focused on a real clinical case of a patient presenting an ACC in the hard palate. In this scenario, introducing surgical navigation enabled a more conservative approach and avoided the complete removal of the maxilla, minimizing the need for reconstruction. We studied the case and proposed three different non-invasive navigation solutions. Two solutions were based on an OTS with different registration methods and one on AR. All solutions used 3D-printed tools fabricated with desktop 3D printers to track the patient and surgical instruments. The accuracy of each system was measured with a 3D-printed patient-specific phantom. We obtained similar results for all solutions with errors below or close to 1 mm. Finally, one of the solutions based on the OTS was applied for surgical navigation during the intervention, although AR was also tested for visualization. The results obtained from the postoperative CT demonstrated high accuracy, with errors below 2 mm in 90% of the points recorded intraoperatively along the resection margins. The surgical outcomes demonstrated clear margins, and after two years the patient was free of disease.

The four studies included in this thesis demonstrate the multiple options 3D printing presents in surgical scenarios. We have used 3D printing not only to fabricate surgical guides but also to create AR markers, fabricate patient-specific phantoms, create patient-specific splints, or manufacture other surgical tools such as reference frames to track the movements of the patient or surgical instruments. All these devices have been fabricated using a desktop 3D printer, obtaining accurate results at a lower cost than industrial 3D printers. These printers present an affordable price and can be included in the hospitals for faster production, allowing cost-effective on-demand manufacturing [174]. However, 3D printing requires the

introduction of well-trained engineers in the hospital and the implication of surgeons in the production process.

One factor worth mentioning is that the application of all these systems requires extra preoperative time from both engineers and surgeons to plan the surgery, develop the software, design the 3D-printed tools, fabricate, and test them. This is a common entry barrier for the use of these technologies. However, it presents several potential benefits. Intraoperative time is reduced, and the procedure is performed with a higher control [41] without increasing the risk of complications [43], [44].

Although the OTS device used for the studies presented in this thesis (NDI Polaris Spectra, CA) is expensive, there is alternative and more accessible hardware such as OptiTrack V120:Duo or V120:Trio (Natural Point Inc., Corvallis, OR, US), that can also be used with the free, open-source software used for navigation, 3D Slicer.

This thesis has proposed several solutions that help minimize the invasiveness of current setups for surgical navigation. Although these solutions have been applied to two specific scenarios, selected for their complexity, similar solutions could be translated to other procedures where CAS can improve surgical outcomes.

8

CONCLUSIONS

The main contributions and conclusions of this thesis are as follows:

- We proposed a less invasive setup for osteotomy guidance in pelvic tumor resections, based on small PSIs fabricated with desktop 3D printers at a low cost. The solution was tested in a cadaveric experiment with a large sample following a realistic workflow. Their placement accuracy was analyzed for the four most common osteotomy locations, obtaining similar results to previous studies with more invasive setups. The results obtained from the analysis allowed us to identify the ilium as the region more prone to errors in placement.
- We studied how small PSIs can also be used for surgical navigation with an OTS in pelvic tumor resections to reduce the invasiveness associated with its setup. Anatomical landmarks and bone surfaces usually exposed for patient-to-image registration are substituted with artificial landmarks included in the PSIs, minimizing the exposed area. The installation of the dynamic reference frame for patient tracking is also optimized by attaching it to the PSIs. We validated the proposed setup in cadavers and evaluated its accuracy, defining the optimum PSIs configurations for surgical navigation in the three most common scenarios of tumor resection in the pelvis.
- To avoid high placement errors of PSIs in the ilium, we proposed AR guidance. We developed an AR application for smartphones and HoloLens 2 that displays the correct location of the PSIs intraoperatively. We evaluated its accuracy in a 3D-printed phantom, comparing the results with freehand placement. The analysis was also performed in a realistic phantom version which included a layer of silicone to simulate tissue. The results demonstrated how this layer hindered their placement

similarly to real scenarios. High deviations were significantly reduced in those cases where AR was used, with similar results for both devices.

- We proposed and tested in a phantom three solutions for surgical navigation in palate tumor resection based on OTS and AR. The solutions presented less invasive setups compared to previous studies. The tools used to track the patient and instruments were fabricated with desktop 3D printers at a low cost. One solution was finally applied in a surgical case. The postoperative results demonstrated a high navigation accuracy with errors below 2 mm. The proposed solution enabled a less invasive setup and a conservative approach with adequate surgical outcomes presenting clear margins.

9

PUBLICATIONS

9.1. Included in this thesis

9.1.1. Articles in peer-reviewed journals

M. García-Sevilla, L. Mediavilla-Santos, M. T. Ruiz-Alba, R. Pérez-Mañanes, J. A. Calvo-Haro, J. Pascau. *Patient-specific desktop 3D-printed guides for pelvic tumour resection surgery: a precision study on cadavers*. Int J CARS, vol. 16, no. 3, pp. 397–406, 2021. [https://doi.org/10.1007/s11548-021-02322-3] - Impact factor: 2.924 (Q2)

M. García-Sevilla, L. Mediavilla-Santos, R. Moreta-Martinez, D. García-Mato, R. Pérez-Mañanes, J. A. Calvo-Haro, J. Pascau. *Combining Surgical Navigation and 3D Printing for Less Invasive Pelvic Tumor Resections*. IEEE Access, vol. 9, pp. 133541-133551, 2021. [https://doi.org/10.1109/ACCESS.2021.3115984] - Impact factor: 3.367 (Q2)

M. García-Sevilla, R. Moreta-Martinez, D. García-Mato, A. Pose-Diez-de-la-Lastra, R. Pérez-Mañanes, J. A. Calvo-Haro and J. Pascau. *Augmented reality as a tool to guide PSI placement in pelvic tumor resections*. Sensors, vol. 21, no. 23, pp. 7824, 2021. [https://doi.org/10.3390/s21237824] - Impact factor: 3.576 (Q1)

M. García-Sevilla, R. Moreta-Martinez, D. García-Mato, G. Arenas de Frutos, S. Ochandiano, C. Navarro-Cuéllar, G. Sanjuán de Moreta, J. Pascau. *Surgical Navigation, Augmented Reality, and 3D Printing for Hard Palate Adenoid Cystic Carcinoma En-Bloc Resection: Case Report and Literature Review*. Frontiers in Oncology, vol. 11, pp. 5327, 2022. [https://doi.org/10.3389/fonc.2021.741191] - Impact factor: 6.244 (Q2)

L. Mediavilla-Santos, **M. García-Sevilla**, J. A. Calvo-Haro, M.T. Ruiz Alba, R. Pérez-Mañanes, J. Pascau, M. Cuervo Dehesa, F. J. Vaquero Martín. *Validación de los modelos de impresión 3D paciente-específicos para cirugía ortopédica oncológica pélvica*. Revista Española de Cirugía Ortopédica y Traumatología, 2021. [https://doi.org/10.1016/j.recot.2021.07.001]

9.1.2. International conferences

M. García-Sevilla, D. García-Mato, J. Calvo-Haro, R. Pérez-Mañanes, J. Pascau. *Optimizing navigation with patient-specific 3D printed guides in pelvic tumor resection surgery*. In: CARS 2019 - Computer Assisted Radiology and Surgery Proceedings of the 33rd International Congress and Exhibition, Rennes, France, June 18–21, 2019. Int J CARS, vol. 14, pp. 1–194, 2019. [https://doi.org/10.1007/s11548-019-01969-3]

M. García-Sevilla, D. García-Mato, R. Moreta-Martinez, S. Ochandiano, M. Tousidonis, C. Navarro-Cuéllar, J. Pascau. *Surgical navigation for palate carcinoma resection using a non-invasive 3D-printed reference frame*. In: CARS 2020 - Computer Assisted Radiology and Surgery Proceedings of the 34th International Congress and Exhibition, Munich, Germany, June 23–27, 2020. Int J CARS, vol. 15, pp. 1–214, 2020. [https://doi.org/10.1007/s11548-020-02171-6]

M. García-Sevilla, R. Moreta-Martinez, D. García-Mato, A. Pose-Díez-de-la-Lastra, R. Pérez-Mañanes, J. Calvo-Haro, J. Pascau. *Augmented reality for improved PSI placement in pelvic tumour resections*. In: CARS 2021: Computer Assisted Radiology and Surgery Proceedings of the 35th International Congress and Exhibition Munich, Germany, June 21-25, 2021. Int J CARS, vol. 16, pp. 1-119, 2021 [https://doi.org/10.1007/s11548-021-02375-4]

9.2. Related to this thesis

9.2.1. Articles in peer-reviewed journals

D. García-Mato, R. Moreta-Martinez, **M. García-Sevilla**, S. Ochandiano, R. García-Leal, R. Pérez-Mañanes, J. A. Calvo-Haro, J. I. Salmerón, J. Pascau. *Augmented reality visualization for craniosynostosis surgery*. Computer Methods in Biomechanics and Biomedical Engineering: Imaging & Visualization, vol. 9, no. 4, pp. 392-399, 2020. [https://doi.org/10.1080/21681163.2020.1834876] – Impact factor: 1.502 (Q3)

D. García-Mato, S. Ochandiano, **M. García-Sevilla**, C. Navarro-Cuéllar, J. V. Darriba-Allés, R. García-Leal, J. A. Calvo-Haro, R. Pérez-Mañanes, J. I. Salmerón, J. Pascau. *Craniosynostosis surgery: workflow based on virtual surgical planning, intraoperative navigation and 3D printed patient-specific guides and templates*. Scientific Reports, vol. 9, 17691, 2019. [https://doi.org/10.1038/s41598-019-54148-4] – Impact factor: 3.998 (Q1)

R Moreta-Martinez, D. García-Mato, **M. García-Sevilla**, R. Pérez-Mañanes, J. A. Calvo-Haro, J. Pascau. *Combining Augmented Reality and 3D Printing to Display Patient Models on a Smartphone*. J. Vis. Exp., 155, e60618, 2020. [https://doi.org/10.3791/60618] – Impact factor: 1.163 (Q3)

R. Moreta-Martinez, D. García-Mato, **M. García-Sevilla**, R. Pérez-Mañanes, J. A. Calvo, J. Pascau. *Augmented reality in computer-assisted interventions based on patient-specific 3D printed reference*. Healthcare Technology Letters, vol. 5, pp. 162-166, 2018. [https://doi.org/10.1049/htl.2018.5072]

R. Moreta-Martinez, J. A. Calvo-Haro, R. Pérez-Mañanes, **M. García-Sevilla**, L. Mediavilla-Santos, and J. Pascau. *Desktop 3D Printing: Key for Surgical Navigation in Acral Tumors?* Applied Sciences, vol. 10, no. 24, pp. 8984, 2020. [https://doi.org/10.3390/app10248984] – Impact Factor: 2.474 (Q2)

9.2.2. International conferences

D. García-Mato, R. Moreta-Martinez, **M. García-Sevilla**, S. Ochandiano, R. García-Leal, R. Pérez-Mañanes, J. A. Calvo-Haro, J. I. Salmerón, J. Pascau. *Augmented Reality Visualization for Craniosynostosis Surgery*. 23rd International Conference on Medical Image Computing & Computer Assisted Intervention (MICCAI), Lima, Peru, 2020.

R. Moreta-Martinez, D. García-Mato, **M. García-Sevilla**, S. Ochandiano, R. García-Leal, R. Pérez-Mañanes, J. A. Calvo-Haro, J. I. Salmerón, J. Pascau. *Augmented reality for bone fragment positioning during craniosynostosis reconstruction surgery*. In: CARS 2020 - Computer Assisted Radiology and Surgery Proceedings of the 34th International Congress and Exhibition, Munich, Germany, June 23–27, 2020. Int J CARS, vol. 15, pp. 1–214, 2020. [https://doi.org/10.1007/s11548-020-02171-6]

R. Moreta-Martinez, D. García-Mato, **M. García-Sevilla**, R. Pérez-Mañanes, J. A. Calvo, J. Pascau. *AR in computer-assisted interventions based on patient-specific 3D printed*

reference. Augmented Environments for Computer-Assisted Interventions Workshop, 21st International Conference on Medical Image Computing & Computer Assisted Intervention (MICCAI), Granada, Spain, 2018.

D. García-Mato, S. Ochandiano, S. Espías-Alonso, **M. García-Sevilla**, R. Moreta-Martinez, J. A. Calvo-Haro, R. Pérez-Mañanes, J. Pascau. *Non-invasive computer-assisted dental implant surgery based on optical tracking and 3D printing*. In: CARS 2019 - Computer Assisted Radiology and Surgery Proceedings of the 33rd International Congress and Exhibition, Rennes, France, June 18–21, 2019. Int J CARS, vol. 14, pp. 1–194, 2019.

D. García-Mato, S. Ochandiano, M. Tousidonis, R. Moreta-Martínez, **M. García-Sevilla**, M. Desco, J. Pascau *Orbital Floor Reconstruction Workflow based on 3D Printing and Surgical Navigation*. In: CARS 2018 - Computer Assisted Radiology and Surgery Proceedings of the 32nd International Congress and Exhibition, Berlin, Germany, June 20–23, 2018. Int J CARS, vol. 13, pp. 1–273, 2018.

9.3. Other publications

9.3.1. Articles in peer-reviewed journals

M. García-Sevilla, J. De León-Luis, R. Moreta-Martínez, D. García-Mato, R. Pérez-Mañanes, J. A. Calvo-Haro, J. Pascau. *Performance Evaluation to Improve Training in Forceps-Assisted Delivery*. OR 2.0 Context-Aware Operating Theaters, Computer Assisted Robotic Endoscopy, Clinical Image-Based Procedures, and Skin Image Analysis. Lecture Notes in Computer Science, vol 11041, pp. 69-77, 2018. [https://doi.org/10.1007/978-3-030-01201-4_9]

D. García-Mato**, M. García-Sevilla**, A.R. Porras, S. Ochandiano, J.V. Darriba-Allés, R. García-Leal, J.I. Salmerón, M.G. Linguraru, J. Pascau. *Three-Dimensional Photography for Intraoperative Morphometric Analysis in Metopic Craniosynostosis Surgery*. Int J CARS, vol. 16, pp. 277–287, 2021. [https://doi.org/10.1007/s11548-020-02301-0] - Impact factor: 2.924 (Q2)

F. Alfano, J.E. Ortuño Fisac, **M. García-Sevilla**, M. Herrero Conde, O. Bueno Zamora, S. Lizarraga, A. Santos, J. Pascau, M.J. Ledesma Carbayo. *Prone to Supine Surface Based Registration Workflow for Breast Tumor Localization in Surgical Planning*. 2019

IEEE 16th International Symposium on Biomedical Imaging (ISBI 2019), pp. 1150-1153, 2019. [https://doi.org/10.1109/ISBI.2019.8759104]

E. Marinetto, J.G. Victores, **M. García-Sevilla**, M. Muñoz, F.Á. Calvo, C. Balaguer, M. Desco, and J. Pascau. *Technical Note: Mobile accelerator guidance using an optical tracker during docking in IOERT procedures*. Medical Physics, vol. 44: 5061-5069, 2017. [https://doi.org/10.1002/mp.12482]

9.3.2. International conferences

M. García-Sevilla, J. De León-Luis, R. Moreta-Martínez, D. García-Mato, R. Pérez-Mañanes, J. A. Calvo-Haro, and J. Pascau. *Performance Evaluation to Improve Training in Forceps-Assisted Delivery*. OR 2.0 Context-Aware Operating Theaters Workshop, 21st International Conference on Medical Image Computing & Computer Assisted Intervention (MICCAI), Granada, Spain, 2018.

D. García-Mato, **M. García-Sevilla**, S. Ochandiano, R. Moreta-Martinez, J. V. Darriba-Allés, R. García-Leal, J. I. Salmerón, J. Pascau. *Intraoperative Outcome Evaluation in Craniosynostosis Reconstruction Surgery using 3D Photography*. In: CARS 2020 - Computer Assisted Radiology and Surgery Proceedings of the 34th International Congress and Exhibition, Munich, Germany, June 23–27, 2020. Int J CARS, vol. 15, pp. 1–214, 2020. [https://doi.org/10.1007/s11548-020-02171-6]

D. García-Mato, **M. García-Sevilla**, S. Ochandiano, C. Navarro-Cuéllar, J. V. Darriba-Allés, R. García-Leal, J. Pascau. *Morphometric Analysis in Craniosynostosis Reconstruction Surgery based on Structured Light Scanning*. 18th meeting of the International Society of Craniofacial Surgery (ISCFS) 2019, Paris, France. Plastic and Reconstructive Surgery - Global Open: August 2019, vol. 7, no. 8S-2, pp. 196, 2019.

D. García-Mato, **M. García-Sevilla**, S. Ochandiano, C. Navarro-Cuéllar, J. V. Darriba-Allés, R. García-Leal, J. Pascau. *Structured Light Scanning for Morphometric Analysis in Craniosynostosis Reconstruction Surgery*. In: CARS 2019 - Computer Assisted Radiology and Surgery Proceedings of the 33rd International Congress and Exhibition, Rennes, France, June 18–21, 2019. Int J CARS, vol. 14, pp. 1–194, 2019. [https://doi.org/10.1007/s11548-019-01969-3]

R. Moreta-Martinez, **M. García-Sevilla**, D. García-Mato, A. Pose-Díez-de-la-Lastra, I. Rubio-Pérez, and J. Pascau. *Smartphone-based augmented reality system for needle insertion guidance in sacral nerve stimulation*. In: CARS 2021 - Computer Assisted Radiology and Surgery Proceedings of the 35th International Congress and Exhibition, Munich, Germany, June 21–25, 2021. Int J CARS, vol. 15, pp. 1–214, 2021. [https://doi.org/10.1007/s11548-021-02375-4]

R. Moreta-Martinez, D. García-Mato, **M. García-Sevilla**, R. Pérez-Mañanes, J. A. Calvo, and J. Pascau. *AR in computer-assisted interventions based on patient-specific 3D printed reference*. Augmented Environments for Computer-Assisted Interventions Workshop (AECAI), 21st International Conference on Medical Image Computing & Computer Assisted Intervention (MICCAI), Granada, Spain, 2018.

M. Concepción-Brito, R. Moreta-Martinez, J. Serrano, D. García-Mato, **M. García-Sevilla**, and J. Pascau. *Segmentation of Organs at Risk in Head and Neck Radiation Therapy with 3D Convolutional Networks*. In: CARS 2019 - Computer Assisted Radiology and Surgery Proceedings of the 33rd International Congress and Exhibition, Rennes, France, June 18–21, 2019. Int J CARS, vol. 14, pp. 1–194, 2019. [https://doi.org/10.1007/s11548-019-01969-3]

10

REFERENCES

[1] V. T. DeVita and S. A. Rosenberg, “Two Hundred Years of Cancer Research,” *N. Engl. J. Med.*, vol. 366, no. 23, pp. 2207–2214, May 2012, doi: 10.1056/NEJMra1204479.

[2] D. Trichopoulos, F. P. Li, and D. J. Hunter, “What Causes Cancer?,” *Sci. Am.*, vol. 275, no. 3, pp. 80–87, Oct. 1996, doi: 10.1038/scientificamerican0996-80.

[3] R. A. DePinho, “The age of cancer,” *Nature*, vol. 408, no. 6809, pp. 248–254, 2000, doi: 10.1038/35041694.

[4] W. H. Clark, “Tumour progression and the nature of cancer,” *Br. J. Cancer*, vol. 64, no. 4, pp. 631–644, 1991, doi: 10.1038/bjc.1991.375.

[5] S. I. Hajdu, “A note from history: landmarks in history of cancer, part 3.,” *Cancer*, vol. 118, no. 4, pp. 1155–1168, Feb. 2012, doi: 10.1002/cncr.26320.

[6] C. L. Chaffer and R. A. Weinberg, “A Perspective on Cancer Cell Metastasis,” *Science (80-.).*, vol. 331, no. 6024, pp. 1559–1564, 2011, doi: 10.1126/science.1203543.

[7] J. C. A. Récamier, *Recherches sur le traitement du cancer par la compression méthodique simple ou combinée, et sur l’histoire général de la même maladie*. Paris: Gabon, 1829.

[8] M. E. Miller, “Cancer.” Momentum Press, New York, 2018.

[9] National Cancer Institute, “What Is Cancer?” https://www.cancer.gov/about-cancer/understanding/what-is-cancer (accessed Sep. 21, 2021).

[10] J. Ferlay *et al.*, “Cancer incidence and mortality worldwide: sources, methods and

major patterns in GLOBOCAN 2012.," *Int. J. cancer*, vol. 136, no. 5, pp. E359-86, Mar. 2015, doi: 10.1002/ijc.29210.

[11] C. de Martel, D. Georges, F. Bray, J. Ferlay, and G. M. Clifford, "Global burden of cancer attributable to infections in 2018: a worldwide incidence analysis," *Lancet Glob. Heal.*, vol. 8, no. 2, pp. e180–e190, Feb. 2020, doi: 10.1016/S2214-109X(19)30488-7.

[12] P. S. Harper, *Practical genetic counselling*, 6th ed. London : Arnold, 2004.

[13] F. K. Tangka, J. G. Trogdon, L. C. Richardson, D. Howard, S. A. Sabatino, and E. A. Finkelstein, "Cancer treatment cost in the United States," *Cancer*, vol. 116, no. 14, pp. 3477–3484, Jul. 2010, doi: https://doi.org/10.1002/cncr.25150.

[14] W. H. Organization and Others, "WHO report on cancer: setting priorities, investing wisely and providing care for all," 2020, [Online]. Available: https://apps.who.int/iris/handle/10665/330745.

[15] S. I. Hajdu and M. Vadmal, "A note from history: Landmarks in history of cancer, Part 6.," *Cancer*, vol. 119, no. 23, pp. 4058–4082, Dec. 2013, doi: 10.1002/cncr.28319.

[16] S. I. Hajdu, M. Vadmal, and P. Tang, "A note from history: Landmarks in history of cancer, part 7.," *Cancer*, vol. 121, no. 15, pp. 2480–2513, Aug. 2015, doi: 10.1002/cncr.29365.

[17] J. Eggert, *Cancer Basics*. Oncology Nursing Society, 2017.

[18] American Cancer Society, "How surgery is used for cancer." https://www.cancer.org/treatment/treatments-and-side-effects/treatment-types/surgery/how-surgery-is-used-for-cancer.html (accessed Sep. 19, 2021).

[19] S. I. Hajdu, "A note from history: Landmarks in history of cancer, part 1," *Cancer*, vol. 117, no. 5, pp. 1097–1102, Mar. 2011, doi: https://doi.org/10.1002/cncr.25553.

[20] W. S. Halsted, "The results of operations for the cure of cancer of the breast performed at the Johns Hopkins Hospital from June, 1889, to January, 1894," *Ann. Surg.*, vol. 20, 1894.

[21] B. Fisher *et al.*, "Ten-Year Results of a Randomized Clinical Trial Comparing Radical Mastectomy and Total Mastectomy with or without Radiation," *N. Engl. J. Med.*, vol.

312, no. 11, pp. 674–681, Mar. 1985, doi: 10.1056/NEJM198503143121102.

[22] B. Fisher *et al.*, “L-Phenylalanine Mustard (L-PAM) in the Management of Primary Breast Cancer,” *N. Engl. J. Med.*, vol. 292, no. 3, pp. 117–122, Jan. 1975, doi: 10.1056/NEJM197501162920301.

[23] B. Fisher *et al.*, “Treatment of Primary Breast Cancer with Chemotherapy and Tamoxifen,” *N. Engl. J. Med.*, vol. 305, no. 1, pp. 1–6, Jul. 1981, doi: 10.1056/NEJM198107023050101.

[24] B. Fisher *et al.*, “Twenty-Year Follow-up of a Randomized Trial Comparing Total Mastectomy, Lumpectomy, and Lumpectomy plus Irradiation for the Treatment of Invasive Breast Cancer,” *N. Engl. J. Med.*, vol. 347, no. 16, pp. 1233–1241, Oct. 2002, doi: 10.1056/NEJMoa022152.

[25] S. Sukegawa, T. Kanno, and Y. Furuki, “Application of computer-assisted navigation systems in oral and maxillofacial surgery,” *Jpn. Dent. Sci. Rev.*, vol. 54, no. 3, pp. 139–149, 2018, doi: 10.1016/j.jdsr.2018.03.005.

[26] U. Sure, O. Alberti, M. Petermeyer, R. Becker, and H. Bertalanffy, “Advanced image-guided skull base surgery,” *Surg. Neurol.*, vol. 53, no. 6, pp. 563–572, Jun. 2000, doi: 10.1016/S0090-3019(00)00243-3.

[27] S. Micali, “Computer Assisted Surgery,” *Urol. J.*, vol. 78, no. 1, pp. 52–59, Jan. 2011, doi: 10.5301/RU.2011.6438.

[28] G. D. Dockery, “Surgical principles,” in *Lower Extremity Soft Tissue & Cutaneous Plastic Surgery: Second Edition*, G. D. Dockery and M. E. B. T.-L. E. S. T. & C. P. S. (Second E. Crawford, Eds. Oxford: W.B. Saunders, 2012, pp. 23–27.

[29] R. A. Mischkowski, M. J. Zinser, L. Ritter, J. Neugebauer, E. Keeve, and J. E. Zöller, “Intraoperative navigation in the maxillofacial area based on 3D imaging obtained by a cone-beam device.,” *Int. J. Oral Maxillofac. Surg.*, vol. 36, no. 8, pp. 687–694, Aug. 2007, doi: 10.1016/j.ijom.2007.04.001.

[30] K. Cleary and T. M. Peters, “Image-Guided Interventions: Technology Review and Clinical Applications,” *Annu. Rev. Biomed. Eng.*, vol. 12, no. 1, pp. 119–142, 2010, doi: 10.1146/annurev-bioeng-070909-105249.

[31] V. Petrik, V. Apok, J. A. Britton, B. A. Bell, and M. C. Papadopoulos, “Godfrey

Hounsfield and the Dawn of Computed Tomography," *Neurosurgery*, vol. 58, no. 4, pp. 780–787, Apr. 2006, doi: 10.1227/01.NEU.0000204309.91666.06.

[32] M. W. Vannier, J. L. Marsh, and J. O. Warren, "Three dimensional CT reconstruction images for craniofacial surgical planning and evaluation.," *Radiology*, vol. 150, no. 1, pp. 179–184, Jan. 1984, doi: 10.1148/radiology.150.1.6689758.

[33] O. H. Karatas and E. Toy, "Three-dimensional imaging techniques: A literature review," *Eur. J. Dent.*, vol. 8, no. 1, pp. 132–140, Jan. 2014, doi: 10.4103/1305-7456.126269.

[34] R. A. Drebin, L. Carpenter, and P. Hanrahan, "Volume Rendering," *SIGGRAPH Comput. Graph.*, vol. 22, no. 4, pp. 65–74, Jun. 1988, doi: 10.1145/378456.378484.

[35] F. Nielsen and R. Nock, "On region merging: the statistical soundness of fast sorting, with applications," in *2003 IEEE Computer Society Conference on Computer Vision and Pattern Recognition, 2003. Proceedings.*, 2003, vol. 2, pp. II–19, doi: 10.1109/CVPR.2003.1211447.

[36] L. Zhao, P. K. Patel, and M. Cohen, "Application of virtual surgical planning with computer assisted design and manufacturing technology to cranio-maxillofacial surgery," *Arch. Plast. Surg.*, vol. 39, no. 4, pp. 309–316, Jul. 2012, doi: 10.5999/aps.2012.39.4.309.

[37] K. R. Smith, K. J. Frank, and R. D. Bucholz, "The NeurostationTM—A highly accurate, minimally invasive solution to frameless stereotactic neurosurgery," *Comput. Med. Imaging Graph.*, vol. 18, no. 4, pp. 247–256, 1994, doi: https://doi.org/10.1016/0895-6111(94)90049-3.

[38] S. Vilsmeier and F. Nisiropoulos, "Introduction of the Passive Marker Neuronavigation System VectorVision BT - Computer-Assisted Neurosurgery," 1997, pp. 23–37.

[39] R. Marmulla and H. Niederdellmann, "Surgical Planning of Computer-Assisted Repositioning Osteotomies," *Plast. Reconstr. Surg.*, vol. 104, no. 4, 1999, doi: 10.1097/00006534-199909040-00007.

[40] R. A. Kockro *et al.*, "Planning and Simulation of Neurosurgery in a Virtual Reality Environment," *Neurosurgery*, vol. 46, no. 1, pp. 118–137, Jan. 2000, doi:

10.1093/neurosurgery/46.1.118.

[41] J. I. Efanov, A.-A. Roy, K. N. Huang, and D. E. Borsuk, “Virtual Surgical Planning: The Pearls and Pitfalls,” *Plast. Reconstr. surgery. Glob. open*, vol. 6, no. 1, pp. e1443–e1443, Jan. 2018, doi: 10.1097/GOX.0000000000001443.

[42] Z. Chen, S. Mo, X. Fan, Y. You, G. Ye, and N. Zhou, “A Meta-analysis and Systematic Review Comparing the Effectiveness of Traditional and Virtual Surgical Planning for Orthognathic Surgery: Based on Randomized Clinical Trials,” *J. Oral Maxillofac. Surg.*, vol. 79, no. 2, pp. 471.e1-471.e19, 2021, doi: https://doi.org/10.1016/j.joms.2020.09.005.

[43] E. I. Chang, M. P. Jenkins, S. A. Patel, and N. S. Topham, “Long-Term Operative Outcomes of Preoperative Computed Tomography-Guided Virtual Surgical Planning for Osteocutaneous Free Flap Mandible Reconstruction.,” *Plast. Reconstr. Surg.*, vol. 137, no. 2, pp. 619–623, Feb. 2016, doi: 10.1097/01.prs.0000475796.61855.a7.

[44] J. M. Toto, E. I. Chang, R. Agag, K. Devarajan, S. A. Patel, and N. S. Topham, “Improved operative efficiency of free fibula flap mandible reconstruction with patient-specific, computer-guided preoperative planning.,” *Head Neck*, vol. 37, no. 11, pp. 1660–1664, Nov. 2015, doi: 10.1002/hed.23815.

[45] G. Succo *et al.*, “Step-by-step surgical technique for mandibular reconstruction with fibular free flap: application of digital technology in virtual surgical planning,” *Eur. Arch. Oto-Rhino-Laryngology*, vol. 272, no. 6, pp. 1491–1501, 2015, doi: 10.1007/s00405-014-3078-3.

[46] D. Hoang, D. Perrault, M. Stevanovic, and A. Ghiassi, “Surgical applications of three-dimensional printing: a review of the current literature & how to get started,” *Ann. Transl. Med. Vol 4, No 23 (December 2016) Ann. Transl. Med. (Focus “Innovations Technol. Surgery”)*, vol. 4, no. 23, p. 456, 2016, doi: 10.21037/atm.2016.12.18.

[47] M. McGurk, A. A. Amis, P. Potamianos, and N. M. Goodger, “Rapid prototyping techniques for anatomical modelling in medicine,” *Ann. R. Coll. Surg. Engl.*, vol. 79, no. 3, pp. 169–174, May 1997.

[48] D. Pramanik, N. Roy, and A. S. B. T.-R. M. in M. S. and M. E. Kuar, “Additive Manufacturing of Polymer Materials: Recent Developments,” Elsevier, 2021.

[49] R. H. Awad, S. A. Habash, and C. J. Hansen, “Chapter 2 - 3D Printing Methods,” S. J. Al’Aref, B. Mosadegh, S. Dunham, and J. K. B. T.-3D P. A. in C. M. Min, Eds. Boston: Academic Press, 2018, pp. 11–32.

[50] A. Su and S. J. Al’Aref, “Chapter 1 - History of 3D Printing,” S. J. Al’Aref, B. Mosadegh, S. Dunham, and J. K. B. T.-3D P. A. in C. M. Min, Eds. Boston: Academic Press, 2018, pp. 1–10.

[51] A. Mazzoli, “Selective laser sintering in biomedical engineering,” *Med. Biol. Eng. Comput.*, vol. 51, no. 3, pp. 245–256, 2013, doi: 10.1007/s11517-012-1001-x.

[52] C. Derekas and D. Kiss, “Development of desktop 3D printer,” *Des. Mach. Struct.*, vol. 10, no. 2, pp. 20–26, 2020, doi: 10.32972/dms.2020.009.

[53] G. B. Kim *et al.*, “Three-Dimensional Printing: Basic Principles and Applications in Medicine and Radiology,” *Korean J. Radiol.*, vol. 17, no. 2, pp. 182–197, 2016, doi: 10.3348/kjr.2016.17.2.182.

[54] V. Filippou and C. Tsoumpas, “Recent advances on the development of phantoms using 3D printing for imaging with CT, MRI, PET, SPECT, and ultrasound,” *Med. Phys.*, vol. 45, no. 9, pp. e740–e760, Sep. 2018, doi: https://doi.org/10.1002/mp.13058.

[55] A. Mahmoud and M. Bennett, “Introducing 3-Dimensional Printing of a Human Anatomic Pathology Specimen: Potential Benefits for Undergraduate and Postgraduate Education and Anatomic Pathology Practice,” *Arch. Pathol. Lab. Med.*, vol. 139, no. 8, pp. 1048–1051, Aug. 2015, doi: 10.5858/arpa.2014-0408-OA.

[56] J. T. Lambrecht, D. C. Berndt, R. Schumacher, and M. Zehnder, “Generation of three-dimensional prototype models based on cone beam computed tomography,” *Int. J. Comput. Assist. Radiol. Surg.*, vol. 4, no. 2, pp. 175–180, 2009, doi: 10.1007/s11548-008-0275-9.

[57] E. A. Gillaspie *et al.*, “From 3-Dimensional Printing to 5-Dimensional Printing: Enhancing Thoracic Surgical Planning and Resection of Complex Tumors,” *Ann. Thorac. Surg.*, vol. 101, no. 5, pp. 1958–1962, May 2016, doi: 10.1016/j.athoracsur.2015.12.075.

[58] S. N. Kurenov, C. Ionita, D. Sammons, and T. L. Demmy, “Three-dimensional printing to facilitate anatomic study, device development, simulation, and planning in

thoracic surgery.," *J. Thorac. Cardiovasc. Surg.*, vol. 149, no. 4, pp. 973–9.e1, Apr. 2015, doi: 10.1016/j.jtcvs.2014.12.059.

[59] P. Fiaschi *et al.*, "Surgical results of cranioplasty with a polymethylmethacrylate customized cranial implant in pediatric patients: a single-center experience.," *J. Neurosurg. Pediatr.*, vol. 17, no. 6, pp. 705–710, Jun. 2016, doi: 10.3171/2015.10.PEDS15489.

[60] L. Wang, T. Cao, X. Li, and L. Huang, "Three-dimensional printing titanium ribs for complex reconstruction after extensive posterolateral chest wall resection in lung cancer.," *J. Thorac. Cardiovasc. Surg.*, vol. 152, no. 1, pp. e5-7, Jul. 2016, doi: 10.1016/j.jtcvs.2016.02.064.

[61] U.-L. Lee, J.-S. Kwon, and Y.-J. Choi, "Keyhole System: A Computer-Assisted Designed and Computer-Assisted Manufactured Maxillomandibular Complex Repositioner in Orthognathic Surgery.," *J. oral Maxillofac. Surg. Off. J. Am. Assoc. Oral Maxillofac. Surg.*, vol. 73, no. 10, pp. 2024–2029, Oct. 2015, doi: 10.1016/j.joms.2015.03.026.

[62] F. Qiao, D. Li, Z. Jin, D. Hao, Y. Liao, and S. Gong, "A novel combination of computer-assisted reduction technique and three dimensional printed patient-specific external fixator for treatment of tibial fractures.," *Int. Orthop.*, vol. 40, no. 4, pp. 835–841, Apr. 2016, doi: 10.1007/s00264-015-2943-z.

[63] H. Chen, D. Wu, H. Yang, and K. Guo, "Clinical Use of 3D Printing Guide Plate in Posterior Lumbar Pedicle Screw Fixation," *Med. Sci. Monit.*, vol. 21, pp. 3948–3954, Dec. 2015, doi: 10.12659/msm.895597.

[64] A. W. Yu and M. Khan, "On-demand three-dimensional printing of surgical supplies in conflict zones.," *J. Trauma Acute Care Surg.*, vol. 78, no. 1, pp. 201–203, Jan. 2015, doi: 10.1097/TA.0000000000000481.

[65] T. M. Rankin, N. A. Giovinco, D. J. Cucher, G. Watts, B. Hurwitz, and D. G. Armstrong, "Three-dimensional printing surgical instruments: are we there yet?," *J. Surg. Res.*, vol. 189, no. 2, pp. 193–197, Jun. 2014, doi: 10.1016/j.jss.2014.02.020.

[66] K. C. Wong, S. M. Kumta, N. V Geel, and J. Demol, "One-step reconstruction with a 3D-printed, biomechanically evaluated custom implant after complex pelvic tumor

resection.," *Comput. aided Surg. Off. J. Int. Soc. Comput. Aided Surg.*, vol. 20, no. 1, pp. 14–23, 2015, doi: 10.3109/10929088.2015.1076039.

[67] H. Li, X. Qu, Y. Mao, K. Dai, and Z. Zhu, "Custom Acetabular Cages Offer Stable Fixation and Improved Hip Scores for Revision THA With Severe Bone Defects," *Clin. Orthop. Relat. Res.*, vol. 474, no. 3, pp. 731–740, Mar. 2016, doi: 10.1007/s11999-015-4587-0.

[68] F. Qiao *et al.*, "Application of 3D printed customized external fixator in fracture reduction.," *Injury*, vol. 46, no. 6, pp. 1150–1155, 2015, doi: 10.1016/j.injury.2015.01.020.

[69] L. Ma *et al.*, "3D-printed guiding templates for improved osteosarcoma resection," *Sci. Rep.*, vol. 6, p. 23335, Mar. 2016, doi: 10.1038/srep23335.

[70] M. Hirao *et al.*, "Computer assisted planning and custom-made surgical guide for malunited pronation deformity after first metatarsophalangeal joint arthrodesis in rheumatoid arthritis: a case report.," *Comput. aided Surg. Off. J. Int. Soc. Comput. Aided Surg.*, vol. 19, no. 1–3, pp. 13–19, 2014, doi: 10.3109/10929088.2014.885992.

[71] Z. Jaffry *et al.*, "Unicompartmental knee arthroplasties: robot vs. patient specific instrumentation.," *Knee*, vol. 21, no. 2, pp. 428–434, Mar. 2014, doi: 10.1016/j.knee.2013.11.017.

[72] S. Kaneyama, T. Sugawara, and M. Sumi, "Safe and accurate midcervical pedicle screw insertion procedure with the patient-specific screw guide template system.," *Spine (Phila. Pa. 1976).*, vol. 40, no. 6, pp. E341-8, Mar. 2015, doi: 10.1097/BRS.0000000000000772.

[73] H. Huang *et al.*, "Improved accuracy of 3D-printed navigational template during complicated tibial plateau fracture surgery.," *Australas. Phys. Eng. Sci. Med.*, vol. 38, no. 1, pp. 109–117, Mar. 2015, doi: 10.1007/s13246-015-0330-0.

[74] V. Reiser *et al.*, "V-stand--a versatile surgical platform for oromandibular reconstruction using a 3-dimensional virtual modeling system.," *J. oral Maxillofac. Surg. Off. J. Am. Assoc. Oral Maxillofac. Surg.*, vol. 73, no. 6, pp. 1211–1226, Jun. 2015, doi: 10.1016/j.joms.2014.12.033.

[75] S. Mazzoni, A. Bianchi, G. Schiariti, G. Badiali, and C. Marchetti, "Computer-aided

design and computer-aided manufacturing cutting guides and customized titanium plates are useful in upper maxilla waferless repositioning.," *J. oral Maxillofac. Surg. Off. J. Am. Assoc. Oral Maxillofac. Surg.*, vol. 73, no. 4, pp. 701–707, Apr. 2015, doi: 10.1016/j.joms.2014.10.028.

[76] S.-H. Kang, M.-K. Kim, T.-K. You, and J.-Y. Lee, "Modification of planned postoperative occlusion in orthognathic surgery, based on computer-aided design/computer-aided manufacturing-engineered preoperative surgical simulation.," *J. oral Maxillofac. Surg. Off. J. Am. Assoc. Oral Maxillofac. Surg.*, vol. 73, no. 1, pp. 134–151, Jan. 2015, doi: 10.1016/j.joms.2014.07.021.

[77] B. Li, L. Zhang, H. Sun, J. Yuan, S. G. F. Shen, and X. Wang, "A novel method of computer aided orthognathic surgery using individual CAD/CAM templates: a combination of osteotomy and repositioning guides.," *Br. J. Oral Maxillofac. Surg.*, vol. 51, no. 8, pp. e239-44, Dec. 2013, doi: 10.1016/j.bjoms.2013.03.007.

[78] M. el-Gengehi and S. A. Seif, "Evaluation of the Accuracy of Computer-Guided Mandibular Fracture Reduction.," *J. Craniofac. Surg.*, vol. 26, no. 5, pp. 1587–1591, Jul. 2015, doi: 10.1097/SCS.0000000000001773.

[79] A. Shqaidef, A. F. Ayoub, and B. S. Khambay, "How accurate are rapid prototyped (RP) final orthognathic surgical wafers? A pilot study.," *Br. J. Oral Maxillofac. Surg.*, vol. 52, no. 7, pp. 609–614, Sep. 2014, doi: 10.1016/j.bjoms.2014.04.010.

[80] S.-H. Kang, M.-K. Kim, B. C. Kim, and S.-H. Lee, "Orthognathic Y-splint: a CAD/CAM-engineered maxillary repositioning wafer assembly.," *Br. J. Oral Maxillofac. Surg.*, vol. 52, no. 7, pp. 667–669, Sep. 2014, doi: 10.1016/j.bjoms.2014.01.023.

[81] N. Adolphs, W. Liu, E. Keeve, and B. Hoffmeister, "RapidSplint: virtual splint generation for orthognathic surgery - results of a pilot series.," *Comput. aided Surg. Off. J. Int. Soc. Comput. Aided Surg.*, vol. 19, no. 1–3, pp. 20–28, 2014, doi: 10.3109/10929088.2014.887778.

[82] E. Shaheen, A. Alhelwani, E. Van De Casteele, C. Politis, and R. Jacobs, "Evaluation of Dimensional Changes of 3D Printed Models After Sterilization: A Pilot Study," *Open Dent. J.*, vol. 12, pp. 72–79, Jan. 2018, doi: 10.2174/1874210601812010072.

[83] H. H. Malik *et al.*, “Three-dimensional printing in surgery: a review of current surgical applications.,” *J. Surg. Res.*, vol. 199, no. 2, pp. 512–522, Dec. 2015, doi: 10.1016/j.jss.2015.06.051.

[84] S. M. Fuller, D. R. Butz, C. B. Vevang, and M. V Makhlouf, “Application of 3-dimensional printing in hand surgery for production of a novel bone reduction clamp.,” *J. Hand Surg. Am.*, vol. 39, no. 9, pp. 1840–1845, Sep. 2014, doi: 10.1016/j.jhsa.2014.06.009.

[85] N. Martelli *et al.*, “Advantages and disadvantages of 3-dimensional printing in surgery: A systematic review.,” *Surgery*, vol. 159, no. 6, pp. 1485–1500, Jun. 2016, doi: 10.1016/j.surg.2015.12.017.

[86] Y.-T. Wang, X.-J. Yang, B. Yan, T.-H. Zeng, Y.-Y. Qiu, and S.-J. Chen, “Clinical application of three-dimensional printing in the personalized treatment of complex spinal disorders.,” *Chinese J. Traumatol. = Zhonghua chuang shang za zhi*, vol. 19, no. 1, pp. 31–34, 2016, doi: 10.1016/j.cjtee.2015.09.009.

[87] C. Li *et al.*, “Application of the polystyrene model made by 3-D printing rapid prototyping technology for operation planning in revision lumbar discectomy.,” *J. Orthop. Sci. Off. J. Japanese Orthop. Assoc.*, vol. 20, no. 3, pp. 475–480, May 2015, doi: 10.1007/s00776-015-0706-8.

[88] U. Mezger, C. Jendrewski, and M. Bartels, “Navigation in surgery,” *Langenbeck’s Arch. Surg.*, vol. 398, no. 4, pp. 501–514, Apr. 2013, doi: 10.1007/s00423-013-1059-4.

[89] R. B. Bell, “Computer Planning and Intraoperative Navigation in Orthognathic Surgery,” *J. Oral Maxillofac. Surg.*, vol. 69, no. 3, pp. 592–605, 2011, doi: https://doi.org/10.1016/j.joms.2009.06.030.

[90] D. J. Cantor, “E. H. Burrows, Pioneers and early years. A history of British radiology , Alderney, Colophon, 1986, 4to, pp. viii, 264, illus.,” *Med. Hist.*, vol. 32, no. 2, p. 224, 1988, doi: 10.1017/S0025727300048146.

[91] J. Cox and R. C. Kirkpatrick, “The new photography: with report of a case in which a bullet was photographed in the leg,” *Montr. Med. J.*, vol. 24, no. 661, p. 65, 1896.

[92] A. Compston, “The structure and functions of the cerebellum examined by a new method. By Sir Victor Horsley, FRS, FRCS and R.H. Clarke, MA, MB. Brain 1908:

31; 45–124.," *Brain*, vol. 130, no. 6, pp. 1449–1452, Jun. 2007, doi: 10.1093/brain/awm115.

[93] E. M. Friets, J. W. Strohbehn, J. F. Hatch, and D. W. Roberts, "A frameless stereotaxic operating microscope for neurosurgery.," *IEEE Trans. Biomed. Eng.*, vol. 36, no. 6, pp. 608–617, Jun. 1989, doi: 10.1109/10.29455.

[94] R. L. G. Jr., C. A. E. II, J. T. Lewis, and R. J. Maciunas, "Image display and surgical visualization in interactive image-guided neurosurgery," *Opt. Eng.*, vol. 32, no. 8, pp. 1955–1962, Aug. 1993, doi: 10.1117/12.143712.

[95] N. D. Glossop, "Advantages of optical compared with electromagnetic tracking.," *J. Bone Joint Surg. Am.*, vol. 91 Suppl 1, pp. 23–28, Feb. 2009, doi: 10.2106/JBJS.H.01362.

[96] B. Preim and C. Botha, "Chapter 18 - Image-Guided Surgery and Augmented Reality," B. Preim and C. B. T.-V. C. for M. (Second E. Botha, Eds. Boston: Morgan Kaufmann, 2014, pp. 625–663.

[97] P. J. Slomka and R. P. Baum, "Multimodality image registration with software: state-of-the-art.," *Eur. J. Nucl. Med. Mol. Imaging*, vol. 36 Suppl 1, pp. S44-55, Mar. 2009, doi: 10.1007/s00259-008-0941-8.

[98] K. S. Arun, T. S. Huang, and S. D. Blostein, "Least-Squares Fitting of Two 3-D Point Sets," *IEEE Trans. Pattern Anal. Mach. Intell.*, vol. PAMI-9, no. 5, pp. 698–700, 1987, doi: 10.1109/TPAMI.1987.4767965.

[99] J. M. Fitzpatrick, J. B. West, and C. R. Maurer, "Predicting error in rigid-body point-based registration.," *IEEE Trans. Med. Imaging*, vol. 17, no. 5, pp. 694–702, 1998, doi: 10.1109/42.736021.

[100] J. B. West, J. M. Fitzpatrick, S. A. Toms, C. R. Maurer Jr., and R. J. Maciunas, "Fiducial Point Placement and the Accuracy of Point-based, Rigid Body Registration," *Neurosurgery*, vol. 48, no. 4, pp. 810–817, Apr. 2001, doi: 10.1097/00006123-200104000-00023.

[101] T. Guo, K. W. Finnis, A. G. Parrent, and T. M. Peters, "Visualization and navigation system development and application for stereotactic deep-brain neurosurgeries.," *Comput. aided Surg. Off. J. Int. Soc. Comput. Aided Surg.*, vol. 11, no. 5, pp. 231–

239, Sep. 2006, doi: 10.3109/10929080600997232.

[102] S. Noachtar and I. Borggraefe, “Epilepsy surgery: a critical review.,” *Epilepsy Behav.*, vol. 15, no. 1, pp. 66–72, May 2009, doi: 10.1016/j.yebeh.2009.02.028.

[103] R. M. Comeau, A. F. Sadikot, A. Fenster, and T. M. Peters, “Intraoperative ultrasound for guidance and tissue shift correction in image-guided neurosurgery.,” *Med. Phys.*, vol. 27, no. 4, pp. 787–800, Apr. 2000, doi: 10.1118/1.598942.

[104] V. Kosmopoulos and C. Schizas, “Pedicle screw placement accuracy: a meta-analysis.,” *Spine (Phila. Pa. 1976).*, vol. 32, no. 3, pp. E111-20, Feb. 2007, doi: 10.1097/01.brs.0000254048.79024.8b.

[105] B. Jaramaz, A. M. 3rd DiGioia, M. Blackwell, and C. Nikou, “Computer assisted measurement of cup placement in total hip replacement.,” *Clin. Orthop. Relat. Res.*, no. 354, pp. 70–81, Sep. 1998, doi: 10.1097/00003086-199809000-00010.

[106] S. Fehlberg, S. Eulenstein, T. Lange, D. Andreou, and P. U. Tunn, “Computer-assisted pelvic tumor resection: Fields of application, limits, and perspectives,” *Recent Results Cancer Res.*, vol. 179, pp. 169–182, 2009, doi: 10.1007/978-3-540-77960-5_11.

[107] S. L. Bobek, “Applications of Navigation for Orthognathic Surgery,” *Oral Maxillofac. Surg. Clin. North Am.*, vol. 26, no. 4, pp. 587–598, 2014, doi: https://doi.org/10.1016/j.coms.2014.08.003.

[108] D. García-Mato *et al.*, “Craniosynostosis surgery: workflow based on virtual surgical planning, intraoperative navigation and 3D printed patient-specific guides and templates,” *Sci. Rep.*, vol. 9, no. 1, p. 17691, 2019, doi: 10.1038/s41598-019-54148-4.

[109] M. Feichtinger, M. Pau, W. Zemann, R. M. Aigner, and H. Kärcher, “Intraoperative control of resection margins in advanced head and neck cancer using a 3D-navigation system based on PET/CT image fusion,” *J. Cranio-Maxillofacial Surg.*, vol. 38, no. 8, pp. 589–594, 2010, doi: https://doi.org/10.1016/j.jcms.2010.02.004.

[110] H. K. Gumprecht, D. C. Widenka, and C. B. Lumenta, “BrainLab VectorVision Neuronavigation System: technology and clinical experiences in 131 cases.,” *Neurosurgery*, vol. 44, no. 1, pp. 95–97, Jan. 1999, doi: 10.1097/00006123-199901000-00056.

[111] G. M. Malham and R. M. Parker, “Early experience of placing image-guided

minimally invasive pedicle screws without K-wires or bone-anchored trackers.," *J. Neurosurg. Spine*, vol. 28, no. 4, pp. 357–363, Apr. 2018, doi: 10.3171/2017.7.SPINE17528.

[112] H. Gui, H. Yang, S. G. F. Shen, B. Xu, S. Zhang, and J. S. Bautista, "Image-guided surgical navigation for removal of foreign bodies in the deep maxillofacial region.," *J. oral Maxillofac. Surg. Off. J. Am. Assoc. Oral Maxillofac. Surg.*, vol. 71, no. 9, pp. 1563–1571, Sep. 2013, doi: 10.1016/j.joms.2013.04.001.

[113] A. Khanna and A. Sama, "New instrumentations in the operating room for sinus surgery," *Curr. Opin. Otolaryngol. Head Neck Surg.*, vol. 26, no. 1, 2018, doi: 10.1097/MOO.0000000000000433.

[114] R. L., "Open Source Licensing: Software Freedom and Intellectual Property Law," *Up. Saddle River, NJ Prentice Hall PTR*, 2005.

[115] I. Wolf *et al.*, "The medical imaging interaction toolkit (MITK): a toolkit facilitating the creation of interactive software by extending VTK and ITK," in *Proc.SPIE*, May 2004, vol. 5367, doi: 10.1117/12.535112.

[116] A. Enquobahrie *et al.*, "The Image-Guided Surgery Toolkit IGSTK: An Open Source C++ Software Toolkit," *J. Digit. Imaging*, vol. 20, no. 1, pp. 21–33, 2007, doi: 10.1007/s10278-007-9054-3.

[117] A. Fedorov *et al.*, "3D Slicer as an image computing platform for the Quantitative Imaging Network," *Magn. Reson. Imaging*, vol. 30, no. 9, pp. 1323–1341, 2012, doi: 10.1016/j.mri.2012.05.001.

[118] R. Azuma, Y. Baillot, R. Behringer, S. Feiner, S. Julier, and B. MacIntyre, "Recent advances in augmented reality," *IEEE Comput. Graph. Appl.*, vol. 21, no. 6, pp. 34–47, 2001, doi: 10.1109/38.963459.

[119] F. A. Casari *et al.*, "Augmented Reality in Orthopedic Surgery Is Emerging from Proof of Concept Towards Clinical Studies: a Literature Review Explaining the Technology and Current State of the Art," *Current Reviews in Musculoskeletal Medicine*, vol. 14, no. 2. Springer, pp. 192–203, Apr. 01, 2021, doi: 10.1007/s12178-021-09699-3.

[120] P. Vávra *et al.*, "Recent Development of Augmented Reality in Surgery: A Review," *Journal of Healthcare Engineering*, vol. 2017. Hindawi Limited, 2017, doi:

10.1155/2017/4574172.

[121] M. Akçayır and G. Akçayır, “Advantages and challenges associated with augmented reality for education: A systematic review of the literature,” *Educ. Res. Rev.*, vol. 20, pp. 1–11, 2017, doi: https://doi.org/10.1016/j.edurev.2016.11.002.

[122] I. E. Sutherland, “A Head-Mounted Three Dimensional Display,” in *Proceedings of the December 9-11, 1968, Fall Joint Computer Conference, Part I*, 1968, pp. 757–764, doi: 10.1145/1476589.1476686.

[123] C. T. Tan and D. Soh, “Augmented reality games: A review,” *Proc. Gameon-Arabia, Eurosis*, 2010.

[124] F. LeBlanc *et al.*, “A comparison of human cadaver and augmented reality simulator models for straight laparoscopic colorectal skills acquisition training.,” *J. Am. Coll. Surg.*, vol. 211, no. 2, pp. 250–255, Aug. 2010, doi: 10.1016/j.jamcollsurg.2010.04.002.

[125] V. Lahanas, C. Loukas, N. Smailis, and E. Georgiou, “A novel augmented reality simulator for skills assessment in minimal invasive surgery.,” *Surg. Endosc.*, vol. 29, no. 8, pp. 2224–2234, Aug. 2015, doi: 10.1007/s00464-014-3930-y.

[126] A. M. Vera, M. Russo, A. Mohsin, and S. Tsuda, “Augmented reality telementoring (ART) platform: a randomized controlled trial to assess the efficacy of a new surgical education technology.,” *Surg. Endosc.*, vol. 28, no. 12, pp. 3467–3472, Dec. 2014, doi: 10.1007/s00464-014-3625-4.

[127] O. F. Rahman, M. Y. Nahabedian, and J. C. Sinkin, “Augmented Reality and Wearable Technology in Image-guided Navigation and Preoperative Planning,” *Plast. Reconstr. Surg. – Glob. Open*, vol. 4, no. 9, 2016, doi: 10.1097/GOX.0000000000001057.

[128] R. Tang *et al.*, “Augmented reality technology for preoperative planning and intraoperative navigation during hepatobiliary surgery: A review of current methods,” *Hepatobiliary Pancreat. Dis. Int.*, vol. 17, no. 2, pp. 101–112, 2018, doi: https://doi.org/10.1016/j.hbpd.2018.02.002.

[129] R. Moreta-Martinez, D. García-Mato, M. García-Sevilla, R. Pérez-Mañanes, J. Calvo-Haro, and J. Pascau, “Augmented reality in computer-assisted interventions based on patient-specific 3D printed reference.,” *Healthc. Technol. Lett.*, vol. 5, no. 5, pp. 162–

166, Oct. 2018, doi: 10.1049/htl.2018.5072.

[130] D. García-Mato *et al.*, "Augmented reality visualization for craniosynostosis surgery," *Comput. Methods Biomech. Biomed. Eng. Imaging Vis.*, pp. 1–8, Oct. 2020, doi: 10.1080/21681163.2020.1834876.

[131] C. M. Andrews, A. B. Henry, I. M. Soriano, M. K. Southworth, and J. R. Silva, "Registration Techniques for Clinical Applications of Three-Dimensional Augmented Reality Devices," *IEEE J. Transl. Eng. Heal. Med.*, vol. 9, 2021, doi: 10.1109/JTEHM.2020.3045642.

[132] D. Andersen *et al.*, "Virtual annotations of the surgical field through an augmented reality transparent display," *Vis. Comput.*, vol. 32, no. 11, pp. 1481–1498, 2016, doi: 10.1007/s00371-015-1135-6.

[133] A. Elmi-Terander *et al.*, "Pedicle Screw Placement Using Augmented Reality Surgical Navigation With Intraoperative 3D Imaging: A First In-Human Prospective Cohort Study.," *Spine (Phila. Pa. 1976).*, vol. 44, no. 7, pp. 517–525, Apr. 2019, doi: 10.1097/BRS.0000000000002876.

[134] P. Fallavollita *et al.*, "An augmented reality C-arm for intraoperative assessment of the mechanical axis: a preclinical study.," *Int. J. Comput. Assist. Radiol. Surg.*, vol. 11, no. 11, pp. 2111–2117, Nov. 2016, doi: 10.1007/s11548-016-1426-z.

[135] H. Ogawa, K. Kurosaka, A. Sato, N. Hirasawa, M. Matsubara, and S. Tsukada, "Does An Augmented Reality-based Portable Navigation System Improve the Accuracy of Acetabular Component Orientation During THA? A Randomized Controlled Trial.," *Clin. Orthop. Relat. Res.*, vol. 478, no. 5, pp. 935–943, May 2020, doi: 10.1097/CORR.0000000000001083.

[136] R. Moreta-Martinez, A. Pose-Díez-de-la-Lastra, J. A. Calvo-Haro, L. Mediavilla-Santos, R. Pérez-Mañanes, and J. Pascau, "Combining Augmented Reality and 3D Printing to Improve Surgical Workflows in Orthopedic Oncology: Smartphone Application and Clinical Evaluation," *Sensors* , vol. 21, no. 4. 2021, doi: 10.3390/s21041370.

[137] H. S. Cho *et al.*, "Can Augmented Reality Be Helpful in Pelvic Bone Cancer Surgery? An In Vitro Study.," *Clin. Orthop. Relat. Res.*, vol. 476, no. 9, pp. 1719–1725, Sep.

2018, doi: 10.1007/s11999.0000000000000233.

[138] H. S. Cho *et al.*, “Augmented reality in bone tumour resection: An experimental study.,” *Bone Joint Res.*, vol. 6, no. 3, pp. 137–143, Mar. 2017, doi: 10.1302/2046-3758.63.BJR-2016-0289.R1.

[139] F. Müller, S. Roner, F. Liebmann, J. M. Spirig, P. Fürnstahl, and M. Farshad, “Augmented reality navigation for spinal pedicle screw instrumentation using intraoperative 3D imaging,” *Spine J.*, vol. 20, no. 4, pp. 621–628, 2020, doi: https://doi.org/10.1016/j.spinee.2019.10.012.

[140] F. Liebmann *et al.*, “Pedicle screw navigation using surface digitization on the Microsoft HoloLens,” *Int. J. Comput. Assist. Radiol. Surg.*, vol. 14, no. 7, pp. 1157–1165, 2019, doi: 10.1007/s11548-019-01973-7.

[141] J. W. Yoon, R. E. Chen, P. K. Han, P. Si, W. D. Freeman, and S. M. Pirris, “Technical feasibility and safety of an intraoperative head-up display device during spine instrumentation.,” *Int. J. Med. Robot.*, vol. 13, no. 3, Sep. 2017, doi: 10.1002/rcs.1770.

[142] F. Shen, B. Chen, Q. Guo, Y. Qi, and Y. Shen, “Augmented reality patient-specific reconstruction plate design for pelvic and acetabular fracture surgery.,” *Int. J. Comput. Assist. Radiol. Surg.*, vol. 8, no. 2, pp. 169–179, Mar. 2013, doi: 10.1007/s11548-012-0775-5.

[143] X. Chen *et al.*, “Development of a surgical navigation system based on augmented reality using an optical see-through head-mounted display.,” *J. Biomed. Inform.*, vol. 55, pp. 124–131, Jun. 2015, doi: 10.1016/j.jbi.2015.04.003.

[144] B. Fiani, F. De Stefano, A. Kondilis, C. Covarrubias, L. Reier, and K. Sarhadi, “Virtual Reality in Neurosurgery: ‘Can You See It?’–A Review of the Current Applications and Future Potential,” *World Neurosurg.*, vol. 141, pp. 291–298, 2020, doi: https://doi.org/10.1016/j.wneu.2020.06.066.

[145] A. S. Vemuri, J. C.-H. Wu, K.-C. Liu, and H.-S. Wu, “Deformable three-dimensional model architecture for interactive augmented reality in minimally invasive surgery.,” *Surg. Endosc.*, vol. 26, no. 12, pp. 3655–3662, Dec. 2012, doi: 10.1007/s00464-012-2395-0.

[146] K. Gavaghan *et al.*, “Evaluation of a portable image overlay projector for the

visualisation of surgical navigation data: phantom studies.," *Int. J. Comput. Assist. Radiol. Surg.*, vol. 7, no. 4, pp. 547–556, Jul. 2012, doi: 10.1007/s11548-011-0660-7.

[147] D. Inoue *et al.*, "Preliminary study on the clinical application of augmented reality neuronavigation.," *J. Neurol. Surg. A. Cent. Eur. Neurosurg.*, vol. 74, no. 2, pp. 71–76, Mar. 2013, doi: 10.1055/s-0032-1333415.

[148] T. Okamoto, S. Onda, K. Yanaga, N. Suzuki, and A. Hattori, "Clinical application of navigation surgery using augmented reality in the abdominal field.," *Surg. Today*, vol. 45, no. 4, pp. 397–406, Apr. 2015, doi: 10.1007/s00595-014-0946-9.

[149] S. Ieiri *et al.*, "Augmented reality navigation system for laparoscopic splenectomy in children based on preoperative CT image using optical tracking device.," *Pediatr. Surg. Int.*, vol. 28, no. 4, pp. 341–346, Apr. 2012, doi: 10.1007/s00383-011-3034-x.

[150] E. Wild *et al.*, "Robust augmented reality guidance with fluorescent markers in laparoscopic surgery.," *Int. J. Comput. Assist. Radiol. Surg.*, vol. 11, no. 6, pp. 899–907, Jun. 2016, doi: 10.1007/s11548-016-1385-4.

[151] X. Kang *et al.*, "Stereoscopic augmented reality for laparoscopic surgery.," *Surg. Endosc.*, vol. 28, no. 7, pp. 2227–2235, Jul. 2014, doi: 10.1007/s00464-014-3433-x.

[152] T. Okamoto *et al.*, "Utility of augmented reality system in hepatobiliary surgery.," *J. Hepatobiliary. Pancreat. Sci.*, vol. 20, no. 2, pp. 249–253, Feb. 2013, doi: 10.1007/s00534-012-0504-z.

[153] M. Qu *et al.*, "Precise positioning of an intraoral distractor using augmented reality in patients with hemifacial microsomia.," *J. cranio-maxillo-facial Surg. Off. Publ. Eur. Assoc. Cranio-Maxillo-Facial Surg.*, vol. 43, no. 1, pp. 106–112, Jan. 2015, doi: 10.1016/j.jcms.2014.10.019.

[154] T. Kilgus *et al.*, "Mobile markerless augmented reality and its application in forensic medicine.," *Int. J. Comput. Assist. Radiol. Surg.*, vol. 10, no. 5, pp. 573–586, May 2015, doi: 10.1007/s11548-014-1106-9.

[155] Y. Hayashi, K. Misawa, D. J. Hawkes, and K. Mori, "Progressive internal landmark registration for surgical navigation in laparoscopic gastrectomy for gastric cancer.," *Int. J. Comput. Assist. Radiol. Surg.*, vol. 11, no. 5, pp. 837–845, May 2016, doi: 10.1007/s11548-015-1346-3.

[156] R. Krishnan, A. Raabe, and V. Seifert, “Accuracy and applicability of laser surface scanning as new registration technique in image-guided neurosurgery,” in *CARS*, 2004.

[157] K. Schicho *et al.*, “Comparison of laser surface scanning and fiducial marker-based registration in frameless stereotaxy. Technical note.,” *J. Neurosurg.*, vol. 106, no. 4, pp. 704–709, Apr. 2007, doi: 10.3171/jns.2007.106.4.704.

[158] K. Konishi *et al.*, “Augmented reality navigation system for endoscopic surgery based on three-dimensional ultrasound and computed tomography: Application to 20 clinical cases,” *Int. Congr. Ser.*, vol. 1281, pp. 537–542, 2005, doi: https://doi.org/10.1016/j.ics.2005.03.234.

[159] S. Nicolau, L. Soler, D. Mutter, and J. Marescaux, “Augmented reality in laparoscopic surgical oncology.,” *Surg. Oncol.*, vol. 20, no. 3, pp. 189–201, Sep. 2011, doi: 10.1016/j.suronc.2011.07.002.

[160] L. Besharati Tabrizi and M. Mahvash, “Augmented reality–guided neurosurgery: accuracy and intraoperative application of an image projection technique,” *J. Neurosurg. JNS*, vol. 123, no. 1, pp. 206–211, 2015, doi: 10.3171/2014.9.JNS141001.

[161] G. Badiali *et al.*, “Augmented reality as an aid in maxillofacial surgery: validation of a wearable system allowing maxillary repositioning.,” *J. cranio-maxillo-facial Surg. Off. Publ. Eur. Assoc. Cranio-Maxillo-Facial Surg.*, vol. 42, no. 8, pp. 1970–1976, Dec. 2014, doi: 10.1016/j.jcms.2014.09.001.

[162] M. Kersten-Oertel *et al.*, “Augmented reality in neurovascular surgery: feasibility and first uses in the operating room.,” *Int. J. Comput. Assist. Radiol. Surg.*, vol. 10, no. 11, pp. 1823–1836, Nov. 2015, doi: 10.1007/s11548-015-1163-8.

[163] R. Londei *et al.*, “Intra-operative augmented reality in distal locking.,” *Int. J. Comput. Assist. Radiol. Surg.*, vol. 10, no. 9, pp. 1395–1403, Sep. 2015, doi: 10.1007/s11548-015-1169-2.

[164] D. Katić *et al.*, “A system for context-aware intraoperative augmented reality in dental implant surgery.,” *Int. J. Comput. Assist. Radiol. Surg.*, vol. 10, no. 1, pp. 101–108, Jan. 2015, doi: 10.1007/s11548-014-1005-0.

[165] N. Loy Rodas and N. Padoy, “Seeing is believing: increasing intraoperative awareness to scattered radiation in interventional procedures by combining augmented reality,

Monte Carlo simulations and wireless dosimeters.," *Int. J. Comput. Assist. Radiol. Surg.*, vol. 10, no. 8, pp. 1181–1191, Aug. 2015, doi: 10.1007/s11548-015-1161-x.

[166] A. Hughes-Hallett, E. K. Mayer, P. Pratt, A. Mottrie, A. Darzi, and J. Vale, "The current and future use of imaging in urological robotic surgery: a survey of the European Association of Robotic Urological Surgeons.," *Int. J. Med. Robot.*, vol. 11, no. 1, pp. 8–14, Mar. 2015, doi: 10.1002/rcs.1596.

[167] F. Volonté *et al.*, "Console-integrated stereoscopic OsiriX 3D volume-rendered images for da Vinci colorectal robotic surgery.," *Surg. Innov.*, vol. 20, no. 2, pp. 158–163, Apr. 2013, doi: 10.1177/1553350612446353.

[168] P. Pessaux, M. Diana, L. Soler, T. Piardi, D. Mutter, and J. Marescaux, "Towards cybernetic surgery: robotic and augmented reality-assisted liver segmentectomy.," *Langenbeck's Arch. Surg.*, vol. 400, no. 3, pp. 381–385, Apr. 2015, doi: 10.1007/s00423-014-1256-9.

[169] S. Condino *et al.*, "Wearable Augmented Reality Platform for Aiding Complex 3D Trajectory Tracing.," *Sensors (Basel).*, vol. 20, no. 6, Mar. 2020, doi: 10.3390/s20061612.

[170] F. Volonté, F. Pugin, P. Bucher, M. Sugimoto, O. Ratib, and P. Morel, "Augmented reality and image overlay navigation with OsiriX in laparoscopic and robotic surgery: not only a matter of fashion.," *J. Hepatobiliary. Pancreat. Sci.*, vol. 18, no. 4, pp. 506–509, Jul. 2011, doi: 10.1007/s00534-011-0385-6.

[171] R. Härtl, K. S. Lam, J. Wang, A. Korge, F. Kandziora, and L. Audigé, "Worldwide survey on the use of navigation in spine surgery.," *World Neurosurg.*, vol. 79, no. 1, pp. 162–172, Jan. 2013, doi: 10.1016/j.wneu.2012.03.011.

[172] R. H. Taylor, A. Menciassi, G. Fichtinger, P. Fiorini, and P. Dario, "Medical Robotics and Computer-Integrated Surgery BT - Springer Handbook of Robotics," B. Siciliano and O. Khatib, Eds. Cham: Springer International Publishing, 2016, pp. 1657–1684.

[173] C. Y. Liaw and M. Guvendiren, "Current and emerging applications of 3D printing in medicine," *Biofabrication*, vol. 9, no. 2, 2017, doi: 10.1088/1758-5090/aa7279.

[174] M. Narita, T. Takaki, T. Shibahara, M. Iwamoto, T. Yakushiji, and T. Kamio, "Utilization of desktop 3D printer-fabricated 'Cost-Effective' 3D models in

orthognathic surgery," *Maxillofac. Plast. Reconstr. Surg.*, vol. 42, no. 1, 2020, doi: 10.1186/s40902-020-00269-0.

[175] M. P. Chae, W. M. Rozen, P. G. McMenamin, M. W. Findlay, R. T. Spychal, and D. J. Hunter-Smith, "Emerging Applications of Bedside 3D Printing in Plastic Surgery," *Front. Surg.*, vol. 2, no. June, pp. 1–14, 2015, doi: 10.3389/fsurg.2015.00025.

[176] B. P. Cromeens, W. C. Ray, B. Hoehne, F. Abayneh, B. Adler, and G. E. Besner, "Facilitating surgeon understanding of complex anatomy using a three-dimensional printed model.," *J. Surg. Res.*, vol. 216, pp. 18–25, Aug. 2017, doi: 10.1016/j.jss.2017.04.003.

[177] A. Sallent *et al.*, "How 3D patient-specific instruments improve accuracy of pelvic bone tumour resection in a cadaveric study," *Bone Jt. Res.*, vol. 6, no. 10, pp. 577–583, 2017, doi: 10.1302/2046-3758.610.BJR-2017-0094.R1.

[178] K. C. Wong, K. Y. Sze, I. O. L. Wong, C. M. Wong, and S. M. Kumta, "Patient-specific instrument can achieve same accuracy with less resection time than navigation assistance in periacetabular pelvic tumor surgery: a cadaveric study," *Int. J. Comput. Assist. Radiol. Surg.*, vol. 11, no. 2, pp. 307–316, 2016, doi: 10.1007/s11548-015-1250-x.

[179] O. Cartiaux *et al.*, "Surgical inaccuracy of tumor resection and reconstruction within the pelvis: an experimental study.," *Acta Orthop.*, vol. 79, no. 5, pp. 695–702, 2008, doi: 10.1080/17453670810016731.

[180] B. Ma, T. Park, I. Chun, and K. Yun, "The accuracy of a 3D printing surgical guide determined by CBCT and model analysis," *J. Adv. Prosthodont.*, vol. 10, no. 4, pp. 279–285, 2018, doi: 10.4047/jap.2018.10.4.279.

[181] L. Brouwers, A. Teutelink, F. A. J. B. van Tilborg, M. A. C. de Jongh, K. W. W. Lansink, and M. Bemelman, "Validation study of 3D-printed anatomical models using 2 PLA printers for preoperative planning in trauma surgery, a human cadaver study," *European Journal of Trauma and Emergency Surgery*, vol. 45, no. 6. pp. 1013–1020, 2019, doi: 10.1007/s00068-018-0970-3.

[182] P. J. Besl and N. D. McKay, "A method for registration of 3-D shapes," *IEEE Trans. Pattern Anal. Mach. Intell.*, vol. 14, no. 2, pp. 239–256, 1992, doi: 10.1109/34.121791.

[183] N. Kawaguchi, S. Matumoto, and J. Manabe, “New method of evaluating the surgical margin and safety margin for musculoskeletal sarcoma, analysed on the basis of 457 surgical cases.,” *J. Cancer Res. Clin. Oncol.*, vol. 121, no. 9–10, pp. 555–563, 1995, doi: 10.1007/BF01197769.

[184] F. Gouin, L. Paul, G. A. Odri, and O. Cartiaux, “Computer-Assisted Planning and Patient-Specific Instruments for Bone Tumor Resection within the Pelvis: A Series of 11 Patients.,” *Sarcoma*, vol. 2014, p. 842709, 2014, doi: 10.1155/2014/842709.

[185] T. Jentzsch, L. Vlachopoulos, P. Fürnstahl, D. A. Müller, and B. Fuchs, “Tumor resection at the pelvis using three-dimensional planning and patient-specific instruments: A case series,” *World J. Surg. Oncol.*, vol. 14, no. 1, pp. 1–12, 2016, doi: 10.1186/s12957-016-1006-2.

[186] M. García-Sevilla, D. García-Mato, J. Calvo-Haro, R. Pérez-Mañanes, and J. Pascau, “Optimizing navigation with patient-specific 3D printed guides in pelvic tumor resection surgery,” in *Proceedings of Computer Assisted Radiology and Surgery: CARS June 18–21, 2019, Rennes, France*, 2019, pp. 62–64.

[187] T. Ozaki *et al.*, “Osteosarcoma of the Pelvis: Experience of the Cooperative Osteosarcoma Study Group,” *J. Clin. Oncol.*, vol. 21, no. 2, pp. 334–341, 2003, doi: 10.1200/JCO.2003.01.142.

[188] B. Fuchs, N. Hoekzema, D. R. Larson, C. Y. Inwards, and F. H. Sim, “Osteosarcoma of the pelvis: outcome analysis of surgical treatment.,” *Clin. Orthop. Relat. Res.*, vol. 467, no. 2, pp. 510–518, Feb. 2009, doi: 10.1007/s11999-008-0495-x.

[189] K. C. Wong, X. Niu, H. Xu, Y. Li, and S. Kumta, “Computer navigation in orthopaedic tumour surgery,” *Adv. Exp. Med. Biol.*, vol. 1093, pp. 315–326, 2018, doi: 10.1007/978-981-13-1396-7_24.

[190] P. S. Young, H. Findlay, J. T. S. Patton, and A. Mahendra, “(iii) Computer assisted navigation in musculoskeletal oncology,” *Orthop. Trauma*, vol. 28, no. 5, pp. 294–302, 2014, doi: 10.1016/j.mporth.2014.08.002.

[191] K. C. Wong, S. M. Kumta, K. H. Chiu, G. E. Antonio, P. Unwin, and K. S. Leung, “Precision tumour resection and reconstruction using image-guided computer navigation,” *J. Bone Jt. Surg. - Ser. B*, vol. 89, no. 7, pp. 943–947, 2007, doi:

10.1302/0301-620X.89B7.19067.

[192] R. Moreta-Martinez, J. A. Calvo-Haro, R. Pérez-Mañanes, M. García-Sevilla, L. Mediavilla-Santos, and J. Pascau, “Desktop 3D Printing: Key for Surgical Navigation in Acral Tumors?,” *Applied Sciences* , vol. 10, no. 24. 2020, doi: 10.3390/app10248984.

[193] T. Hüfner *et al.*, “New indications for computer-assisted surgery: Tumor resection in the pelvis,” *Clin. Orthop. Relat. Res.*, no. 426, pp. 219–225, 2004, doi: 10.1097/01.blo.0000138958.11939.94.

[194] L. Jeys, G. S. Matharu, R. S. Nandra, and R. J. Grimer, “Can computer navigation-assisted surgery reduce the risk of an intralesional margin and reduce the rate of local recurrence in patients with a tumour of the pelvis or sacrum?,” *Bone Jt. J.*, vol. 95 B, no. 10, pp. 1417–1424, 2013, doi: 10.1302/0301-620X.95B10.31734.

[195] F. Alam, S. Ur Rahman, S. Ullah, and K. Gulati, “Medical image registration in image guided surgery: Issues, challenges and research opportunities,” *Biocybern. Biomed. Eng.*, vol. 38, Oct. 2017, doi: 10.1016/j.bbe.2017.10.001.

[196] T. M. Wong *et al.*, “The use of three-dimensional printing technology in orthopaedic surgery: A review,” *J. Orthop. Surg.*, vol. 25, no. 1, pp. 1–7, 2017, doi: 10.1177/2309499016684077.

[197] O. Cartiaux, L. Paul, B. G. Francq, X. Banse, and P. L. Docquier, “Improved accuracy with 3D planning and patient-specific instruments during simulated pelvic bone tumor surgery,” *Ann. Biomed. Eng.*, vol. 42, no. 1, pp. 205–213, 2014, doi: 10.1007/s10439-013-0890-7.

[198] M. A. Hafez and K. Moholkar, “Patient-specific instruments: advantages and pitfalls,” *Sicot-J*, vol. 3, p. 66, 2017, doi: 10.1051/sicotj/2017054.

[199] K. C. Wong and S. M. Kumta, “Joint-preserving tumor resection and reconstruction using image-guided computer navigation tumor,” *Clin. Orthop. Relat. Res.*, vol. 471, no. 3, pp. 762–773, 2013, doi: 10.1007/s11999-012-2536-8.

[200] A. J. V Brown, A. Uneri, T. S. De Silva, A. Manbachi, and J. H. Siewerdsen, “Design and validation of an open-source library of dynamic reference frames for research and education in optical tracking,” *J. Med. Imaging*, vol. 5, no. 2, pp. 1–8, 2018, doi:

10.1117/1.JMI.5.2.021215.

[201] R. Elfring, M. de la Fuente, and K. Radermacher, “Assessment of optical localizer accuracy for computer aided surgery systems,” *Comput. Aided Surg.*, vol. 15, no. 1–3, pp. 1–12, Feb. 2010, doi: 10.3109/10929081003647239.

[202] T. Ungi, A. Lasso, and G. Fichtinger, “Open-source platforms for navigated image-guided interventions,” vol. 33, pp. 181–186, 2016, doi: 10.1016/j.media.2016.06.011.

[203] A. Lasso, T. Heffter, A. Rankin, C. Pinter, T. Ungi, and G. Fichtinger, “PLUS: Open-Source Toolkit for Ultrasound-Guided Intervention Systems,” *IEEE Trans. Biomed. Eng.*, vol. 61, no. 10, pp. 2527–2537, 2014, doi: 10.1109/TBME.2014.2322864.

[204] W. F. Enneking and W. K. Dunham, “Resection and reconstruction for primary neoplasms involving the innominate bone.,” *J. Bone Joint Surg. Am.*, vol. 60, no. 6, pp. 731–746, Sep. 1978.

[205] R. Khadem *et al.*, “Comparative Tracking Error Analysis of Five Different Optical Tracking Systems,” *Comput. Aided Surg.*, vol. 5, no. 2, pp. 98–107, 2000, doi: 10.3109/10929080009148876.

[206] T. Y. C. So, Y.-L. Lam, and K.-L. Mak, “Computer-assisted navigation in bone tumor surgery: seamless workflow model and evolution of technique.,” *Clin. Orthop. Relat. Res.*, vol. 468, no. 11, pp. 2985–2991, Nov. 2010, doi: 10.1007/s11999-010-1465-7.

[207] M. García-Sevilla, L. Mediavilla-Santos, M. T. Ruiz-Alba, R. Pérez-Mañanes, J. A. Calvo-Haro, and J. Pascau, “Patient-specific desktop 3D-printed guides for pelvic tumour resection surgery: a precision study on cadavers,” *Int. J. Comput. Assist. Radiol. Surg.*, vol. 16, no. 3, pp. 397–406, 2021, doi: 10.1007/s11548-021-02322-3.

[208] M. García-Sevilla *et al.*, “Combining Surgical Navigation and 3D Printing for Less Invasive Pelvic Tumor Resections,” *IEEE Access*, vol. 9, pp. 133541–133551, 2021, doi: 10.1109/ACCESS.2021.3115984.

[209] L. Jud *et al.*, “Applicability of augmented reality in orthopedic surgery – A systematic review,” *BMC Musculoskelet. Disord.*, vol. 21, no. 1, p. 103, 2020, doi: 10.1186/s12891-020-3110-2.

[210] C. Dennler *et al.*, “Augmented reality in the operating room: a clinical feasibility study,” *BMC Musculoskelet. Disord.*, vol. 22, no. 1, p. 451, 2021, doi:

10.1186/s12891-021-04339-w.

[211] P. Pratt *et al.*, "Through the HoloLens™ looking glass: augmented reality for extremity reconstruction surgery using 3D vascular models with perforating vessels.," *Eur. Radiol. Exp.*, vol. 2, no. 1, p. 2, 2018, doi: 10.1186/s41747-017-0033-2.

[212] I. Kuhlemann, M. Kleemann, P. Jauer, A. Schweikard, and F. Ernst, "Towards X-ray free endovascular interventions - using HoloLens for on-line holographic visualisation.," *Healthc. Technol. Lett.*, vol. 4, no. 5, pp. 184–187, Oct. 2017, doi: 10.1049/htl.2017.0061.

[213] R. Tang *et al.*, "Augmented reality navigation in open surgery for hilar cholangiocarcinoma resection with hemihepatectomy using video-based in situ three-dimensional anatomical modeling: A case report," *Medicine (Baltimore).*, vol. 96, no. 37, 2017, doi: 10.1097/MD.0000000000008083.

[214] R. Plantefève, I. Peterlik, N. Haouchine, and S. Cotin, "Patient-Specific Biomechanical Modeling for Guidance During Minimally-Invasive Hepatic Surgery.," *Ann. Biomed. Eng.*, vol. 44, no. 1, pp. 139–153, Jan. 2016, doi: 10.1007/s10439-015-1419-z.

[215] F. J. Romero-Ramirez, R. Muñoz-Salinas, and R. Medina-Carnicer, "Speeded up detection of squared fiducial markers," *Image Vis. Comput.*, vol. 76, pp. 38–47, 2018, doi: https://doi.org/10.1016/j.imavis.2018.05.004.

[216] J. Ackermann *et al.*, "Augmented Reality Based Surgical Navigation of Complex Pelvic Osteotomies—A Feasibility Study on Cadavers," *Applied Sciences* , vol. 11, no. 3. 2021, doi: 10.3390/app11031228.

[217] T. Kamomae *et al.*, "Three-dimensional printer-generated patient-specific phantom for artificial in vivo dosimetry in radiotherapy quality assurance," *Phys. Medica*, vol. 44, pp. 205–211, 2017, doi: https://doi.org/10.1016/j.ejmp.2017.10.005.

[218] T. Akiyama, J. C. M. Clark, Y. Miki, and P. F. M. Choong, "The non-vascularised fibular graft," *J. Bone Joint Surg. Br.*, vol. 92-B, no. 7, pp. 999–1005, Jul. 2010, doi: 10.1302/0301-620X.92B7.23497.

[219] R. Moreta-Martinez, D. García-Mato, M. García-Sevilla, R. Pérez-Mañanes, J. A. Calvo-Haro, and J. Pascau, "Combining Augmented Reality and 3D Printing to Display Patient Models on a Smartphone," *JoVE*, no. 155, p. e60618, 2020, doi:

doi:10.3791/60618.

[220] H. Boukheris, R. E. Curtis, C. E. Land, and G. M. Dores, “Incidence of carcinoma of the major salivary glands according to the WHO classification, 1992 to 2006: A population-based study in the United States,” *Cancer Epidemiol. Biomarkers Prev.*, vol. 18, no. 11, pp. 2899–2906, 2009, doi: 10.1158/1055-9965.EPI-09-0638.

[221] V. S. H. To, J. Y. W. Chan, R. K. Y. Tsang, and W. I. Wei, “Review of salivary gland neoplasms,” *ISRN Otolaryngol.*, vol. 2012, p. 872982, Feb. 2012, doi: 10.5402/2012/872982.

[222] G. V Shah, “MR imaging of salivary glands,” *Magn. Reson. Imaging Clin.*, vol. 10, no. 4, pp. 631–662, Nov. 2002, doi: 10.1016/S1064-9689(02)00015-6.

[223] E. Son, A. Panwar, C. H. Mosher, and D. Lydiatt, “Cancers of the Major Salivary Gland.,” *J. Oncol. Pract.*, vol. 14, no. 2, pp. 99–108, Feb. 2018, doi: 10.1200/JOP.2017.026856.

[224] N. S. V. Chundru, R. Amudala, P. Thankappan, and C. D. Nagaraju, “Adenoid cystic carcinoma of palate: A case report and review of literature.,” *Dental research journal*, vol. 10, no. 2. pp. 274–278, Mar. 2013, doi: 10.4103/1735-3327.113372.

[225] P. M. Speight and A. W. Barrett, “Salivary gland tumours,” *Oral Dis.*, vol. 8, no. 5, pp. 229–240, Sep. 2002, doi: https://doi.org/10.1034/j.1601-0825.2002.02870.x.

[226] A. Mahajan, M. Kulkarni, M. Parekh, M. Khan, A. Shah, and M. Gabhane, “Adenoid Cystic Carcinoma of Hard Palate: a Case Report,” *Oral Maxillofac. Pathol. J.*, vol. 2, no. 1, pp. 127–131, 2011.

[227] S. Catanzaro *et al.*, “Intraoperative navigation in complex head and neck resections: indications and limits.,” *Int. J. Comput. Assist. Radiol. Surg.*, vol. 12, no. 5, pp. 881–887, May 2017, doi: 10.1007/s11548-016-1486-0.

[228] A. Deganello *et al.*, “Endoscopic-assisted maxillectomy: Operative technique and control of surgical margins.,” *Oral Oncol.*, vol. 93, pp. 29–38, Jun. 2019, doi: 10.1016/j.oraloncology.2019.04.002.

[229] B. Wei, G. Sun, Q. Hu, and E. Tang, “The Safety and Accuracy of Surgical Navigation Technology in the Treatment of Lesions Involving the Skull Base,” *J. Craniofac. Surg.*, vol. 28, no. 6, pp. 1431–1434, 2017, doi: 10.1097/SCS.0000000000003624.

[230] S. M. Hardy, C. Melroy, D. R. White, M. Dubin, and B. Senior, “A Comparison of Computer-Aided Surgery Registration Methods for Endoscopic Sinus Surgery,” *Am. J. Rhinol.*, vol. 20, no. 1, pp. 48–52, Jan. 2006, doi: 10.1177/194589240602000110.

[231] C. Bettschart *et al.*, “Point-to-point registration with mandibulo-maxillary splint in open and closed jaw position. Evaluation of registration accuracy for computer-aided surgery of the mandible,” *J. Cranio-Maxillofacial Surg.*, vol. 40, no. 7, pp. 592–598, 2012, doi: https://doi.org/10.1016/j.jcms.2011.10.016.

[232] B. Šiniković, F.-J. Kramer, G. Swennen, H.-T. Lübbers, and R. Dempf, “Reconstruction of orbital wall defects with calcium phosphate cement: clinical and histological findings in a sheep model,” *Int. J. Oral Maxillofac. Surg.*, vol. 36, no. 1, pp. 54–61, 2007, doi: https://doi.org/10.1016/j.ijom.2006.07.014.

[233] J. Hoffmann, C. Westendorff, C. Leitner, D. Bartz, and S. Reinert, “Validation of 3D-laser surface registration for image-guided cranio-maxillofacial surgery,” *J. Cranio-Maxillofacial Surg.*, vol. 33, no. 1, pp. 13–18, 2005, doi: https://doi.org/10.1016/j.jcms.2004.10.001.

[234] R. Marmulla, G. Eggers, and J. Mühling, “Laser surface registration for lateral skull base surgery.,” *Minim. Invasive Neurosurg.*, vol. 48, no. 3, pp. 181–185, Jun. 2005, doi: 10.1055/s-2005-870906.

[235] I. Azarmehr, K. Stokbro, R. B. Bell, and T. Thygesen, “Surgical Navigation: A Systematic Review of Indications, Treatments, and Outcomes in Oral and Maxillofacial Surgery,” *Journal of Oral and Maxillofacial Surgery*, vol. 75, no. 9. W.B. Saunders, pp. 1987–2005, Sep. 01, 2017, doi: 10.1016/j.joms.2017.01.004.

[236] M. Anand and S. Panwar, “Role of Navigation in Oral and Maxillofacial Surgery: A Surgeon’s Perspectives.,” *Clin. Cosmet. Investig. Dent.*, vol. 13, pp. 127–139, 2021, doi: 10.2147/CCIDE.S299249.

[237] L. Dubois *et al.*, “Predictability in orbital reconstruction: A human cadaver study. Part II: Navigation-assisted orbital reconstruction.,” *J. cranio-maxillo-facial Surg. Off. Publ. Eur. Assoc. Cranio-Maxillo-Facial Surg.*, vol. 43, no. 10, pp. 2042–2049, Dec. 2015, doi: 10.1016/j.jcms.2015.07.020.

[238] L. Dubois *et al.*, “Predictability in orbital reconstruction. A human cadaver study, part

III: Implant-oriented navigation for optimized reconstruction.," *J. cranio-maxillo-facial Surg. Off. Publ. Eur. Assoc. Cranio-Maxillo-Facial Surg.*, vol. 43, no. 10, pp. 2050–2056, Dec. 2015, doi: 10.1016/j.jcms.2015.08.014.

[239] Y. Wu, F. Wang, W. Huang, and S. Fan, "Real-Time Navigation in Zygomatic Implant Placement: Workflow.," *Oral Maxillofac. Surg. Clin. North Am.*, vol. 31, no. 3, pp. 357–367, Aug. 2019, doi: 10.1016/j.coms.2019.03.001.

[240] R. Schmelzeisen, N. C. Gellrich, R. Schoen, R. Gutwald, C. Zizelmann, and A. Schramm, "Navigation-aided reconstruction of medial orbital wall and floor contour in cranio-maxillofacial reconstruction," *Injury*, vol. 35, no. 10, pp. 955–962, 2004, doi: 10.1016/j.injury.2004.06.005.

[241] R. B. Bell and M. R. Markiewicz, "Computer-Assisted Planning, Stereolithographic Modeling, and Intraoperative Navigation for Complex Orbital Reconstruction: A Descriptive Study in a Preliminary Cohort," *J. Oral Maxillofac. Surg.*, vol. 67, no. 12, pp. 2559–2570, Dec. 2009, doi: 10.1016/j.joms.2009.07.098.

[242] B. Li, L. Zhang, H. Sun, S. G. F. Shen, and X. Wang, "A New Method of Surgical Navigation for Orthognathic Surgery: Optical Tracking Guided Free-Hand Repositioning of the Maxillomandibular Complex," *J. Craniofac. Surg.*, vol. 25, no. 2, 2014, doi: 10.1097/SCS.0000000000000673.

[243] N. Casap, A. Wexler, N. Persky, A. Schneider, and J. Lustmann, "Navigation surgery for dental implants: Assessment of accuracy of the image guided implantology system," *J. Oral Maxillofac. Surg.*, vol. 62, no. SUPPL. 2, pp. 116–119, Sep. 2004, doi: 10.1016/j.joms.2004.06.028.

[244] M. Sießegger *et al.*, "Use of an image-guided navigation system in dental implant surgery in anatomically complex operation sites," *J. Cranio-Maxillofacial Surg.*, vol. 29, no. 5, pp. 276–281, Oct. 2001, doi: 10.1054/jcms.2001.0242.

[245] F. Watzinger *et al.*, "Positioning of dental implants using computer-aided navigation and an optical tracking system: Case report and presentation of a new method," *J. Cranio-Maxillo-Facial Surg.*, vol. 27, no. 2, pp. 77–81, Apr. 1999, doi: 10.1016/S1010-5182(99)80017-1.

[246] A. Tarsitano *et al.*, "Navigation-guided resection of maxillary tumours: The accuracy

of computer-assisted surgery in terms of control of resection margins – A feasibility study," *J. Cranio-Maxillofacial Surg.*, vol. 45, no. 12, pp. 2109–2114, 2017, doi: https://doi.org/10.1016/j.jcms.2017.09.023.

[247] A. Schramm *et al.*, "Indications for Computer-Assisted Treatment of Cranio-Maxillofacial Tumors," *Comput. Aided Surg.*, vol. 5, no. 5, pp. 343–352, Jan. 2000, doi: 10.3109/10929080009149852.

[248] R. E. Austin and O. M. Antonyshyn, "Current applications of 3-d intraoperative navigation in craniomaxillofacial surgery: a retrospective clinical review.," *Ann. Plast. Surg.*, vol. 69, no. 3, pp. 271–278, Sep. 2012, doi: 10.1097/SAP.0b013e31822a3ec3.

[249] Y. Hagiwara, M. Koizumi, and T. Igarashi, "Application of CT imaging for dental implant simulation," *J. Oral Sci.*, vol. 41, no. 4, pp. 157–161, 1999, doi: 10.2334/josnusd.41.157.

[250] C. D. Stockham, "Using CT and SIM/Plant to plan implant therapy.," *Alpha Omegan*, vol. 89, no. 4, pp. 35–38, 1996.

[251] A. Wagner *et al.*, "Computer-aided placement of endosseous oral implants in patients after ablative tumour surgery: assessment of accuracy.," *Clin. Oral Implants Res.*, vol. 14, no. 3, pp. 340–348, Jun. 2003, doi: 10.1034/j.1600-0501.2003.110812.x.

[252] F. Wanschitz *et al.*, "Evaluation of accuracy of computer-aided intraoperative positioning of endosseous oral implants in the edentulous mandible.," *Clin. Oral Implants Res.*, vol. 13, no. 1, pp. 59–64, Feb. 2002, doi: 10.1034/j.1600-0501.2002.130107.x.

[253] M. Siessegger *et al.*, "Use of an image-guided navigation system in dental implant surgery in anatomically complex operation sites.," *J. cranio-maxillo-facial Surg. Off. Publ. Eur. Assoc. Cranio-Maxillo-Facial Surg.*, vol. 29, no. 5, pp. 276–281, Oct. 2001, doi: 10.1054/jcms.2001.0242.

[254] Y.-H. Kim, D.-W. Jung, T. G. Kim, J. H. Lee, and I.-K. Kim, "Correction of orbital wall fracture close to the optic canal using computer-assisted navigation surgery.," *J. Craniofac. Surg.*, vol. 24, no. 4, pp. 1118–1122, Jul. 2013, doi: 10.1097/SCS.0b013e318290266a.

[255] A. Wagner, M. Rasse, W. Millesi, and R. Ewers, "Virtual reality for orthognathic

surgery: the augmented reality environment concept.," *J. oral Maxillofac. Surg. Off. J. Am. Assoc. Oral Maxillofac. Surg.*, vol. 55, no. 5, pp. 453–456, May 1997, doi: 10.1016/s0278-2391(97)90689-3.

[256] F. Wanschitz *et al.*, "Computer-enhanced stereoscopic vision in a head-mounted display for oral implant surgery.," *Clin. Oral Implants Res.*, vol. 13, no. 6, pp. 610–616, Dec. 2002, doi: 10.1034/j.1600-0501.2002.130606.x.

[257] R. Guo, Y. X. Guo, Z. Feng, and C. Bin Guo, "Application of a computer-aided navigation technique in surgery for recurrent malignant infratemporal fossa tumors.," *J. Craniofac. Surg.*, vol. 26, no. 2, pp. e126-32, Mar. 2015, doi: 10.1097/SCS.0000000000001350.

[258] E. Hassmann-Poznańska, B. Skotnicka, B. Musiatowicz, and E. Hubert, "Adenoid cystic carcinoma in the head and neck: clinical and pathologic review.," *Otolaryngol. Pol.*, vol. 47, no. 5, pp. 399–405, 1993.

[259] L. Cozzi, A. Fogliata, A. Lomax, and A. Bolsi, "A treatment planning comparison of 3D conformal therapy, intensity modulated photon therapy and proton therapy for treatment of advanced head and neck tumours.," *Radiother. Oncol. J. Eur. Soc. Ther. Radiol. Oncol.*, vol. 61, no. 3, pp. 287–297, Dec. 2001, doi: 10.1016/s0167-8140(01)00403-0.

[260] M. Steneker, A. Lomax, and U. Schneider, "Intensity modulated photon and proton therapy for the treatment of head and neck tumors.," *Radiother. Oncol. J. Eur. Soc. Ther. Radiol. Oncol.*, vol. 80, no. 2, pp. 263–267, Aug. 2006, doi: 10.1016/j.radonc.2006.07.025.

[261] S. Kandula *et al.*, "Spot-scanning beam proton therapy vs intensity-modulated radiation therapy for ipsilateral head and neck malignancies: a treatment planning comparison.," *Med. Dosim. Off. J. Am. Assoc. Med. Dosim.*, vol. 38, no. 4, pp. 390–394, 2013, doi: 10.1016/j.meddos.2013.05.001.

[262] L. D. Locati *et al.*, "Patients with adenoid cystic carcinomas of the salivary glands treated with lenvatinib: Activity and quality of life.," *Cancer*, vol. 126, no. 9, pp. 1888–1894, Jan. 2020, doi: 10.1002/cncr.32754.

[263] E. Zavattero, G. Ramieri, F. Volpe, and C. Borbon, "Navigation-Assisted Resection

and Fibula Free-Flap Reconstruction of an Extensive Maxillary Tumor.," *J. Craniofac. Surg.*, vol. 32, no. 5, pp. e450–e452, 2021, doi: 10.1097/SCS.0000000000007304.

[264] A. Tel *et al.*, "The evolution of craniofacial resection: A new workflow for virtual planning in complex craniofacial procedures.," *J. cranio-maxillo-facial Surg. Off. Publ. Eur. Assoc. Cranio-Maxillo-Facial Surg.*, vol. 47, no. 9, pp. 1475–1483, Sep. 2019, doi: 10.1016/j.jcms.2019.06.016.

[265] F. Ricotta *et al.*, "Navigation-guided resection of maxillary tumors: Can a new volumetric virtual planning method improve outcomes in terms of control of resection margins?," *J. cranio-maxillo-facial Surg. Off. Publ. Eur. Assoc. Cranio-Maxillo-Facial Surg.*, vol. 46, no. 12, pp. 2240–2247, Dec. 2018, doi: 10.1016/j.jcms.2018.09.034.

[266] M. Ferrari *et al.*, "Navigation-guided osteotomies improve margin delineation in tumors involving the sinonasal area: A preclinical study.," *Oral Oncol.*, vol. 99, p. 104463, Dec. 2019, doi: 10.1016/j.oraloncology.2019.104463.

[267] G. Burström *et al.*, "Frameless Patient Tracking With Adhesive Optical Skin Markers for Augmented Reality Surgical Navigation in Spine Surgery.," *Spine (Phila. Pa. 1976).*, vol. 45, no. 22, pp. 1598–1604, Nov. 2020, doi: 10.1097/BRS.0000000000003628.

[268] F. Manni *et al.*, "Towards Optical Imaging for Spine Tracking without Markers in Navigated Spine Surgery," *Sensors*, vol. 20, no. 13, 2020, doi: 10.3390/s20133641.

[269] F. Manni *et al.*, "Hyperspectral Imaging for Skin Feature Detection: Advances in Markerless Tracking for Spine Surgery," *Appl. Sci.*, vol. 10, no. 12, 2020, doi: 10.3390/app10124078.

[270] Y. Xue *et al.*, "High-accuracy and real-time 3D positioning, tracking system for medical imaging applications based on 3D digital image correlation," *Opt. Lasers Eng.*, vol. 88, pp. 82–90, 2017, doi: https://doi.org/10.1016/j.optlaseng.2016.07.002.

[271] J. T. Gibby, S. A. Swenson, S. Cvetko, R. Rao, and R. Javan, "Head-mounted display augmented reality to guide pedicle screw placement utilizing computed tomography.," *Int. J. Comput. Assist. Radiol. Surg.*, vol. 14, no. 3, pp. 525–535, Mar. 2019, doi:

10.1007/s11548-018-1814-7.

[272] J. W. Meulstee *et al.*, “Toward Holographic-Guided Surgery,” *Surg. Innov.*, vol. 26, no. 1, pp. 86–94, Sep. 2018, doi: 10.1177/1553350618799552.

[273] J. J. Pu, W. S. Choi, P. Yu, M. C. M. Wong, A. W. I. Lo, and Y.-X. Su, “Do predetermined surgical margins compromise oncological safety in computer-assisted head and neck reconstruction?,” *Oral Oncol.*, vol. 111, p. 104914, Dec. 2020, doi: 10.1016/j.oraloncology.2020.104914.